FACULDADE DE ENGENHARIA DA UNIVERSIDADE DO PORTO

Design of a Combined Torsion and Bending Fatigue Testing Machine

Beatriz Marques Ferreira



Mechanical Engineering Master's Degree

FEUP Supervisor: Prof. Pedro Sousa

INEGI Supervisor: Eng. Tiago Domingues

INEGI Supervisor: Dr. Daniel Braga

INEGI Supervisor: Prof. Francisco Queirós de Melo

October 6, 2023

Design of a Combined Torsion and Bending Fatigue Testing Machine

Beatriz Marques Ferreira

Mechanical Engineering Master's Degree

October 6, 2023

Resumo

No domínio da engenharia e da análise estrutural, o estudo da fadiga multiaxial desempenha um papel crucial na compreensão das interacções complexas entre cargas, frequências e orientações variáveis experienciadas pelos componentes. Com a sua relevância a estender-se a diversas indústrias, tais como a aeroespacial, a automóvel e a indústria da manufatura, a investigação da fadiga multiaxial não só informa a conceção de estruturas para aplicações no mundo real, como também contribui para o avanço dos modelos preditivos.

Embora os componentes de engenharia sofram frequentemente cargas complexas, a maioria dos estudos centra-se em condições uniaxiais, baseando-se em dados de ensaios uniaxiais para a caraterização da fadiga. No entanto, sob cargas multiaxiais, os materiais podem comportar-se de forma imprevisível e apresentar propriedades variáveis, necessitando de uma caraterização abrangente do material.

Os ensaios de fadiga que envolvem torção e flexão combinadas ganharam destaque devido à sua relevância em vários cenários do mundo real. No entanto, um desafio significativo reside na escassez de máquinas disponíveis, necessitando de um maior foque neste campo para eventualmente comercializar tais soluções e expandir a base de conhecimento.

Esta dissertação foi realizada em ambiente empresarial, no Instituto de Ciência e Inovação em Engenharia Mecânica e Engenharia Industrial (INEGI), na Unidade de Monitorização Avançada e Integridade Estrutural (UMAI). O objetivo principal foi projetar uma nova máquina de ensaios de fadiga combinada de torção e flexão para combater a falta de soluções oferecidas e melhorar as já existentes.

O processo de projeto iniciou-se com uma revisão bibliográfica, onde se identificaram os vários tipos de ensaios de fadiga, os diferentes aparelhos, e outras características relevantes, de onde é possível conceber melhor a solução pretendida. O projeto final tem em conta os diferentes requisitos e utiliza diferentes soluções adaptadas de outras máquinas, tornando-o num conceito muito diversificado.

Para garantir a segurança da máquina, todos os componentes têm cálculos de validação que asseguram a sua estabilidade quando submetidos às cargas implícitas no ensaio. A máquina é capaz de aplicar um momento de 210 N.m através de um sistema excêntrico que fornece cargas cíclicas.

A dissertação conclui com a apresentação dos resultados e sugere novos projetos com o objetivo de avançar a compreensão dos ensaios de fadiga multiaxial.

Abstract

In the realm of engineering and structural analysis, the study of multiaxial fatigue holds a crucial role in understanding the complex interactions between varying loads, frequencies, and orientations experienced by components. With its relevance extending to diverse industries such as aerospace, automotive, and manufacturing, the research of multiaxial fatigue not only informs the design of structures for real-world applications but also contributes to advancing predictive models.

While engineering components are often submitted to complex loads, the majority of studies focuses on uniaxial conditions, relying on data from uniaxial tests for fatigue characterization. However, under multiaxial loads, materials can behave unpredictably and display varying properties, necessitating comprehensive material characterization.

Fatigue tests involving combined torsion and bending have gained prominence due to their relevance in various real-world scenarios. However, a significant challenge lies in the scarcity of available machines, needing a stronger focus in this field to eventually commercialize such solutions and expand the knowledge base.

This dissertation was carried out in a business environment, in the Instituto de Ciência e Inovação em Engenharia Mecânica e Engenharia Industrial (INEGI), in the Unidade de Monitorização Avançada e Integridade Estrutural (UMAI). The main objective was to design a new combined torsion and bending fatigue testing machine to fight the lack of solutions offered and improve the ones already existing.

The design process began with a literature review, which identified the various types of fatigue testing, different apparatus, and other relevant features, from where is possible to better design the intended solution.

The final design takes into account the different requirements and uses different adapted solutions from other machines, turning it into a very diverse concept.

To ensure the safety of the machine, every component has validation calculus that assure their stability when submitted to the loads implied by the test. The machine is capable of applying a 210 Nm moment by the means of an eccentric system that provides cyclic loads.

The dissertation concludes with the presentation of findings and suggests further projects aimed at advancing our understanding of multiaxial fatigue testing.

Acknowledgements

Firstly, to INEGI, a renowned technological innovation centre, for giving me the opportunity to carry out this thesis in a corporate environment. The authors acknowledge the project POCI- 01-0247-FEDER-072260, financed by the European Funds, through the programme COMPETE2020, under the Eureka Smart Label S0318-STREAM -Surface TREatment for Additive Manufacturing. I would also like to express my gratitude to the staff at INEGI who welcomed me and helped me whenever I needed it.

I would also like to individually thank my supervisors, Pedro Sousa, Daniel Braga, Tiago Domingues and Francisco Queirós de Melo, for all their support throughout the development of this work. A special thank you to prof. Queirós for spending hours on end on this work, giving me the opportunity to work with such an intelligent and kind mind.

To my family, parents and siblings, who have always supported me in everything and, regardless of the result, make sure I know they are proud of me. The person I am today comes a lot from you and I hope you know that.

To all my friends, especially those who came along with the best part of university, the academic traditions, whether from other courses or different years, you have all marked me in some way and are part of the growth that these five years have been. I couldn't fail to mention Maria, who quickly went from stranger to sister. Just as we're both a bit special, so is our relationship. There are no words for the support and trust we see in each other.

Now for someone I'll never be able to put into words what means to me. These years haven't been the easiest, and if anyone knows that, it's you. In one way or another, ever since we met, we've always been there for each other. You've always been there to help when it's bad and celebrate when it's good. You've been by far the person I've learnt the most from, and the person I've grown up with. I'll carry with me for life the best experiences with the person who became my life itself. I'd do everything the same way again with you, otherwise I wouldn't be me. Thank you for being who you are and for everything you do. I love you.

Finally, a thank you that is both difficult and easy, and that I really wish didn't have to be on paper. Difficult because by little you didn't see me finish this stage of my life, easy because of the example of a person you've always been. You and Grandma have always been as much parents as my own parents, and you've always done everything to make me happy. Thank you for giving me everything, and don't worry, I'll take good care of Grandma, Grandad.

The experiences I carry with me can never be described because they've been lived, and that's the beauty of them. Each one has shaped me a little and made me the person I am today. How much I've changed in these five years is absurd, but this change isn't all bad. The Beatriz of always is still here, and now she realises that growing up isn't a bad thing and only makes us better people. Thank you to all the persons, mentioned or not, who have surrounded me over the years and made me realise a more beautiful side of life.

"I need to grow even though I'm grown."

Denzel Curry

Contents

1 Introduction **1**
- 1.1 Background and Motivation . . . 1
- 1.2 Objectives . . . 2
- 1.3 Research Methodology . . . 2
- 1.4 Document Structure . . . 2

2 State of the Art **4**
- 2.1 Introduction to Fatigue . . . 4
  - 2.1.1 Types of Fatigue . . . 5
  - 2.1.2 Factors Influencing Fatigue . . . 6
- 2.2 Fatigue Testing . . . 7
  - 2.2.1 Axial Fatigue Test . . . 8
  - 2.2.2 Torsion Fatigue Test . . . 9
  - 2.2.3 Bending Fatigue Test . . . 10
- 2.3 Multiaxial Fatigue . . . 11
  - 2.3.1 Multiaxial Fatigue Testing . . . 12
- 2.4 Combined Bending and Torsion Apparatus . . . 13
  - 2.4.1 Ogawa's Apparatus . . . 13
  - 2.4.2 Shawki's Apparatus . . . 15

3 Machine Design **17**
- 3.1 System Requirements . . . 17
  - 3.1.1 Testing Specimens . . . 18
  - 3.1.2 Reference Materials . . . 19
  - 3.1.3 Load Capacity . . . 19
- 3.2 Conceptual Design . . . 20
- 3.3 Final Design . . . 21
- 3.4 Main Body . . . 22
  - 3.4.1 Chucks (1) . . . 23
  - 3.4.2 Mirrors . . . 26
  - 3.4.3 Horizontal Articulation (4) . . . 31
  - 3.4.4 Balance Triangles (5 and 6) . . . 31
  - 3.4.5 Vertical Articulation (7) . . . 32
- 3.5 Eccentric System . . . 35
  - 3.5.1 Fixed eccentric (18) . . . 39
  - 3.5.2 Free eccentric (17) . . . 41
  - 3.5.3 Locking cap (19) . . . 43
  - 3.5.4 Movement transmission (15 and 16) . . . 45

3.5.5 Fixation (21) . . . 46
3.6 Equilibrium Structure . . . 47
3.6.1 Profiles . . . 47
3.6.2 Steel cables and pulleys . . . 50
3.7 Base (23) . . . 52
3.8 Shafts sizing . . . 52
3.8.1 Shaft connecting the horizontal articulations (9) . . . 53
3.8.2 Shaft connecting the balance triangles and vertical articulations (10) . . . 55
3.8.3 Shaft connecting the vertical articulations to the support (29) . . . 57
3.8.4 Shaft connecting the balance triangles and eccentric system (9) . . . 58
3.8.5 Eccentric system's central shaft (20) . . . 59
3.9 Bearings sizing . . . 60
3.9.1 Plain Bearings (34) . . . 60
3.9.2 Ball Bearings (35) . . . 61
3.10 Screws, Nuts and Washers . . . 64
3.11 Design for Manufacturing . . . 65
3.12 System Actuating Power Requirements . . . 66
3.13 Chapter Summary . . . 67

4 Conclusion **68**
4.1 Final Conclusions . . . 68
4.2 Future Works . . . 69

References **71**

A Final Design technical drawings **75**

B BOM - Bill of Materials **77**

C Technical drawings **80**

D Wispeco Catalog **112**

E Orplex Catalog **114**

F SKF Bearing Technical Sheet **116**

G Fabory Spring Plunger Technical Sheet **119**

List of Figures

2.1 Stress distribution with sharp ends. . . . 5
2.2 Stress distribution with round ends. . . . 5
2.3 Bimodal fatigue curve for LCF, HCF and VHCF modes [11]. . . . 5
2.4 S-N curve example [14]. . . . 6
2.5 Cyclic load graphic. . . . 7
2.6 Axial load scheme. . . . 8
2.7 Stress distribution of a specimen subjected to axial stress (porjected view). . . . 8
2.8 Torsion load scheme. . . . 9
2.9 Stress distribution of a specimen subjected to torsion. . . . 10
2.10 Bending load scheme. . . . 10
2.11 3-point bending test. . . . 11
2.12 4-point bending test. . . . 11
2.13 Stress distribution of a specimen subjected to bending (projected view). . . . 11
2.14 Ogawa's machine display [43]. . . . 13
2.15 Bending loading test [43]. . . . 14
2.16 Combined bending and torsion loading test [43]. . . . 14
2.17 Layout of the testing machine and respective legend [44]. . . . 16

3.1 ASTM E2207-02 [45]. . . . 18
3.2 Curved pipes testing machine [51]. . . . 21
3.3 Final design. . . . 22
3.4 Bending main body. . . . 23
3.5 Torsion main body. . . . 23
3.6 SCHUNK ROTA-S plus 2.0 250-62 C5-SFG. . . . 24
3.7 Jaw adaptor assembly. . . . 26
3.8 Jaw adaptor assembly: section view. . . . 26
3.9 Bending mirror. . . . 27
3.10 Torsion mirror. . . . 28
3.11 Chuck-mirror adaptor. . . . 29
3.12 Separation created between the mirror and the chuck. . . . 29
3.13 Imaginary displacement scheme for mirror. . . . 30
3.14 Horizontal articulation. . . . 31
3.15 Balance triangle. . . . 32
3.16 Vertical articulation. . . . 33
3.17 Vertical articulation's support. . . . 35
3.18 Press eccentric mechanism [53]. . . . 36
3.19 Eccentric system. . . . 36
3.20 Subsystem when θ is imposed. . . . 38

3.21 Fixed eccentric. . . . 39
3.22 Key scheme. . . . 40
3.23 Free eccentric. . . . 41
3.24 Eccentric centre trajectory. . . . 42
3.25 Eccentricity scheme. . . . 42
3.26 Locking cap. . . . 44
3.27 Spring plunger setup. . . . 45
3.28 Eccentric system 46
3.29 Eccentric system support. . . . 47
3.30 Profile scheme. . . . 48
3.31 Forces diagram of the profiles. . . . 49
3.32 Bending moment diagram of the profiles. . . . 49
3.33 Pulley scheme. . . . 50
3.34 Imaginary displacement scheme. . . . 51
3.35 Base. . . . 52
3.36 Threaded hole on the end of a shaft. . . . 53
3.37 Free body diagram of section of the system. . . . 53
3.38 Forces diagram of the shaft (9). . . . 54
3.39 Bending moment diagram of the shaft (9). . . . 54
3.40 Free body diagram of section of the system. . . . 55
3.41 Forces diagram of the shaft (10). . . . 55
3.42 Bending moment diagram of the shaft (10). . . . 56
3.43 Stress concentration factor for shafts with a change in cross-section [46]. . . . 56
3.44 Forces diagram of the shaft (29). . . . 58
3.45 Bending moment diagram of the shaft (29). . . . 58
3.46 Forces diagram of the shaft (9). . . . 59
3.47 Bending moment diagram of the shaft (9). . . . 59
3.48 Forces diagram of the shaft (20). . . . 59
3.49 Bending moment diagram of the shaft (20). . . . 60
3.50 Permaglide bearing. . . . 61
3.51 16004 SKF bearing scheme. . . . 62

List of Tables

3.1 Specimen dimensions. 18
3.2 AA2024 and Inconel 718 mechanical properties [50]. 19
3.3 Necessary moments for Specimen A. 20
3.4 Necessary moments for Specimen B. 20
3.5 New Specimen B dimensions. 24
3.6 Necessary moments for the new Specimen B. 25
3.7 θ_t, δ_b and θ_b for Specimen A. 37
3.8 θ_t, δ_b and θ_b for Specimen B. 37
3.9 Course y required values. 38
3.10 Key dimensions. 40
3.11 Conversion table for eccentric mechanism. 43
3.12 16004 SKF bearing dimensions. 62
3.13 Variation of the safety factor [46]. 62

Chapter 1

Introduction

In this chapter, the subject of this dissertation is introduced. As such, this chapter contains a brief background, the motivation, the goals, the empolyed methodology and the organisation of the present document.

1.1 Background and Motivation

In the realm of engineering and structural analysis, the study of multiaxial fatigue holds a crucial role in understanding the complex interactions between varying loads, frequencies, and orientations experienced by components [1]. Unlike uniaxial fatigue, which deals with simpler single-load scenarios, multiaxial fatigue involves intricate stress and strain states arising from diverse loading and geometric conditions. This distinction emphasizes the need for tailored approaches to predict and address fatigue failures under different loading conditions. With its relevance extending to diverse industries such as aerospace, automotive, and manufacturing, the investigation of multiaxial fatigue not only informs the design of structures for real-world applications but also contributes to advancing predictive models and engineering practices [2].

While engineering components often experience complex loads, the majority of studies focuses on uniaxial conditions, relying on data from uniaxial tests for fatigue characterization [2]. However, under multiaxial loads, materials can behave unpredictably and display varying properties, necessitating comprehensive material characterization. Multiaxial fatigue testing, particularly under combined loads like axial, bending, and torsion, simulates real-life conditions and is essential for evaluating fatigue life [3]. Among multiaxial tests, the axial-torsion combination is widely used and standardized, while axial-bending and bending-torsion combinations are gaining attention.

Fatigue tests involving combined torsion and bending have gained prominence due to their relevance in various real-world scenarios. However, a significant challenge lies in the scarcity of available machines, necessitating a stronger focus in this field to eventually commercialize such solutions and expand the knowledge base. Overcoming the considerable time consumption and limited diversity in applying test forces remains a hurdle in the realm of multiaxial fatigue testing

machines. As this area continues to evolve, addressing these challenges is essential for unlocking the full potential of multiaxial fatigue testing and advancing its practical applications.

1.2 Objectives

The primary objectives of this dissertation are as follows:

- Design a combined torsion and bending fatigue testing machine;
- The machine having the capability to perform tests solely for torsion or solely for bending;
- Being able to adjust and vary the R ratio within a range;
- The final design being portable and relatively low in footprint.

1.3 Research Methodology

The objectives of this dissertation were achieved by doing the following, which can be broken down into:

- Research about fatigue, both uniaxial and multiaxial, and why and how to test it;
- Literature review of the already existing solutions to multiaxial fatigue testing, specifically combined bending and torsion;
- Development of the machine design and manufacturing designs of its components;
- Validation calculus of the designed solution.

1.4 Document Structure

The present dissertation is composed of five chapters, commencing with the current chapter 1. This initial chapter offers an introduction to the document, outlining the contextual background, the primary goals, the methodology employed, and the structure of the document. It also explores the existing technologies of interest that have inspired the creation of this dissertation.

In chapter 2, an introduction about the concept of fatigue is made, presenting its most interesting facts, such as its consequences and existing types. The importance of testing is also mentioned, making a quick reference and analysis to its three principal facets. Furthermore, the concept of multiaxial fatigue is presented, where its principal interest and challenges are addressed. Finally, is done a more in depth analysis and comparison between apparatus related to the theme of this dissertation.

In chapter 3, is demonstrated how the process of designing the machine occurred. The system requirements, mechanisms that served as inspiration and both conceptual and final designs

are shown. Furthermore, based on the determined requirements and associated concepts, the dissertation progresses forward to the detailed design phase, displaying the design options and their reasoning. This section addresses the dimensioning of the parts and other necessary components, such as bearings and shafts. It also addresses the validation calculus to confirm that some features or parts don't break while functioning. Towards the end of the chapter, the focus shifts to the manufacturing processes and designs, as the intention is to manufacture certain parts of the machine.

Finally, in the last chapter, chapter 4, conclusions about the developed solutions and future development suggestions are presented.

Chapter 2

State of the Art

2.1 Introduction to Fatigue

Fatigue is the phenomenon of mechanical failure in a material resulting from the repetitive application of stresses or deformations. This leads to changes in the material's properties and the formation of cracks, which ultimately propagate and culminate in the total failure of the component [4] [5]. These failures usually occur due to the influence of cyclic loads, whose peak values are below the ultimate tensile stress, or even the yield stress of the material [4]. Different from a static load applied in a component, with a stress so high that automatically causes its failure, cyclic loading is based on the concept that the material becomes "tired" and fails over time [6]. The gradual growth of failure can go unnoticed until it reaches the critical point because it does not alter the component's behaviour, potentially leading to the loss of human lives, equipment, and structures. Therefore, studying fatigue life is essential [5].

Numerous industries in the engineering world suffer from this phenomenon and its consequences, such as aerospace, automotive, civil engineering, manufacturing, among others. There are several real-life examples of accidents caused by failure due to mechanical fatigue. Two examples of historical situations are the British Overseas Airways Corporation (BOAC) flight 781 in 1954 and the Hatfield rail crash in 2000. In the first example, a de Havilland Comet operated by BOAC was flying from Rome to London. The Comet plunged into the waters close to Elba, off the shores of Italy, resulting in the loss of all 35 individuals aboard. The cause was attributed to metal fatigue, stemming from the repetitive pressurization and depressurization of the aircraft's fuselage during regular operations [7]. In the second, the Great North Eastern Railway (GNER) train ID38, travelling from London Kings Cross to Leeds, derailed approximately 0.8 km south of Hatfield Station. The train was carrying a total of 170 passengers and 12 GNER staff members. Tragically, four passengers lost their lives, while over seventy individuals sustained injuries, including four severe cases. Similarly to the plain crash, the cause was attributed to metal fatigue [8]. The steel rails on the railway track experience metal fatigue due to factors such as the frequent passage of trains, the presence of 'out of round' wheels causing flat spots, inadequate connections between rail sections, or insufficient packing and support beneath the rails [8].

With the acknowledgement of this problem, it was a natural response to start looking for solutions to try to prevent failure. This interest in discovering and developing new and better design solutions to prevent fatigue failure is always growing. A well-known solution is the use of different materials, for example composites. Also, adding fillets and round surfaces instead of sharp ends, reducing the stress concentrations in that zone [9], as seen in images 2.1 and 2.2. The avoidance of abrupt cross-section changes and use of improved surface treatments are other examples of design considerations that arm in arm with a appropriated fatigue study help to prevent fatigue failures [10].

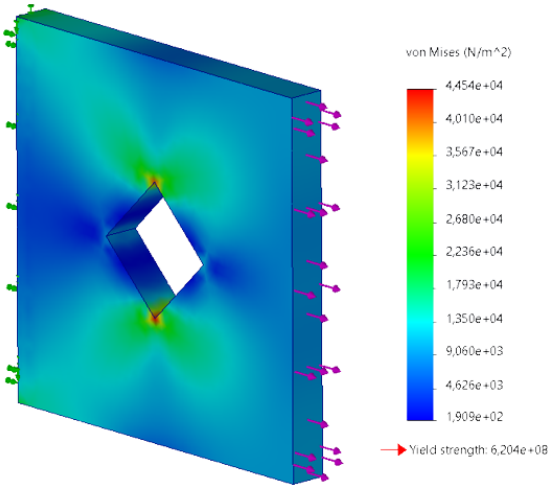


Figure 2.1: Stress distribution with sharp ends.

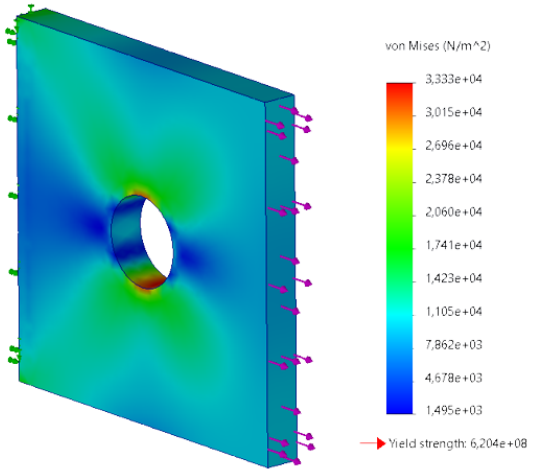


Figure 2.2: Stress distribution with round ends.

2.1.1 Types of Fatigue

As the knowledge in the field of fatigue continued growing, the areas of study related to it became more specialized. Three types of fatigue were subsequently identified, depending on the number of cycles: low cycle fatigue (LCF), high cylce fatigue (HCF) and very high cycle fatigue (VHCF) [11].

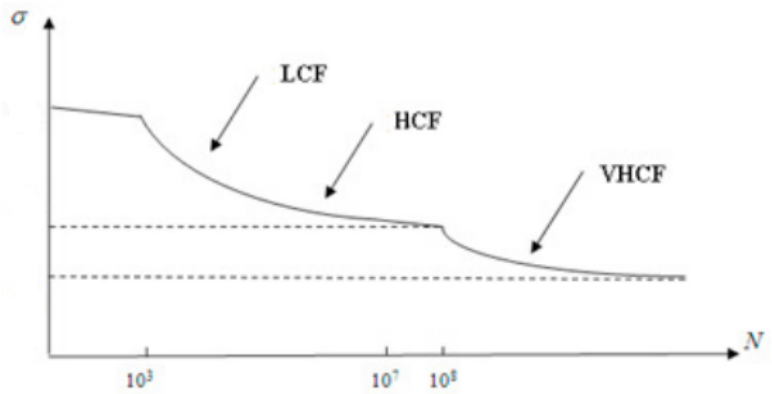


Figure 2.3: Bimodal fatigue curve for LCF, HCF and VHCF modes [11].

LCF arises when a material experiences repeated loading under elevated stress levels, leading to its failure after a relatively limited count of cycles, typically less than 10^4, and is commonly linked to plastic deformation. This was studied the latest because of the little knowledge about plasticity compared to elasticity at the time [12]. HCF occurs when a material is subjected to cyclic loading at a low stress level, causing it to fail after a large number of cycles, 10^4 up to 10^8 in some cases, and is characterized by elastic deformation. VHCF occurs when a material is subjected to cyclic loading at a very low stress level, causing it to fail after an extremely large number of cycles, typically greater than 10^7 [13]. LCF runs in strain control, the load is a dependent variable, while HCF and VHCF run in stress control.

2.1.2 Factors Influencing Fatigue

The fatigue strength of a component is highly sensitive to various internal and external factors. From the material properties and surface conditions to environmental factors, in a real-world application there are several potential influences that need to be taken into account. But the most critical factors that govern the fatigue behaviour of materials are related to the stresses and number of cycles applied. This two parameters are commonly represented by S-N curves, which play an important role in understanding how materials respond to repeated loading over time [14].

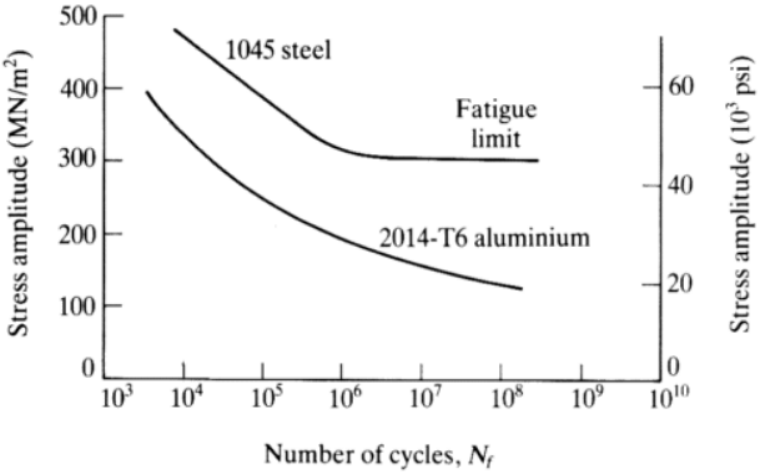


Figure 2.4: S-N curve example [14].

On an S-N curve, the vertical axis typically represents the stress amplitude, while the horizontal axis represents the logarithm of the number of cycles to failure. S-N curves are divided into distinct regions that offer valuable insights into a material's behavior. One such region is the endurance limit, which indicates the stress amplitude below which a material can theoretically endure an infinite number of cycles without failing. Above the endurance limit, the material's fatigue life gradually decreases as stress amplitudes increase [14].

Because the amplitude of the cyclic load greatly influences fatigue performance, the S-N relationship is established for a particular loading amplitude. This amplitude is presented through

the R ratio, represented in figure 2.5, denoting the minimum peak stress divided by the maximum peak stress [6].

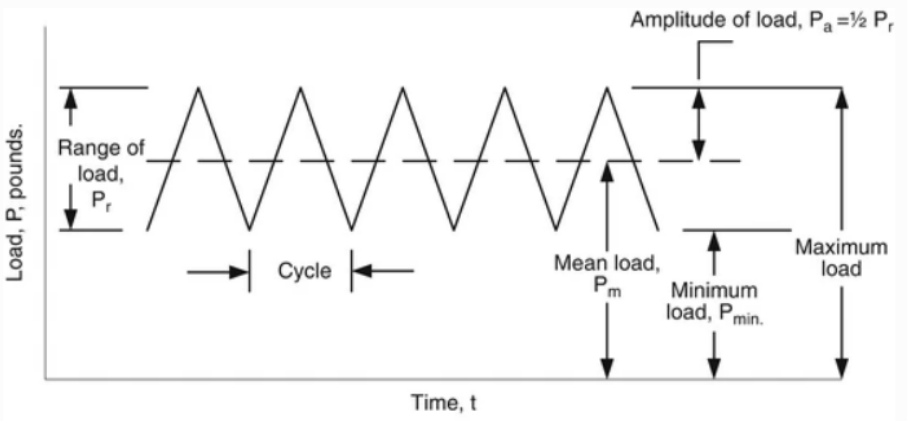


Figure 2.5: Cyclic load graphic.

In terms of frequency, it can influence life time to increase, decrease or have no effect also. In general, the frequency can affect fatigue behaviour of a material but, to produce a reasonable influence in fatigue life, the frequency needs to change in order of magnitudes [15].

2.2 Fatigue Testing

Nowadays, a well done fatigue design involves testing. A component subjected to a stress higher than the ultimate tensile strength fails. However, as seen above, it is often observed that components fail before reaching this value. Materials must then be tested to determine how many cycles they can endure before failing, producing data to build various S-N curves [16]. It's essential to evaluate the cases experimentally since theoretical equations often do not fit the reality. Therefore, there is a need to conduct fatigue tests of various types on different materials to correctly design engineering components subjected to loads, preventing failure [3].

The first evidences of fatigue testing go back to 1837 when Wilhelm August Julius Albert released the first findings from the earliest-known fatigue tests, employing a testing apparatus for conveyor chains that had experienced failure during operations in the Clausthal mines. But it was years later, between 1850 and 1860, that August Wöhler revolutionized the fatigue world. The German's engineer work was the first to systematically characterize the fatigue behavior of materials using S-N Curves. He also created a device to apply repetitive loads to railway axles and demonstrated conclusively that fatigue failure takes place due to the propagation of cracks from surface imperfections until the load can no longer be sustained [17].

Fatigue testing machines usually apply cyclic loads to test specimens. Therefore, fatigue testing is a dynamic testing mode, which can be used to simulate the behaviour of a material under real life loading conditions. They can incorporate axial, torsion or bending loading [18].

2.2.1 Axial Fatigue Test

When the specimen is subjected to cyclic loading along its longitudinal axis, repeated tension and compression, we come across a scenery of axial fatigue, as represented in figure 2.6.

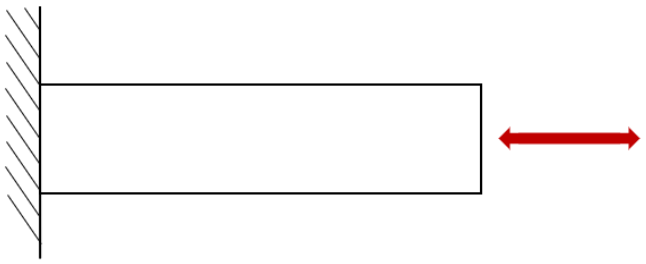


Figure 2.6: Axial load scheme.

Axial loading is a common type of loading that is present in many structural components. One example are trusses that are used to support roofs, bridges, and other structures. They are made up of a series of interconnected triangles that are designed to carry loads in tension and compression along their axis [19]. A similar example to this are columns [20].

In terms of axial testing, most machines have a similar display. Torontech [21] developed an axial load fatigue testing machine specially designed to conduct tests on strand. The test involves subjecting the strand to an alternating axial tensile force, following a sinusoidal waveform with a consistent frequency within the elastic range. The examination continues either until the strand fails or until the specified number of loading cycles is achieved without encountering failure. Generally, this type of machines are built vertically and the actuator is mounted on the upper crosshead for maximum versatility, embracing different length specimens.

When a sample undergoes axial loading, the force applied is evenly spread over the cross-sectional area. As of that, the stress magnitude remains constant at any location across the cross-section [22].

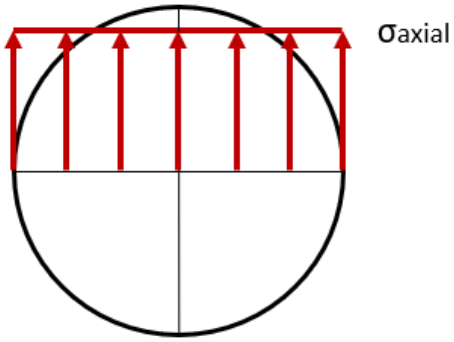


Figure 2.7: Stress distribution of a specimen subjected to axial stress (porjected view).

2.2.2 Torsion Fatigue Test

When the specimen is subjected to cyclic twisting deformation through a torsion moment inducing shear stresses along its cross-section, we came across a scenery of torsion fatigue, as represented in figure 2.8.

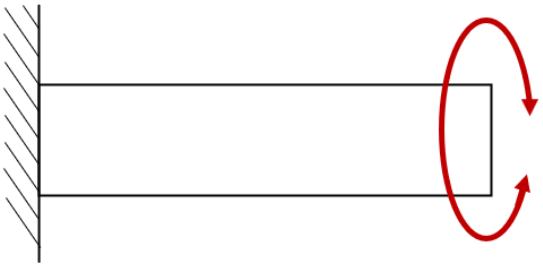


Figure 2.8: Torsion load scheme.

Torsion loading is mostly present in rotating applications. The major example of components submitted to this type of load are shafts. Transmission shafts can be found on motors and gearboxes, which are used to transmit power from one point to another, and are often subjected to torsion loading due to the torque generated by the components they connect [23]. Other examples are components of human-powered vehicles, such as the shaft in the bottom bracket of a bike, the propeller shaft of an aircraft or boat, or the wing of an aircraft [24].

Torsion fatigue testing has gained a lot of attention in the last years, since bending and axial tests were more known due to its simplicity. Nowadays, the market already offers a lot of solutions with variety of display. ADMET [25] and TestResources [26] for example, offer multiple machines with a vertical or horizontal configuration option. The systems are capable of static constant angular speed or torsion load rate tests with a cyclic mode for repetitive sinusoidal or triangular wave forms that can cycle between angular positions or torque load limits. Tests last millions of cycles, or until sample failure. Some machines can reach frequencies up to 20 Hz.

Some researchers have also attempted new design solutions for torsion fatigue testing machines. Fernanda [3] opted for servomotors mounted with a linear motion mechanism and the machine allows working at different load ratios R by applying an initial static angle before the initiation of torsion testing. Bustos [27] on the other hand, based the operation on the alternating movement that the transmission of a washing machine produces. A flywheel located at the top of the machine causes the inertial load. This design tries to illustrate how the acceleration-induced inertial forces on the mechanical components generate cyclic loads, leading to fatigue failures over time.

Under torsion loading, there is an absence of normal stress as the applied force aligns parallel to the object's cross-sectional area. Torsional stress, on the other hand, is the shear stress impacting a cross-section perpendicular to the member's length, generated due to twisting action. The shear stress varies from zero at the center to a maximum at the surface.

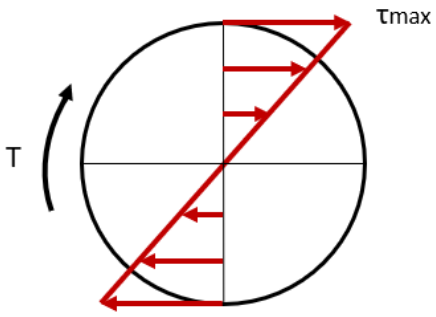


Figure 2.9: Stress distribution of a specimen subjected to torsion.

Shear stresses are at their lowest point close to the center. As a result, the material situated near this central area makes only a minor contribution to the torsional strength. This is the reason why hollow shafts are frequently employed in power transmission [28].

2.2.3 Bending Fatigue Test

When the specimen is subjected to cyclic bending deformation through a pure bending moment we came across a scenery of bending fatigue, as represented in figure 2.10. Pure bending is defined as only a bending moment, without axial and torsional stress [16].

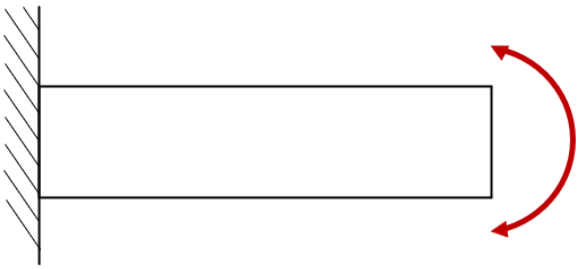


Figure 2.10: Bending load scheme.

An instance of bending loading can be seen in crane applications. Crane booms are the long horizontal arms of cranes that extend out to lift and move heavy loads. They are subjected to bending loading as they support the weight of the load and transfer it to the crane's base [29]. Other example are bicycle frames, components that are designed to withstand the forces and loads experienced during riding. They experience bending loading as they flex and deform under the rider's weight and the forces applied during pedaling and maneuvering [30].

Testing equipment for this type of fatigue test can be found in habitual testing machine suppliers, such as TestResources [31] and Matest [32]. These machines can be specific for three or four point bending tests, although some solutions offer adaptors to switch off between, which allow the same machine to perform these two variants of the test.

3-point and 4-point bending fatigue tests are similar, yet different. The primary distinction between 3-point and 4-point bending fatigue tests lies in the region where the maximum bending stress is experienced. In 3-point tests, figure 2.11, the stress concentration is small and concentrated under the center of the loading point, while in 4-point tests, figure 2.12, the stress concentration is over a larger region, avoiding premature failure [33]. Also, during bending tests, shear stresses occur within the specimen being tested. In 3-point bending, shear stress is present everywhere in the bent specimen except along the vertical plane containing the central loading nose. Consequently, pure bending occurs only on that plane. In 4-point bending, shear stress is absent in the region between the two loading noses (a zone of pure bending) [34].

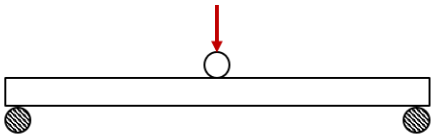


Figure 2.11: 3-point bending test.

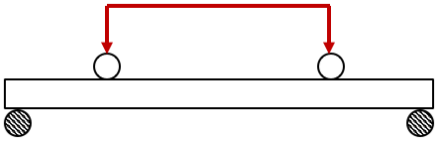


Figure 2.12: 4-point bending test.

When a sample undergoes bending, it encounters a spectrum of stresses throughout its thickness. At the concave face's edge of the specimen (upper point), the normal stress reaches its peak compressive level. On the convex face of the specimen (lower point), the normal stress reaches its maximum tensile intensity [35].

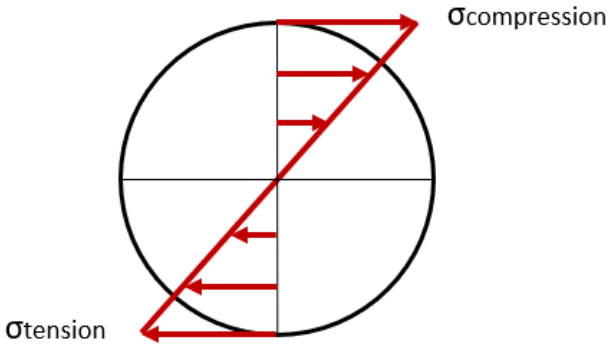


Figure 2.13: Stress distribution of a specimen subjected to bending (projected view).

2.3 Multiaxial Fatigue

In multiaxial fatigue, components undergo diverse loads with varying frequencies, amplitudes, and orientations, leading to biaxial or multiaxial fatigue [2]. This overarching concept encompasses complex stress and strain states, both local and global, arising from loading and/or geometry conditions. Specifically, multiaxial loading engenders stress and/or strain patterns characterized by two or more components in the stress or strain tensor [36]. In essence, multiaxial fatigue occurs in more complex loading scenarios, while uniaxial fatigue manifests under simpler, single-loading

conditions. This distinction underscores the need for tailored approaches in predicting and mitigating fatigue failures across different types of loading scenarios.

Studying multiaxial fatigue holds significant importance for various compelling reasons, one being its widespread presence in everyday structures, where multiaxial fatigue is commonly observed. By delving into the intricacies of multiaxial fatigue, engineers and researchers can gain invaluable insights to inform the design and analysis of structures, ensuring their reliability and safety within real-world applications [37]. Research efforts in the domain of multiaxial fatigue also contribute to the refinement of predictive models, driving advancements in the field.

Multiaxial fatigue analysis has practical applications in various industries, such as aerospace, automotive, medical, manufacturing and even energy. However, there are numerous situations that present certain conditions that require a suitable multiaxial study. For instance, multiaxial fatigue becomes relevant when applied loadings are not proportional to each other [38]. This occurs in scenarios where different types of loadings, such as tension, compression, bending, and torsion, are simultaneously applied. It's also crucial in components featuring geometric discontinuities like holes, notches, or chamfers due to increased stress concentration in these regions [39].

2.3.1 Multiaxial Fatigue Testing

Although most engineering components are subjected to complex loads, the majority of existing studies are conducted under uniaxial conditions [2]. The characterization of materials for fatigue is typically carried out using data obtained from uniaxial tests, hence there is data available for many materials under such conditions [40]. However, when subjected to multiaxial loads, materials can exhibit unpredictable behavior and display varying material properties. Hence, it becomes crucial to characterize these material properties across a diverse range of materials, particularly due to the prevalence of products designed to withstand biaxial loading in their regular operational scenarios.

Among all experimental methods to study multiaxial fatigue, testing under a multiaxial loading is the most promising due to its effort to recreate real-life conditions. Multiaxial fatigue testing machines are designed to apply complex loading conditions to a specimen, such as axial, bending, and torsion loads, to evaluate its fatigue life. These machines can simulate the actual conditions to which various elements of machines and structures are generally subjected.

Of all of the multiaxial tests, the combination of torsion and axial loading stands out as one of the most frequently employed methods. This approach is well-established and has yielded valuable data, contributing to a deeper understanding of material responses. Additionally, combined axial and torsion testing has been standardized, providing a structured framework for evaluation. It has some commercialized solutions as well, supplied by Instron [41] and TestResources [42]. In contrast, the combined axial-bending test remains less explored, with a limited body of research. On the other hand, the combination of bending and torsion has sparked interest due to its relevance in practical applications. While commercial solutions for this test type might not yet be prevalent, the scholarly realm is abuzz with studies investigating this very subject. This highlights the evolving

interest of multiaxial testing, with each variant offering unique insights into materials' behavior under the diverse forces that real-world applications impose.

2.4 Combined Bending and Torsion Apparatus

Since the theme of this dissertation is the design of a combined torsion and bending fatigue testing machine, we will delve deeper into the analysis of two examples of such machine designs presented in scientific articles. This will enable us to attain a comprehensive understanding of the existing machines, facilitating discussions regarding the merits and drawbacks of their designs. These insights can also serve as inspiration for the final design of this project.

2.4.1 Ogawa's Apparatus

Fumio Ogawa's work [43] led to the development of a combined bending and torsion fatigue testing machine. The primary objective behind this innovation was to minimize testing duration without compromising the accuracy of results, hence the machine having a capability to conduct tests at a significantly high frequency. Ogawa's machine lies in its versatility, as it caters to both proportional and non-proportional loading conditions. By simulating real-world scenarios in a controlled environment, the machine facilitates a comprehensive examination of material responses to varying stress states.

The testing machine's design encompasses essential components such as a revolution control motor, a timing belt, wheels, and a connecting shaft for bilateral wheels. Notably, weights are affixed to the wheels to induce the intended bending and torsion loads. The motor orchestrates the rotation of both wheels and weights through the timing belt, ensuring precise load application. A pivotal concept behind this machine was to achieve equilibrium by suspending the loading head, including the overhead wheels, directly above the test specimen.

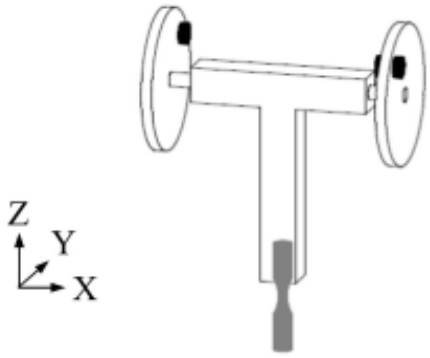


Figure 2.14: Ogawa's machine display [43].

The machine's versatility hinged upon the strategic positioning of weights, enabling the generation of both bending and torsion loading. In the absence of weights on the wheels, minimal

bending was observed on the specimen due to the absence of a direct connection between the specimen and timing belt. Altering the amount of weight allowed for the adjustment of maximum axial and bending stress levels. The machine's capability to facilitate various types of fatigue loading was intricately tied to the placement of the weights.

In the survey, the machine executed two types of tests, bending and combined bending and torsion. For Bending Tests, uniform weights on the bilateral wheels yielded consistent results. However, top or bottom positioning led to pull or push loading, while forward or backward positioning induced bending loading. Although push-pull loading emerged, its amplitude remained marginal, warranting the classification of the loading condition as predominantly pure cyclic bending loading. Conducting Combined Tests necessitated the displacement of weights by a 180° angle on the bilateral wheels. With one weight forward and the other backward, torsion loading was applied. Similarly, when weights were placed vertically, resulting in one weight upwards and the other downwards, bending loading ensued. This intricate orchestration allowed the machine to mimic a range of loading conditions with precision.

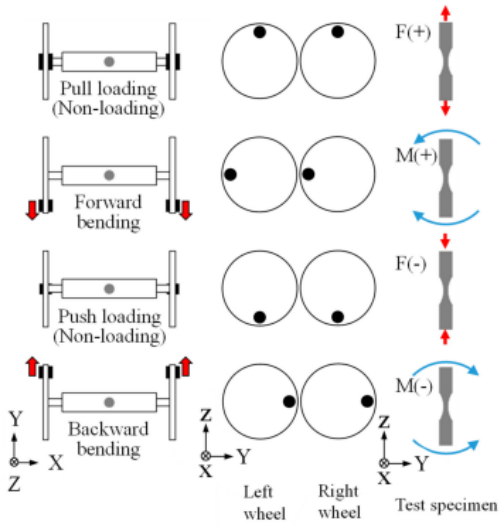


Figure 2.15: Bending loading test [43].

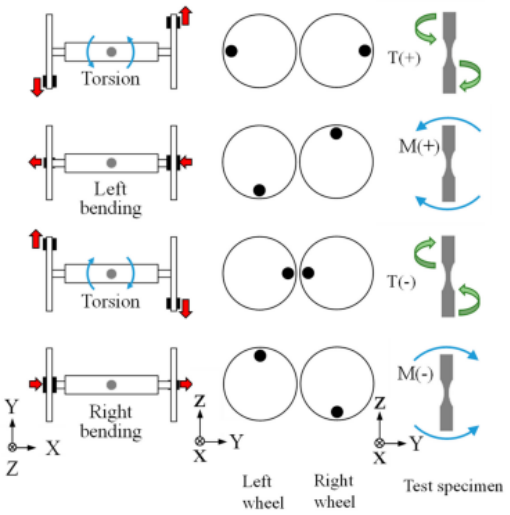


Figure 2.16: Combined bending and torsion loading test [43].

Engineered to accommodate multiaxial fatigue tests, this machine operated at a high frequency, scaling up to 50 Hz. With a resolute objective to perform a staggering 10^7 cycles within a span of three days, the machine exemplified efficiency and precision in its fatigue testing endeavors. In order to achieve such high loads, the revolution speed of the testing machine was calibrated to steer clear of the resonance frequency of the specimen. However, in order to obtain enough power, the revolution speed in the tests was close to the resonance value, for example about 80% of it in the bending test, but never reaching it. This choice was grounded in the realization that sustaining a consistent stress amplitude becomes a challenging feat at the resonance point.

Studying this mechanism is possible to find some advantages:

- Versatility in accommodating various round or cylindrical geometry specimens;

- The ability to combine bending and reverse torsion loading for assessing multiaxial fatigue behavior;
- High-frequency fatigue testing which allows for efficient testing and reduces the time required;
- Flexible load adjustment;
- Constant bending moment over the specimen length.

However, it's also possible to observe some disadvantages:

- The stress range has to be calculated based on the strain value;
- The stress range applicable in the combined test was limited.

2.4.2 Shawki's Apparatus

The primary objective of this study by Shawki [44] is to expand the investigation into low-cycle fatigue. In pursuit of this goal, a dedicated testing machine has been designed and constructed. This machine ensures consistent distributions of bending and twisting moments across the entire length of the test specimen. The machine facilitates the simultaneous application of cyclic bending and twisting forces onto a centrally positioned test specimen. Achieving this functionality relies on the utilization of two loading arms, which offer flexibility in terms of adjustable positions and lengths. This adaptability ensures the exact magnitude of moments required for accurate experimentation.

The loading arms are connected to a loading joint, allowing for both angular oscillation and swiveling motion. The loading unit includes a worm-gear drive and a slotted disk mounted on a shaft supported by angular-contact ball bearings. A sliding block on the slotted disk adjusts the eccentricity, imparting vertical displacement to a scotch-yoke follower, loading rod, and loading arm. This loading mechanism is driven by two identical units, operated by worms connected to a driving shaft, which is powered by the motor. The specimen is held by positive grips at its ends, connected to horizontal rods supported by ball bearings. Integral to the experimental setup is a comprehensive measuring system, comprised of torquemeters, load cells, and a flexural-deflection measuring device.

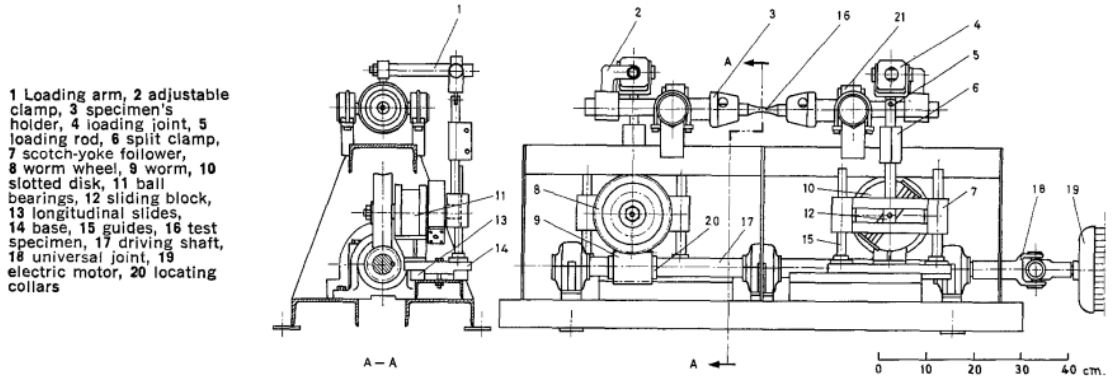


Figure 2.17: Layout of the testing machine and respective legend [44].

The testing machine in question exhibits impressive capabilities, enabling the imposition of a twisting moment reaching 69 Nm. Additionally, it can superimpose a bending moment of up to 34 Nm. These moments are administered at a steady rate of 36 cycles per minute.

The experimental procedure in the machine has multiple initial steps. The loading ratio is initially set by adjusting the position of the loading arm along the specimen holder, where the torque arm remains fixed at specific position. The two loading units' bases are longitudinally shifted until their scotch-yoke follower rods align with the rods of the loading joint, and the slotted disks' slots are horizontally positioned. The worms are then moved along the driving shaft to ensure proper meshing with the gear wheels, secured with collars. Fine-tuning the desired eccentricity is done using screw adjusters, after loosening and subsequently tightening the nuts of the sliding blocks. Then, the driving motor is started, and the test is conducted.

Studying this mechanism is possible to find some advantages:

- The machine is capable of exerting simultaneous cyclic bending and torsion loads on the test specimen;
- The bending-to-torsion moment ratio is adjustable in the range from 0 to 0.5;
- Moments are evenly spread across the entire gage length of the test specimen.

However, it's also possible to observe some disadvantages:

- Although being adjustable, the moment ratio is limited;
- Doesn't allow non-proportional loading;
- According to the available information, the machine doesn't allow different specimens than the ones tested.

Chapter 3

Machine Design

This chapter comprehensively presents the design process of the required machine, including the rationale behind each step and the justification for the chosen design options. It takes into account the apparatuses discussed in chapter 2 and other mechanisms referred later.

During the design process of this combined torsion and bending fatigue testing system, various solutions were carefully considered and evaluated to ensure optimal performance. Each element was thoroughly explored, and the most advantageous solutions were selected to ensure the smooth operation of the apparatus. To aid in the design process, the apparatus was modeled in 3D using Solidworks.

In this chapter, all calculation formulas are obtained from the book Shigley's Mechanical Engineering Design book [45] and Norton's Machine Design book [46].

3.1 System Requirements

System requirements are fundamental in machine design for practical and pragmatic reasons. They serve as a practical roadmap, outlining exactly what the machine needs to do and how it should perform. By clearly defining these requirements, engineers and designers have a concrete set of criteria to work with. This helps in making informed decisions about materials, components, and structural considerations, ensuring the machine meets its intended purpose. Moreover, these requirements are crucial for safety evaluations, enabling the identification and mitigation of potential risks.

Defining the key points related to test frequency, load amplitude, load ratio, and specimen geometry is of maximum importance in the design process. These fundamental elements serve as the foundations upon which all design decisions and component selections are built. Test frequency determines the rate at which the system must operate, being also important. Load amplitude and load ratio specify the range of forces and load patterns that the machine must withstand, influencing the robustness and strength of the chosen components. Additionally, specimen geometry defines the dimensions and shapes of the test samples, impacting the overall configuration of the

machine and the accuracy of results. Therefore, these initial points are crucial in shaping the entire design of the multiaxial fatigue testing machine.

3.1.1 Testing Specimens

In order to start the design of the machine, it's imperative to determine the type of specimens that will be tested. Through research, it was observed that there are no standardized dimensions or geometries for specimens used in combined bending and torsion fatigue tests. However, for multiaxial testing, a standard does exist for combined axial and torsion fatigue tests. As other articles have used specimens with geometries similar to those proposed by this standard, it was decided to use the dimensions proposed by the standard.

The used standard is the ASTM E2207-02 [47], that provides information about standard practice for strain-controlled axial-torsional fatigue testing with thin-walled tubular specimens. A tubular shape is based on the consideration that the uniform distribution of normal and shear stresses caused by bending and torsion, respectively, occurs throughout the slender wall of the specimen. This is in contrast to the uneven stress distribution that arises in a solid bar, particularly in the plastic range [44]. With this information, the determination of the maximum and minimum dimensions of the specimen covered by the standard was carried out. The specimen's scheme and respective dimensions are in the following image 3.1 and table 3.1, respectively.

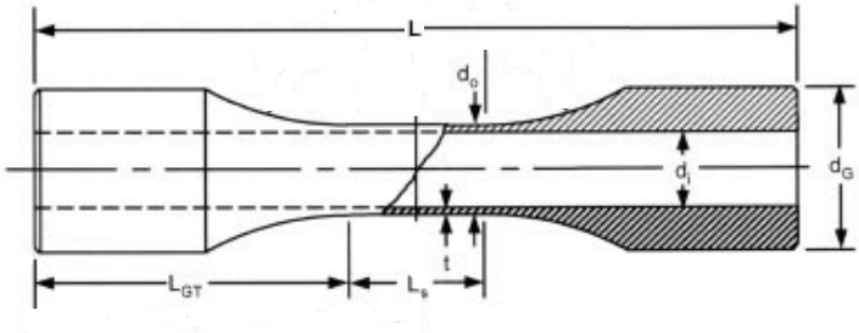


Figure 3.1: ASTM E2207-02 [45].

Table 3.1: Specimen dimensions.

Dimension	Minimum [mm]	Maximum [mm]
t	1.5	2.5
d_o	16.5	42.5
d_i	13.5	37.5
d_G	19.8	85
L	115.5	425
L_{GT}	28.05	97.75
L_s	59.4	229.5

3.1.2 Reference Materials

To gain an understanding of the parameters to be utilized in the machine design, two reference materials were selected. First, we have AA2024 which is an aluminum alloy with good strength properties and fatigue resistance [48]. The other material is Inconel 718, a high-performance nickel-based superalloy with excellent strength, ductility, and corrosion and oxidation resistance [49]. Both of these materials are particularly used in the aerospace industry, for critical applications that require strength and resistance to extreme environments. Hence, they are often submitted to multiaxial loading, making its multiaxial study interesting.

The materials' mechanical properties were obtained from the Granta EduPack software [50]. Values of the properties were selected based on the treatments that hardened them the most, thus utilizing the worst-case scenario to overestimate the dimensions. The properties are presented in the following table.

Table 3.2: AA2024 and Inconel 718 mechanical properties [50].

Property	AA2024	Inconel 718
E [GPa]	73	198
G [GPa]	28	79
σ_y [MPa]	349	1160

Since majority of fatigue tests are performed with a stress under the yield stress, only the yield strength, σ_y, is required to the design of the machine. The shear and Young modulus, G and E respectively, will enter the torsion and bending specific parameters further ahead.

3.1.3 Load Capacity

To understand the limitations of the designed system, it's essential to ascertain the conditions under which it will operate. Once the type of test specimens and the reference materials for the project are known, it becomes imperative to establish the parameters under which the testing will take place.

As previously mentioned, the tests will likely occur below the materials' yield strength. For reference, it will be assumed that the tests take place with a stress ranging from 10 to 100 percent of the material's yield strength. The next step involves determining the bending and torsional moments that need to be applied to the specimen for testing, depending on the stress desired for the test. During the calculations, equations for hollow cylindrical shafts will be used as an approximation to the gauge section of the specimens.

The maximum bending stress supported in the critical section of the specimen of a certain material is given by,

$$\sigma_{max} = \frac{M_{bending} \times R_{exterior}}{I} \tag{3.1}$$

and the maximum shear stress by,

$$\tau_{max} = \frac{M_{torsion} \times R_{exterior}}{J}. \tag{3.2}$$

To determine the moment of inertia, I, and the polar moment of inertia, J, of a specimen, the following equations were used:

$$I = \frac{\pi \times (D_{ext}^4 - D_{int}^4)}{64} \tag{3.3}$$

$$J = \frac{\pi \times (D_{ext}^4 - D_{int}^4)}{32}. \tag{3.4}$$

Finally, using these expressions, it's possible to determine the bending and torsional moments required to apply to each specimen to reach 10 or 100 percent of its yield strength. The maximum shear stresses used were obtained through the yield strength of each material, applying the Tresca criterion, given by the following expression:

$$\tau = \sigma \times 0.5. \tag{3.5}$$

The following tables present the values obtained for specimens of maximum and minimum dimensions for each reference material. For easy reference, minimum specimens will be called Specimen A, and maximum called Specimen B.

Table 3.3: Necessary moments for Specimen A.

	$M_{bending}$ [Nm]		$M_{torsion}$ [Nm]	
Material	10%	100%	10%	100%
AA2024	8.49	84.94	8.49	84.94
Inconel 718	28.23	282.33	28.23	282.33

Table 3.4: Necessary moments for Specimen B.

	$M_{bending}$ [Nm]		$M_{torsion}$ [Nm]	
Material	10%	100%	10%	100%
AA2024	103.60	1035.95	103.60	1035.95
Inconel 718	344.33	3443.28	344.33	3443.28

It's possible to see that the values of torsional and bending moments are equal. This is due to the cylindrical geometry of the specimens, which is symmetric and causes the moment of inertia I to be half of the polar moment of inertia J.

3.2 Conceptual Design

To start the machine design, some testing mechanisms were studied. An interesting mechanism was found in Elmar Wilczek's PhD thesis called "Statische Berechnung Eines Rohrkrummers mit Realen Randbedingungen" [51], which means Static Analysis of Curved Pipes with Realistic

Boundary Conditions. This experimental configuration is based on a 4-bar mechanism that allows the system to apply moments in any direction at the specimen's end.

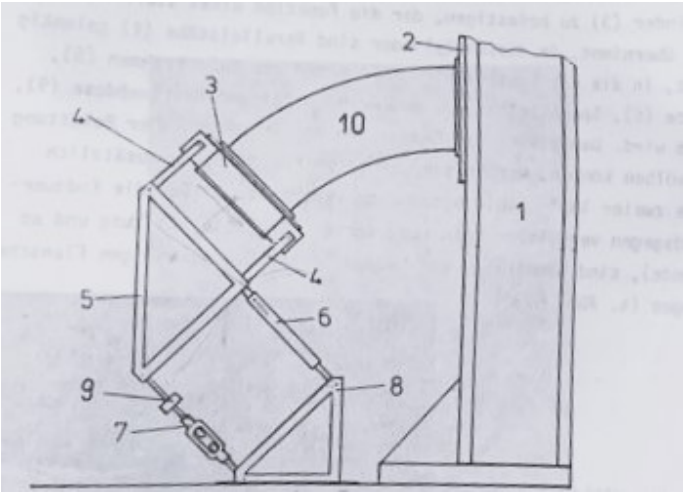


Figure 3.2: Curved pipes testing machine [51].

The specimen (10) is fixed to the base plate (2) through its right flange, which is connected to the rigid column (3). The division of the flange hole allows for a 15° rotation of the test. The load is initiated on the left flange. In the figure's example, a torque is applied to the tube. To accommodate this type of load, a short and rigid connection cylinder (3) is fixed to the left flange, serving as a rigid end flange. Parallel bars (4) are articulated on this cylinder, from which the load harness, consisting of articulated structure (5), floor support (6), locking fixture (7), floor structure (8), and force measuring box (9), is suspended. To prevent the end beams of the collector from buckling under load, they are also tensioned on their free side using two 180° steel ring segments. In addition to the distributed forces and moments introduced into the sample through the connection cylinder (3), concentrated forces or force couples can also be applied. Instead of the connection cylinder, the load harness can attack directly through cutting-edge jaws on the left end flange of the test.

Adapting this concept to the design of the machine in question, the 4-bar linkage system was used to allow the system to adapt to the specimen's axes when subjected to loads. This enables the application of both pure bending moments and torsional moments. To ensure that these two tests are independent, two 4-bar mechanisms will be used, one for each type of test. However, the concept of the machine is to perform both tests simultaneously, which will be possible.

3.3 Final Design

In the figure 3.3, is presented a 3D overview of the machine. It is composed by two systems, torsion and bending, each one composed by three subsystems. These three subsystems are

the main body, responsible for the transmission of movement, the eccentric subsystem, responsible for creating the movement necessary to test, and the equilibrium structure, responsible for compensating the chucks weight (not fully designed in this work).

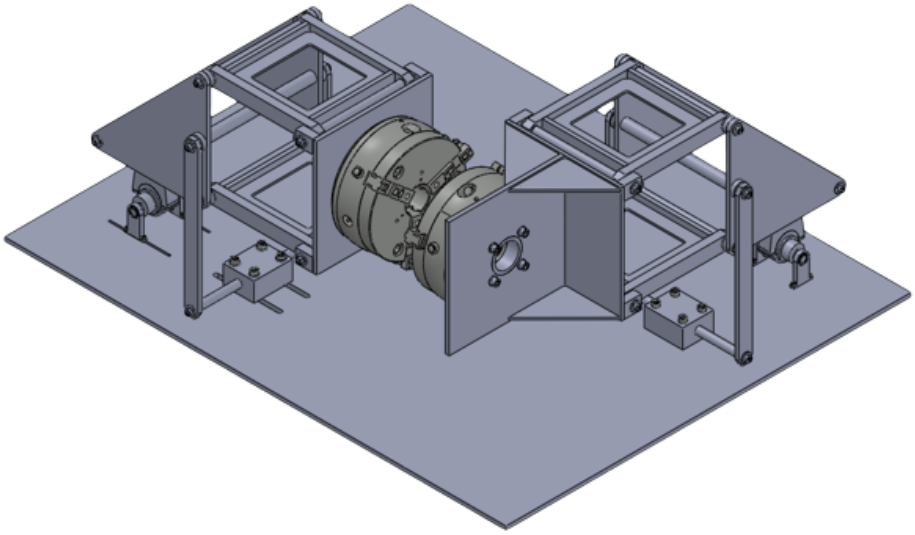


Figure 3.3: Final design.

The respective Bill of Materials and technical drawing with all the parts of the machine numbered can be found in appendix B and A, respectively.

3.4 Main Body

The main body refers to the part of the overall system that moves and adapts to the system's needs during a test. There are two of them, with the torsion one differing slightly from the bending one. This difference lies in the design of the mirrors, which adapt to the needs of their application. In addition to these parts, these systems also consist of the bushing, the balancing triangles, and the articulations. This system is the one that comes into contact with the other two systems discussed later on.

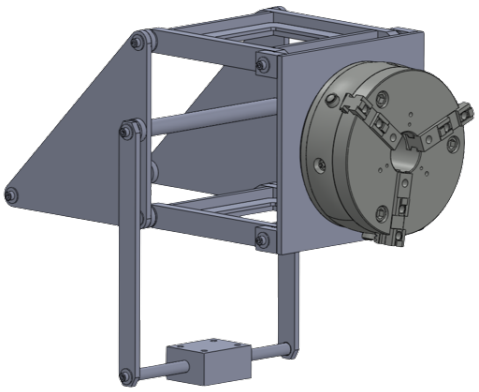


Figure 3.4: Bending main body.

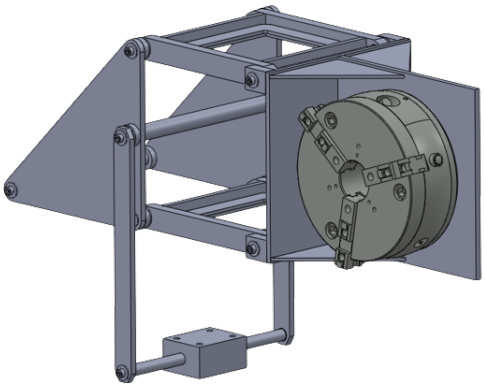


Figure 3.5: Torsion main body.

This mechanism, often referred to as a 4-bar linkage or simply a 4-bar, offers a dynamic way to adjust the testing setup to conform to the specimen's geometry. It consists of four rigid bars interconnected by hinged joints, allowing for both linear and rotational motions. When imposed a bending or torsion moment on the specimen, initially the two identical connecting rods form a rectangle with the mirrors. Then, it becomes distorted and appears as a parallelogram. This change of shape with constant arm lengths, plus the vertical articulations connected to the base, is what allows the adaptability of the system to apply the desired moments.

3.4.1 Chucks (1)

Chucks are an essential component of fatigue testing machines, as they are used to hold the specimen in place during testing. They also center the specimen and can be adjustable to fit test samples of different sizes.

For this component, the chosen solution was obtained from external suppliers, as there is a wide range of options available, and these components are somewhat complex to design. As seen in section 3.1.1, the utilized test samples possess a circular geometry. This aspect had to be taken into account when selecting the chuck. SCHUNK offered a number of compatible solutions and the ROTA-S plus 2.0 250-62 C5-SFG was chosen.

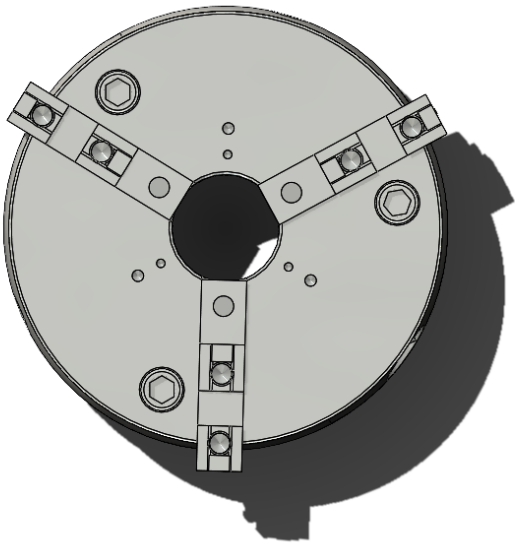


Figure 3.6: SCHUNK ROTA-S plus 2.0 250-62 C5-SFG.

This solution has an outside and inside diameter of 256 mm and 62 mm, respectively. In terms of loads, it supports a maximum torque of 210 Nm and a maximum clamping force of 160 kN. It is a manual chuck with three wedge-bar jaws and an angled serration jaw interface. The quick-change system suggests that the jaws can be easily and quickly changed, allowing them to be removed and replaced without disassembling the entire chuck. It also has a spindle holder that follows the standard ISO 702-1, with intermediate flange.

One limitation found is that the chuck only supports 210 Nm of torque, while the largest reference specimen of Inconel 718 needs 344.3 Nm for it to reach 10% of its yield strength. Since the chuck is already large, it was opted for the decrease of the range of test specimens in order to not compromise the size of the machine. A reasonable compromise was achievable with a 37 mm d_o specimen. These dimensions allow the tests to reach 10% of its yield strength at a 211.8 Nm torque, similar to the torque held by the chuck. With a d_G of 59.2 mm, it's admissible for our system. All the dimensions and required moments are given in the following tables, with this specimen being designated as the new specimen B.

Table 3.5: New Specimen B dimensions.

Dimension	Maximum [mm]
t	2
d_o	37
d_i	33
d_G	59.2
L	314.5
L_{GT}	74
L_s	166.5

Table 3.6: Necessary moments for the new Specimen B.

	$M_{bending}$ [Nm]		$M_{torsion}$ [Nm]	
Material	10%	100%	10%	100%
AA2024	63.73	637.33	63.73	637.33
Inconel 718	211.83	2118.34	211.83	2118.34

3.4.1.1 Jaws

As seen above, the chuck has a clamping mechanism with three jaws. Each of them has a stroke of 7.5 mm, which means a 15 mm range in diameter. Knowing that the trough-hole diameter of the chuck is 62 mm, with the maximum jaw stroke, it can clamp specimens with a d_G of:

$$D_{clamp} = D_{hole} - 2 \cdot x \tag{3.6}$$

$$D_{clamp} = 62 - 2 \cdot 7.5 \tag{3.7}$$

$$D_{clamp} = 47 \text{ mm} \tag{3.8}$$

being D_{clamp} the diameter the clamp can reach and x the jaw stroke.

As seen in the section above, the d_G of the smallest reference specimen is 19.8 mm. Since the jaws only reach 47 mm diameter, a solution to reach our range of specimens is needed. A search for a compatible commercialized solution was done, but none of the results reached the desired diameter. A solution was designed from scratch to solve this problem and make it possible to have a more extensive range of testing specimens.

3.4.1.2 Jaw Adaptors (13 and 14)

Unlike the original jaws, that had a squared tip to tighten the specimen, it was opted for a wedge grip that provides better grip on the designed solution. It was taken advantage of the already existing hole on the jaw and irregular profile shape it offers, with the intention of sliding the adaptor in with a coincident shape, providing a better support and reducing the risk of it giving imprecise results during the test by moving.

Since both the threaded hole and the sliding profile feature were located at the middle of the jaw, the tip of the adaptor was too loose and could easily bend when tightened. A solution to this problem was to create a new fixing point through a screw located close to the end of the jaw. Due to the fact that the jaw didn't have a hole for that purpose, a new M12 threaded hole was made 15 mm from the end. Both holes in the adaptor have a counterbore to rest the bolt's head that reinforce even more the connection longitudinally.

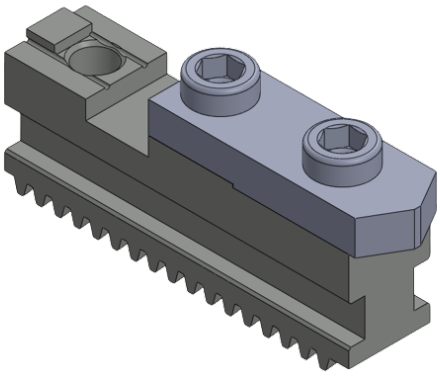


Figure 3.7: Jaw adaptor assembly.

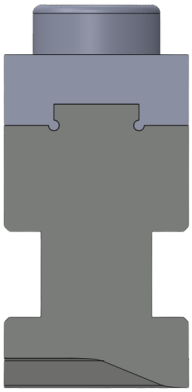


Figure 3.8: Jaw adaptor assembly: section view.

Knowing that with the maximum stroke per jaw is 7.5 mm, diameter variation of 15 mm, it was easily determined how many adaptors are needed to reach the whole range of specimens. The range of each adaptor was overlapped by 0.5 mm for safety:

- From 18 to 33 mm;
- From 32.5 to 47.5 mm;
- From 47 to 62 mm;

It is known that two adaptors are needed. The next step was to determine the length of each one, following the next equation:

$$l_i = l_0 + \frac{62 - d_i^{max}}{2}, i = 1,2 \tag{3.9}$$

where,

- l_i is the length of the adaptor i;
- l_0 is the length of the initial jaw, l_0 = 110 mm;
- d_i^{max} is the maximum diameter the adaptor i can reach.

With this, is concluded that the biggest adaptor, that reaches the smallest specimens, has a length of l_2 = 117.25 mm, and the other of l_1 = 124.5 mm.

3.4.2 Mirrors

The system's movement needs to be transmitted to the specimens in order to test. Therefore, it's necessary the use of a component that connects with both the specimen and the rest of the system structure. As seen in section (conceptual design), the system is composed of two independent subsystems that function in different axis. This translates into the need for two different mirrors,

one for torsion and another for bending. Despite the slightly different designs, the two mirrors have the same purpose.

Since these are components specific for this application, they are self-designed. The main body consists of a 300x300x10 mm plate, large enough to secure the 256 mm diameter chucks. They have a central hole with a 62 mm diameter and four smaller holes around the central one, all with a 10 mm diameter. These five holes are concentric to the chuck ones, allowing the connection between the two components. In addition to this, the mirrors have four 20 mm thick eyelets welded, where the connection with the rest of the system's structure is made. These eyelets have a 18 mm diameter hole each and are welded to the main plate.

3.4.2.1 Bending Mirror (2)

The bending subsystem works in the same axis that the test is made. Therefore, the bending mirror connects directly with the chuck and the system's structure.

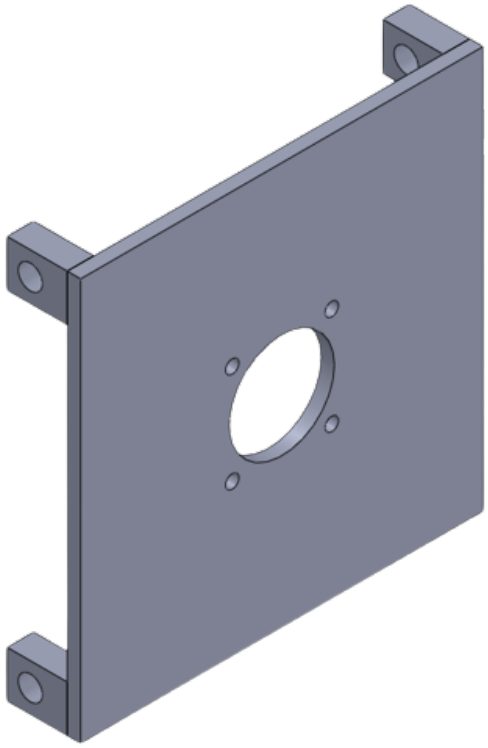


Figure 3.9: Bending mirror.

3.4.2.2 Torsion Mirror (3)

In the torsion case, the subsystem works in a perpendicular axis to the one where the testing occurs. The plate that connects with the chuck is welded to a perpendicular plate, this being the one with the eyelets that connect with the rest of the system's structure. This allows for the rest of the components to be the exact same as the ones in the bending subsystem. To reinforce the two

plates connection, there are four triangle plates welded between the two main plates. They have a 5 mm width.

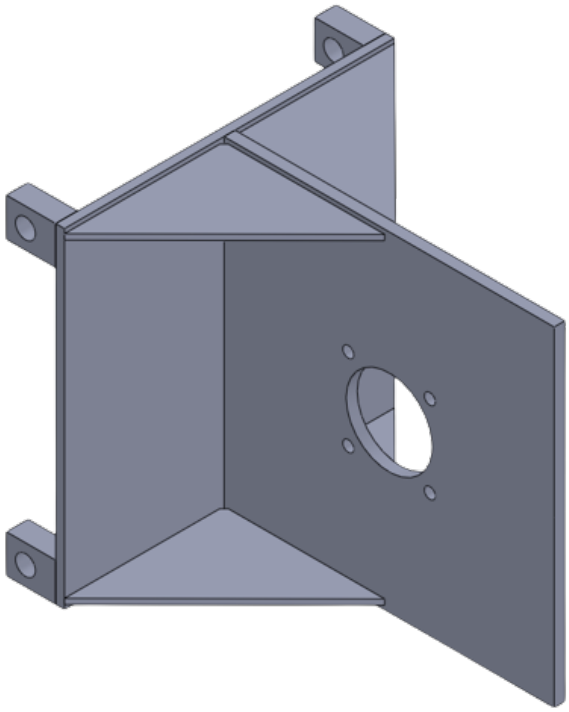


Figure 3.10: Torsion mirror.

3.4.2.3 Chuck-Mirror Adaptor (11)

To improve the connection between the chucks and their respective mirrors, an adapter was designed to be placed between the two. This piece has a central disc with a 135 mm outside diameter and 5 mm thickness. It also has four holes concentric to the ones in the chucks and mirrors. This allows the connection of the three components through four M10x35 screws. On both sides of the central disc there are two outermost faces, one corresponding to the chuck and the other to the mirror. They follow the patter of the element they are going to enter. For example, the chuck side has a conic shape with coincident dimensions to the chuck's through-hole. This piece also conserves the 62 mm inside diameter provided by the chuck that allows specimens to slide in if necessary.

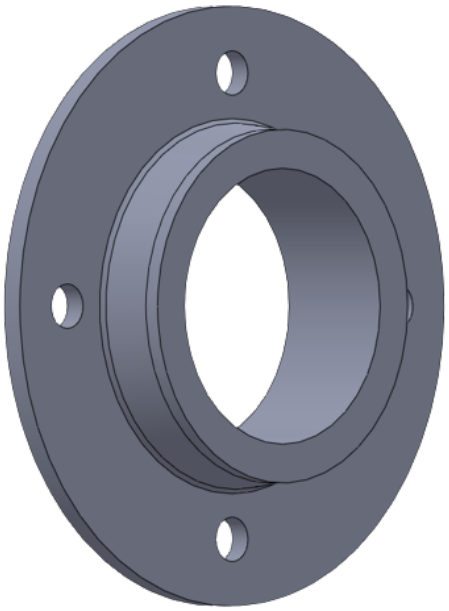


Figure 3.11: Chuck-mirror adaptor.

Due to the thickness, it creates a small separation between the chuck and the mirror, making space for the connecting screws of the chuck.

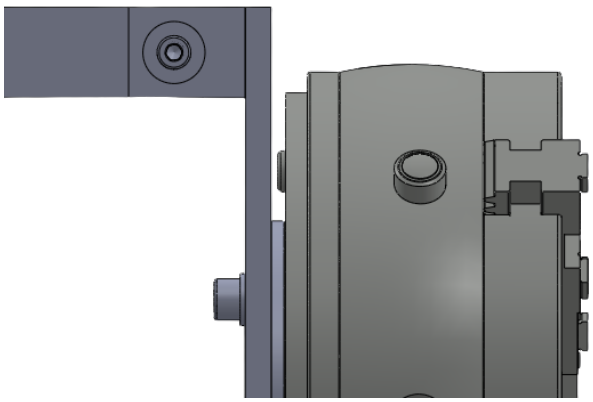


Figure 3.12: Separation created between the mirror and the chuck.

3.4.2.4 Validation calculations

To determine if the mirrors can support the weight of the chucks without deformation or the bolts that hold them, it is necessary to study the stiffness of the connections in comparison to the supported weight.

To perform this study, it will be necessary to consider an imaginary displacement characterized by the angle θ. By considering the total distances from the contact point between the adaptor and

the chuck and the number of bolts, it is possible to determine the forces exerted on the bolts when the counterweights act.

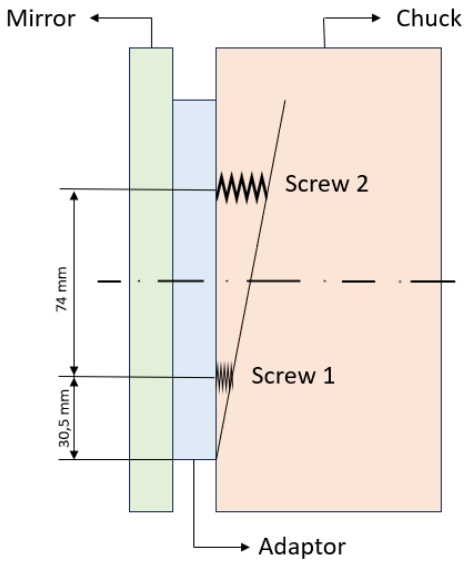


Figure 3.13: Imaginary displacement scheme for mirror.

Considering two bolts per row and the displacements as a function of the angle theta, we can obtain an equality of moments.

$$2 \cdot (K_p \cdot \theta \cdot 30.5) \cdot 30.5 + 2 \cdot (K_p \cdot \theta \cdot 104.5) \cdot 104.5 = M \tag{3.10}$$

$$2 \cdot K_p \cdot \theta \cdot (30.5^2 + 104.5^2) = M \tag{3.11}$$

where K_p is the bolts stiffness and M the maximum torque admissible, 210 Nm.

The stiffness supported by the bolts is then:

$$2 \cdot K_P \cdot \theta = \frac{210}{0.0305^2 + 0.1045^2} = 17.72 \text{ N/mm} \tag{3.12}$$

To determine the force on each bolt, it is necessary to multiply the stiffness obtained by the distance to the contact point. Therefore, we obtain a supported force of 540.48 N and 1851.82 N for each pair of bolts.

Next, it is necessary to determine the force that each hole of the mirror can support. Knowing that the chuck involves the use of M10 bolts, we can find the effective area to determine this force through the yield strength.

$$Area = 2 \cdot \pi \cdot r \cdot t = 2 \cdot \pi \cdot 5 \cdot 10 = 314.16 \text{ mm}^2 \tag{3.13}$$

$$\sigma_{hole} = \frac{1851.82}{314.16} = 5.89 \text{ MPa} \tag{3.14}$$

It's verified that the holes support the force implied by the chucks weight cause the pressure is much smaller that the yield strength of the material.

3.4.3 Horizontal Articulation (4)

In order to transmit the movement of the main system to the mirrors, and subsequently to the specimen, there has to be an articulation part. Both mirrors are connected to two of this parts, one up and another down. A huge feature of this machine is that it self-adapts to the specimen's movement through components of this type. Having these connection components, in both torsion and bending subsystems, allows the system to adapt itself vertically so that the specimen never forces itself wrongly causing interference in tests.

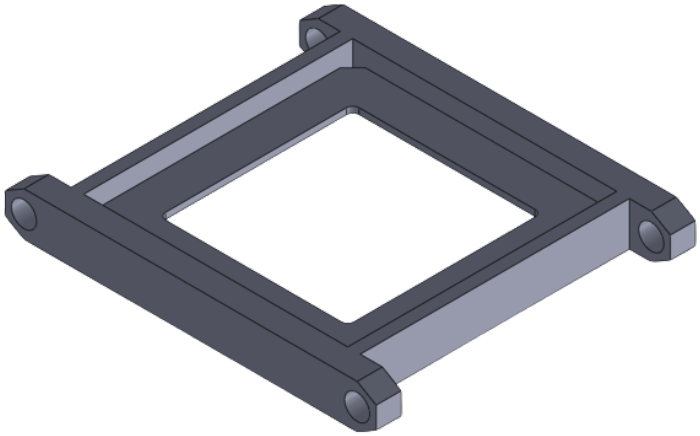


Figure 3.14: Horizontal articulation.

This piece is composed by 3 different types of parts. First, there are two main bars with a 20 mm width that execute the main work, connecting with the respective mirror and balance triangles, showed in section 3.4.4. These connections are made through shafts, therefore each bar has one hole in each tip with a 20 mm diameter. The squared design on the edges was adopted because its manufacturing process is cheaper than round edges. Next, are the structural components that ensure the stability of the whole piece: two 10 mm thick bars, close to the ends of the main bars, and a 5 mm central plate. These ensure that the main bars don't curve while submitted to forces during tests. The central plate is cut to release some unnecessary weight from the machine. All of these are welded.

3.4.4 Balance Triangles (5 and 6)

The balance triangles are the central piece of the mechanism. They connect all the articulation points of its respective system, torsion or bending. These articulations are the horizontal articulations, section 3.4.3, and the vertical articulations and eccentric system, talked about in sections 3.4.5 and 3.5, respectively.

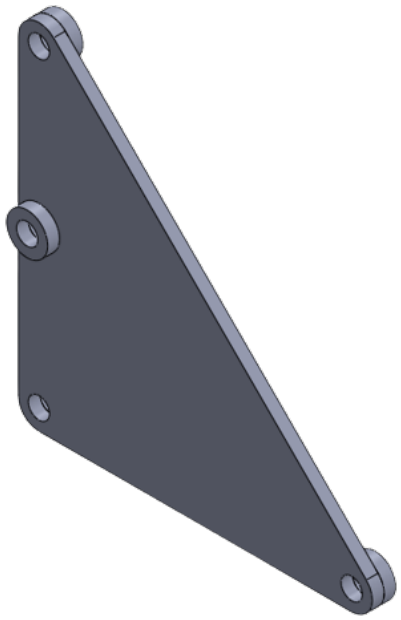


Figure 3.15: Balance triangle.

For this system, it was opted to design a right-angled triangle with a through hole in each vertex, with a 18 mm diameter each. The holes are distanced by 265 mm in width and height, and will connect to the other components through shafts. In these three holes is a cylindrical attachment of 10 mm to space out other pieces from the triangle surface. Additionally, at middle height is another hole, with equal diameter and the same kind of attachment, that will be the fourth connection. The first three are facing the interior surface and the last one the exterior. These attachments are welded to the main triangle piece which has a 10 mm thickness. Each system is composed of two triangles, right and left, that only differ on the side of its parts.

3.4.5 Vertical Articulation (7)

One of the two points of connection between the machine's systems and the base are the vertical joints. As well as making this connection, these components are an important part of adjusting the system to the conditions it is in. In other words, they allow the system to adjust horizontally when the test specimen is subjected to test forces. In this way, the specimen never has its natural adjustment movement constrained, and can adapt better with this freedom of movement.

This piece then consists of a type of bar, 10 mm thick, which is connected to two shafts. For this connection, there are two 18 mm diameter through holes, one at each end. In order to save on manufacturing costs but not jeopardise the design, it was decided to cut 3 sections at the ends of the piece, rather than round ones, which would have been more expensive.

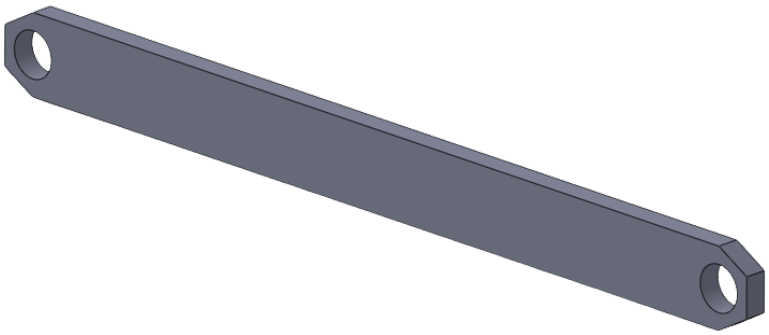


Figure 3.16: Vertical articulation.

In the application of this component, it may be subjected to axial forces that can induce bending, making it important to conduct a confirmatory study on buckling. Buckling is the sudden change in shape of a structural component under load. Through this study, the maximum allowable axial force in this component can be determined. It is known that the total length l of the component under study is 369.5 mm, with a rectangular cross-section having a width b of 35 mm and a height h of 10 mm. Calculating the moment of inertia and cross-sectional area:

$$I = \frac{b \cdot h^3}{12} = \frac{0.035 \cdot 0.010^3}{12} = 2.92 \cdot 10^{-9} \text{ m}^4 \tag{3.15}$$

$$A = b \cdot h = 0.035 \cdot 0.010 = 3.5 \cdot 10^{-4} \text{ m}^2 \tag{3.16}$$

With these two parameters, the radius of gyration i can be determined, which is the ratio of the moment of inertia to the cross-sectional area.

$$i = \sqrt{\frac{I}{A}} = \sqrt{\frac{2.92 \cdot 10^{-9}}{3.5 \cdot 10^{-4}}} = 0.0029 \text{ m} \tag{3.17}$$

The next step is to chose the column effective length factor, μ, whose value depends on the conditions of end support of the column. In this case, is considered that both ends are pinned, which means that μ = 1.0.

In accordance with Eurocode 3 [52], to verify the resistance to buckling of the component, it's necessary to calculate the buckling resistance reduction factor, denoted as, χ, as a function of the reduced slenderness ratio, $\overline{\lambda}$. This parameter depends on the slenderness of the bar, λ, and the Euler slenderness, λ_1 which are determined by the following formulas:

$$\lambda = \frac{\mu \cdot l}{i} = 128.00 \tag{3.18}$$

$$\lambda_1 = \pi \cdot \sqrt{\frac{E}{\sigma_y}} = 83.12 \tag{3.19}$$

$$\overline{\lambda} = \frac{\lambda}{\lambda_1} = 1.54 \tag{3.20}$$

where E and σ_y of Ck45 are 217 GPa and 310 MPa, respectively.

Real imperfections in the components are incorporated into the design process through the imperfection factor α which is defined based on the European buckling design curves. Each resistance curve used depends on parameters such as the cross-sectional geometry, axis of bending, and manufacturing process. For this case, The imperfection factor is "c" with value 0.49. χ is given by:

$$\chi = \frac{1}{\phi + \sqrt{\phi^2 - \overline{\lambda}^2}} \tag{3.21}$$

where,

$$\phi = 0.5 \cdot (\overline{\lambda}^2 + \alpha \cdot (\overline{\lambda} - 0.2) + 1). \tag{3.22}$$

Calculating, it's obtained ϕ = 2.01 and χ = 0.30. Multiplying the value of χ by the yield strength of the material, obtains the reduced strength, which allows to calculate the maximum axial force supported by the component. Therefore,

$$\sigma_{safe} = \chi \cdot \sigma_y = 93.60 \text{ MPa} \tag{3.23}$$

$$F_{adm} = \sigma_{safe} \cdot A = 32.76 \text{ kN} \tag{3.24}$$

Knowing that the component can withstand a force F = 3996.23 N, which is lower than the obtained value, we confirm that it is suitable for this application.

3.4.5.1 Fixation (8)

As mentioned earlier, two vertical articulations that work together are connected by a shaft. However, this shaft needs to be securely fixed to the base, which is why a support was designed. This support consists of a parallelepiped block with considerable width to prevent shaft bending and immobilize it in terms of translation. On the other hand, this support must allow the shaft to pass through and rotate, which occurs during the adjustment of the articulations to the specimen's requirements. The designed support can be seen in the following image.

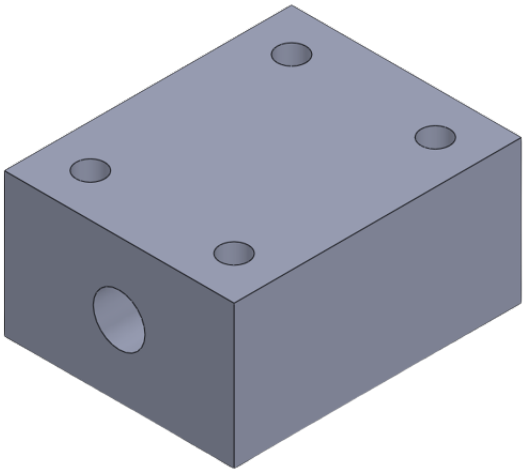


Figure 3.17: Vertical articulation's support.

This support, with dimensions of 80 mm in width, 50 mm in height, and 100 mm in length, is also composed of four holes. These holes are appropriately spaced near each corner of the upper face, in order to avoid intersecting with the longitudinal hole for the passing shaft. These four M10 holes will allow the passage of four M10 screws to secure this support to the base.

3.5 Eccentric System

The idea of this mechanism provided from the book Mechanical Presses [53], where is explained that small and medium sized presses commonly require stroke adjustments for their front crank or eccentric shafts. To achieve this, a specialized eccentric bush, b, is installed around the crank or eccentric journal of the shaft. This component plays a crucial role in modifying the distance between two key centers: the center, O_b, of the eccentric sleeve, which serves as the bearing for the ram connecting rod, and the center, O_w, of the shaft itself. Notably, the center, O_b, traces a circular path around the center, O_z of the journal.

The stroke adjustment entails the capability to set specific and predetermined throw radii. This is made possible through the utilization of radial serrations on the eccentric bush. These serrations, when paired with an adjustable drive ring featuring complementary teeth, effectively prevent the eccentric bush from rotating concerning the journal. Consequently, adjusting the position of the eccentric bush leads to a shift in the top dead center along the circumference of the crank circle.

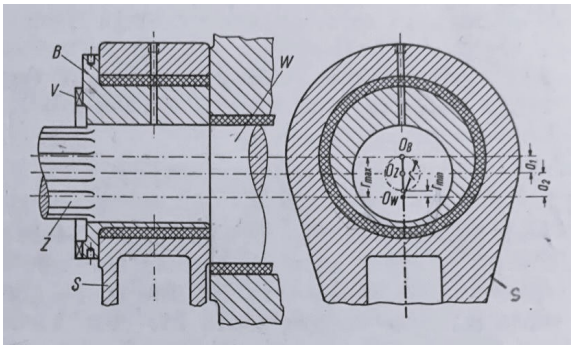


Figure 3.18: Press eccentric mechanism [53].

Adapting this concept made it possible to create a solution that allowed for changing the course of the test while simultaneously generating a cyclic motion. Its components include the main shaft, a fixed eccentric, a free eccentric, a locking cap, and the parts that will connect the eccentrics to the main body. Its operation will consist of transferring power from the main shaft to the fixed eccentric, which will then pass it on to the free eccentric. To enable this transmission between the two eccentrics, something to hold them together is needed, and that's where the locking cap comes in. This cap will lock the desired position for the intended stroke, causing the entire eccentric system to move in harmony to transfer the motion to the main body. Below is an overall 3D view of this system.

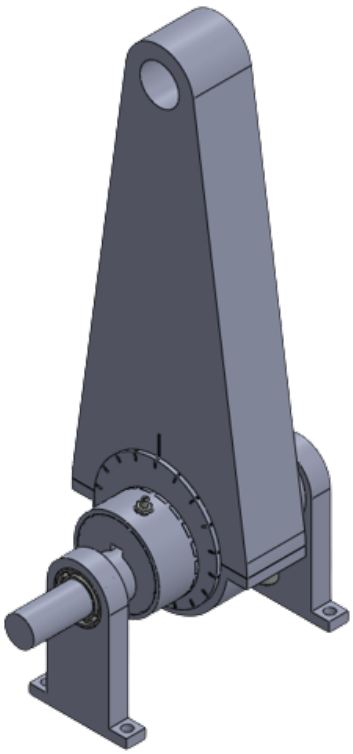


Figure 3.19: Eccentric system.

To dimension this system, the crucial aspect is to determine the necessary eccentricities to reach the requirements. This cannot be determined without first knowing the maximum amplitude of the parameters that characterize the deformation of the specimen, torsion angle, and deflection. After knowing their maximum values, it's possible to dimension the entire eccentric system in a way that allows achieving the necessary displacements to perform tests.

The first step was to calculate the equivalent torsion angles, θ_t, and deflections, δ, using the maximum reference moments determined in section 3.1.3 and 3.4.1. For the bending scenario, the bending angle, θ_b was also determined since the mechanism acts by applying an angular displacement in the plane that induces bending in the specimen. To achieve this, the following expressions were utilized:

$$\theta_t = \frac{M_t \cdot l}{G \cdot J} \tag{3.25}$$

$$\delta = \frac{M_b \cdot l^2}{2 \cdot E \cdot I} \tag{3.26}$$

$$\theta_b = \frac{M_b \cdot l}{E \cdot I} \tag{3.27}$$

where l is the length of the gauge section of a specimen, L_s.

Using the values of tables 3.7 and 3.8, the values for both sizes of specimens are determined.

Table 3.7: θ_t, δ_b and θ_b for Specimen A.

Parameter	AA2024	Inconel 718
θ_t [°]	2.571	2.253
δ_b [mm]	1.022	0.932
θ_b [°]	1.972	1.798

Table 3.8: θ_t, δ_b and θ_b for Specimen B.

Parameter	AA2024	Inconel 718
θ_t [°]	1.059	0.375
δ_b [mm]	1.180	0.435
θ_b [°]	0.812	0.299

The next step was to determine the displacements that the system needed to impose on the specimen using the torsion and deflection angles obtained. For this purpose, the aid diagrams present in images x and y were used. By observing the images, it is possible to see the trigonometric relationships within the system when an angle θ is imposed, both in torsion and bending subsystems.

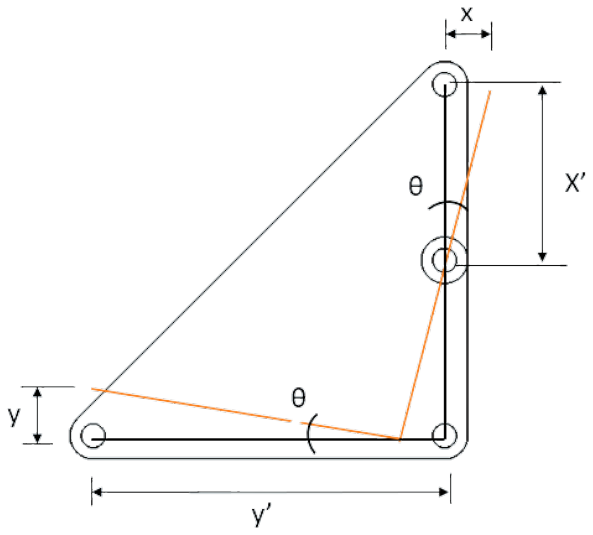


Figure 3.20: Subsystem when θ is imposed.

It is now easy to notice that to impose an angle θ on the specimen, the eccentric system needs to apply a displacement y to the balancing triangles. Knowing that x' = 132.5 mm and y' = 265 mm, the trigonometric relationship is as follows:

$$\tan(\theta) = x/x' = y/y' \tag{3.28}$$

and applying the values of θ_t and θ_b, the course y values required to test torsion and flexion are obtained.

Table 3.9: Course y required values.

	Specimen A		Specimen B	
Course	AA2024	Inconel 718	AA2024	Inconel 718
y_t [mm]	11.898	10.425	4.899	1.736
y_b [mm]	9.125	8.317	3.757	1.385

The maximum value of y required for torsion and flexion is 11.899 mm and 9.125 mm, respectively. Based on these values, it is concluded that the eccentric must be capable of a displacement of at least 12 mm, rounding up. In order to conduct tests on materials that are more fragile than the reference ones and to test different machine limits, the decision was made to dimension this system for a maximum course of 20 mm.

The displacement is dependent on the fixed and free eccentricities, and it is calculated as follows:

$$y = 2 \cdot (e_{fixed} + e_{free}) \tag{3.29}$$

As will be seen later, when the eccentrics are placed in the minimum configuration and the

values of the eccentricities are the same, they cancel each other out. For this reason, equal eccentricities were chosen, allowing the displacement to vary between 0 and 20 mm. It's then known that $e_{fixed} = e_{free} = 5$ mm, so $e_{total} = 10$ mm.

3.5.1 Fixed eccentric (18)

The first eccentric is referred to as the fixed eccentric because it always moves in accordance with the central shaft, and its relative eccentricity is fixed. As mentioned earlier, the eccentricity of this component is 5 mm, meaning that the center of its outer perimeter is displaced from the center of its rotational path by 5 mm. As a result, the center of its perimeter follows a circular trajectory with a radius of 5 mm around the center of its rotational path, which coincides with the center of the main shaft.

In order for the main shaft and the fixed eccentric to move together, there must be a connecting element that can transmit power. This element is a key placed between the two parts. It will be dimensioned in section 3.5.1.1, being presented there its dimensions as well as those of the keysit and keyway. For the keyway, however, a slot will be made along the entire length of the fixed eccentric, in order to simplify its machining.

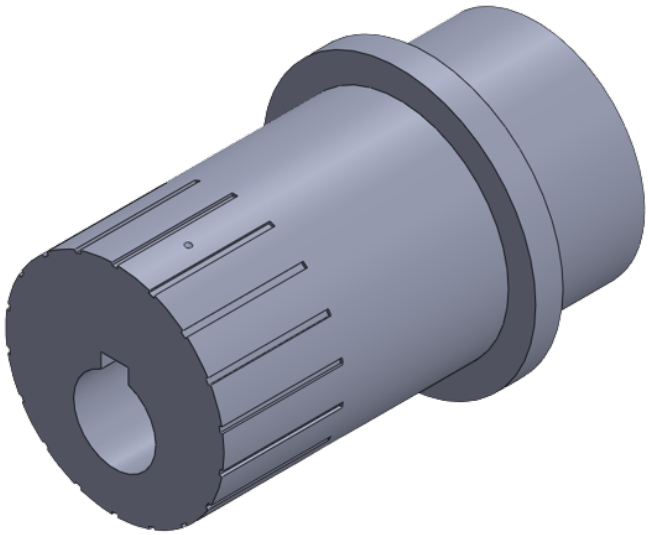


Figure 3.21: Fixed eccentric.

As it can be seen in the image above, there is a subtle change in diameter at just over half the length. This protrusion will act as an impediment to translations of the free eccentric that will surround the fixed eccentric. This piece also has some grooves that, in addition to allowing the connection with the locking cap, enable its guidance, only allowing it to move in the direction of these grooves.

3.5.1.1 Key sizing (22)

To simplify the machining of the parts, it was decided to have a transmitting shaft attached to the fixed eccentric, a keyed joint. The transmission of torque is achieved through the use of a key. To dimension this key, the DIN 6885 standard was consulted, which provides various standardized dimensions for these types of components, depending on the diameter of the shaft on which they are placed.

The keyed shaft has a 20 mm diameter, as the hole on the fixed eccentric. Following DIN 6885, the dimensions for the key for this shaft's diameter are the following:

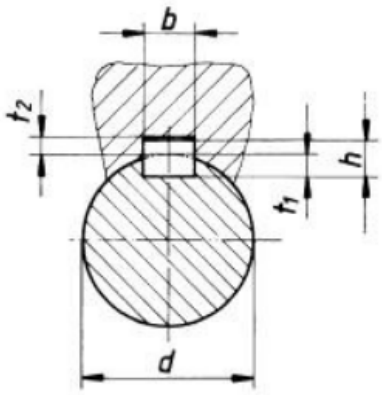


Figure 3.22: Key scheme.

Table 3.10: Key dimensions.

d [mm]	b [mm]	h [mm]	t_1 [mm]	t_2 [mm]
17 ... 22	6	6	3.5	2.8

To determine the length of this component, it's necessary to calculate the minimum lengths required to avoid damage. The equations 3.30 and 3.31 were followed to study crushing and shearing, respectively.

$$\sigma_{adm} = \frac{F \cdot n}{l_1 \cdot (h - t_1)} \tag{3.30}$$

$$\tau_{adm} = \frac{F \cdot n}{l_2 \cdot b} \tag{3.31}$$

The force F represents the stresses acting on the key, at the lower part through the shaft and at the upper part through the fixed eccentric. Considering the maximum torque, calculated in equation 3.72, we thus determine the maximum force F the key is submitted to:

$$F = \frac{2 \cdot T}{d} = \frac{2 \cdot 7.925}{0.020} = 792.453 \text{ N} \tag{3.32}$$

It's proceeded the calculation of the minimum lengths. Considering that the key is made of Ck45, with σ_{adm} = 310 MPa and τ_{adm} = 155 MPa, and a safety factor of n = 2, the results obtained

are l_1 = 2.045 mm and l_2 = 1.704 mm. Since the fixed eccentric has a length of 77 mm, it was chosen a key length of 25 mm, with the intention of placing this piece in the middle of it.

3.5.2 Free eccentric (17)

Next, we encounter the second eccentric, known as the free eccentric. The name of this component originates from its functionality, which revolves around its adjustment according to the desired total eccentricity. This means that by rotating around the fixed eccentric, the movable eccentricity undergoes vertical modification, subsequently altering the total eccentricity. As mentioned earlier, the free eccentricity, e_{free}, is also 5 mm. Below is a 3D view image of the mentioned component.

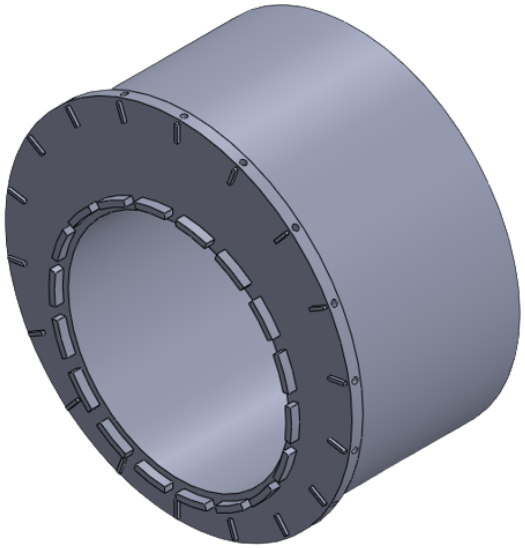


Figure 3.23: Free eccentric.

This component consists of a cylindrical shape with a slight eccentricity, featuring a slightly protruding edge that is larger in diameter than most of the piece's outer surface. The main functionality of this feature is to ensure the correct positioning of the linking components, requiring them to snugly fit against the inner face of this protrusion. The central hole of this component has a diameter that matches the outer diameter of the fixed eccentric.

On the visible top face in the image, a circular pattern of teeth is evident. This pattern of teeth will serve as the connection point with the locking cap that secures the three pieces together during the execution of a test. It consists of 18 teeth, with each tooth corresponding to a calculated total eccentricity. To simplify the machine's use, a conversion table was created between the tooth number positioned at the top and its equivalent eccentricity, knowing that tooth number zero is the one corresponding to maximum e_{total}. The necessary calculations and diagrams are now presented.

Just like the concept of the fixed eccentric, the trajectory that the center of the outer diameter of the free eccentric follows is a circular path around the center of rotation, corresponding to the

outer diameter of the fixed eccentric. With this understanding, it's possible to draw a diagram that illustrates this trajectory when the free eccentric rotates around the fixed one.

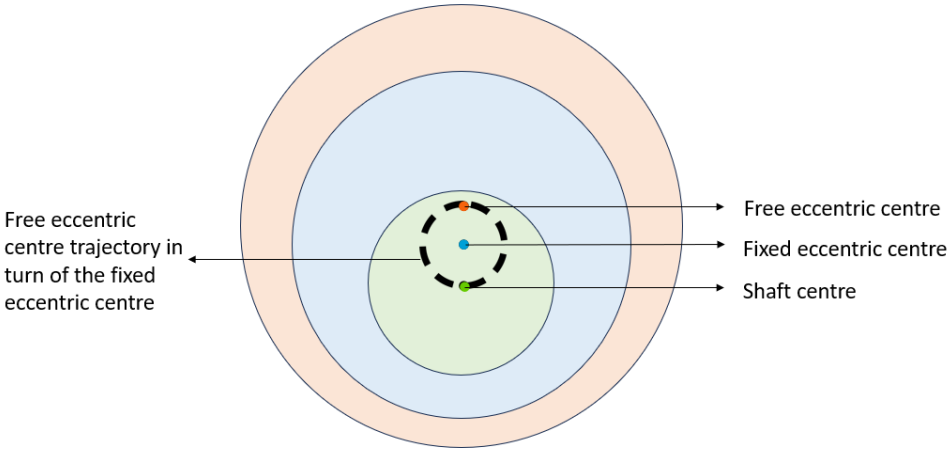


Figure 3.24: Eccentric centre trajectory.

Since the two eccentricities are of equal value, the diagram shows that the lower point of the circular trajectory corresponds to the center of rotation of the system's main shaft. With this understanding, we can calculate e_{total} taking into consideration the vertical variation in distance of e_{free} in relation to e_{fixed}, using trigonometric relationships.

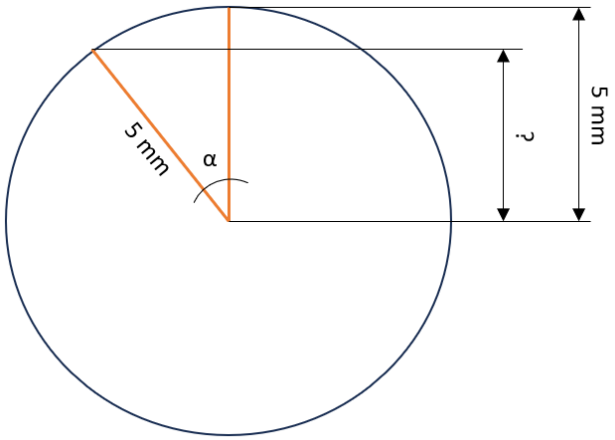


Figure 3.25: Eccentricity scheme.

$$e_{total} = e_{fixed} + e_{free} \cdot cos(\alpha) \tag{3.33}$$

where α corresponds to the angle of the desired tooth relative to the first tooth, in the counter-clockwise direction.

The conversion table is based on the use of equation 3.33 for each tooth, utilizing the corresponding angle α.

Table 3.11: Conversion table for eccentric mechanism.

Tooth no.	α [°]	e_{total} [mm]	y [mm]
0	0	10	20
1	20	9,698	19,397
2	40	8,830	17,660
3	60	7,5	15
4	80	5,868	11,736
5	100	4,132	8,264
6	120	2,5	5
7	140	1,170	2,340
8	160	0,302	0,603
9	180	0	0
10	200	0,302	0,603
...	...	...	...
17	340	9,698	19,397

In the table, the values for teeth 11 to 16 have been omitted because they are the same as the first half, 2 to 7, but in the opposite direction. This is easily understood because $\cos(\alpha) = \cos(\pi + \alpha)$. The ten values for the total course that the machine is capable of achieving for fatigue tests are presented on the table.

To enable this change of course between tests, the part has reference markings accompanied by small holes. With the use of a suitable tool, these markings and holes facilitate the easy rotation of the eccentric to the desired position.

3.5.3 Locking cap (19)

As mentioned earlier, the locking cap is the part that locks the eccentric system in place for testing. It's a cylindrical shell that encases the fixed eccentric, connecting to it through the teeth on its inner surface and securing the movable eccentric through teeth on its end. In the following 3D view, an overview of this piece can be seen:

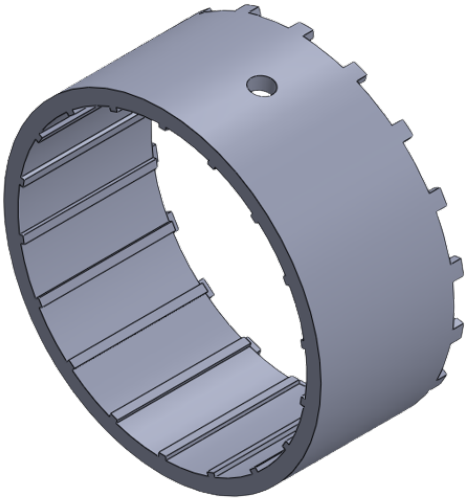


Figure 3.26: Locking cap.

However, the teeth connecting to the free eccentric are subjected to a considerable load, so it is necessary to conduct a study to see if they can withstand the transmission of torque without breaking the teeth. The first step is to calculate the force exerted on each tooth in the worst-case scenario during a test. To do this, it is necessary to consider the maximum torque M_t of 7.92 Nm exerted by the eccentric system and the average radius of the teeth r_m, which has a value of 21.5 mm.

$$F_t = \frac{7.92}{0.0215} = 368.37 \text{ N} \tag{3.34}$$

Knowing that there are eighteen teeth, the tangential force per tooth F_{tooth} is 20.47 N. Next, it is necessary to verify if the contact stress on the tooth and the shear stress experienced at the tooth root are lower than the material's yield stress. To make this calculation, it's necessary to know the dimensions of each tooth. It's known that they have a width b = 1 mm, length l = 2 mm, and height h = 1.5 mm.

$$\sigma_{cont} = \frac{F_{tooth}}{b \cdot h} = \frac{20.47}{0.001 \cdot 0.0015} = 13.64 \text{ MPa} \tag{3.35}$$

$$\tau_{root} = \frac{F_{tooth}}{b \cdot l} = \frac{20.47}{0.001 \cdot 0.002} = 10.24 \text{ MPa} \tag{3.36}$$

Both these stresses experienced by the teeth are considerably lower than the material's yield stress, confirming the safety of using this feature.

3.5.3.1 Locking mechanism (32 and 33)

The hole that can be observe on the surface of the cap is where the locking mechanism will be located. This threaded hole, M3, will house a spring plunger that enables the locking of the

cap's longitudinal movement, which in turn locks the movable eccentric in the desired position. The spring plunger provided by Fabory, model reference 58517.030.001, has a hexagon socket, a sphere, standard spring force and is made of stainless steel, found in appendix G. In the following image it's possible to see it's setup in the machine.

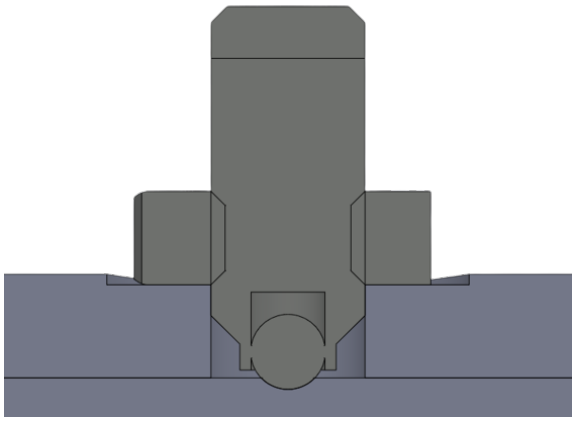


Figure 3.27: Spring plunger setup.

The fixed eccentric has a small concavity to allow the ball of the spring plunger to secure itself in place when the intention is to lock the movement of the components. After being screwed into the threaded hole of the locking cap, a countersunk M3 nut is placed on its exposed surface, due to the cap's small thickness. With this face being slightly chamfered, it allows the nut to seat better and thus improves the tightening. This nut will enable precise and secure tightening of the plunger. When the mechanism is stationary and the position of the free eccentric is to be changed in order to adjust the test course, this plunger, thanks to its spring and ball, allows the cap to slide backwards. Moving it slightly behind the locking cap, it's possible to rotate the free eccentric to the desired position and then slide the locking cap forward again until the spring plunger locks the movement by engaging with the concavity of the fixed eccentric.

3.5.4 Movement transmission (15 and 16)

In order to establish a connection between the eccentrics and the rest of the system, a linking component is necessary to facilitate the transmission of motion. Two pieces were designed that enclose the movable eccentric and simultaneously connect to the shaft that joins the balancing triangles. These two pieces are attached at the mid-height of the movable eccentric, with the lower part having a protrusion that allows the two parts to be bolted together. The connection is established using two M5 screws.

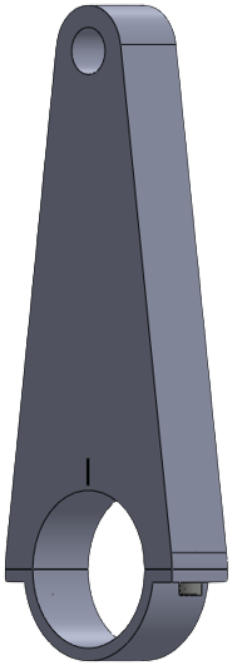


Figure 3.28: Eccentric system

A detail of the upper part is the marking next to the hole, which aids in aligning the movable eccentric. The movable eccentric also features these markings that indicate the possible positions of the teeth. Aligning the markings on both components ensures that the parts are properly positioned.

To hold this part in the centre position of the shaft to which it is attached, two spacers (12) of length x have been designed. These spacers will be sandwiched between the triangle, left or right, and the crank itself.

3.5.5 Fixation (21)

The eccentric system is the other connection of each subsystem to the base. For this purpose, supports were designed to connect with both the main shaft and the base. This component consists of an eyelet with dimensions large enough to be penetrated by the shaft. To allow the free rotation of the main shaft, each support will have a bearing between itself and the shaft. These bearings will be sized in section 3.9.2.

At its base, it has two protrusions, each with a 5 mm diameter hole, through which it will be attached to the base using M5 screws. Each shaft will be supported by two of these supports, equally spaced to ensure that the eccentrics are at identical distances from them.

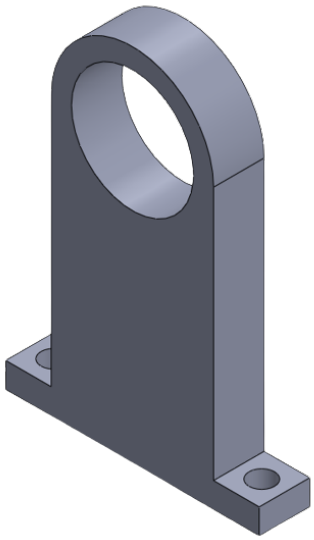


Figure 3.29: Eccentric system support.

3.6 Equilibrium Structure

One of the challenges encountered in this project was the weight of the checks that hold onto the test specimens. With a mass of 30 kg each, which is a significant value, they would interfere with the test and cause undesirable forces on the specimen during testing. To address this, it was necessary to devise a solution for this issue. The solution would have to involve a mechanism that supports the constant force weight without impeding the movement of the chucks, thus avoiding interference with the test.

Since the goal is to keep the machine's design affordable and compact, a pneumatic solution was ruled out. Another considered solution was the application of constant force springs, however, these springs are designed for smaller applications and are not suitable for weights of this magnitude. Conventional springs were not the preferred choice as they are not specifically designed to support constant weight. The solution, therefore, involved creating a counterweight system.

In terms of dimensions, this structure must be taller than the machine and should not hinder the necessary movements of the operator to insert new test specimens. To prevent this issue, two horizontal bars were used to shift the counterweight's point of application. This way, it's possible to create a support structure with 8 bars that is sufficiently tall and allows for the passage of operator's limbs. In addition to the profiles, this structure is also composed of steel cables, pulleys, and the counterweight.

3.6.1 Profiles

The bars that make up the main structure are standardized profiles. In this case, where the load was not excessive for this type of application, the choice was made to use simpler and cost-effective profiles, hence the selection of standardized profiles. From the Wispeco Aluminium

catalog, appendix D, the Tubing Square profiles were chosen. It is worth noting that this solution is just an example, and it is possible to choose more affordable profiles suitable for this application. The selected profile, referenced as 42886, has a width B of 30 mm and a thickness t of 2 mm, which means a inner length b of 26 mm.

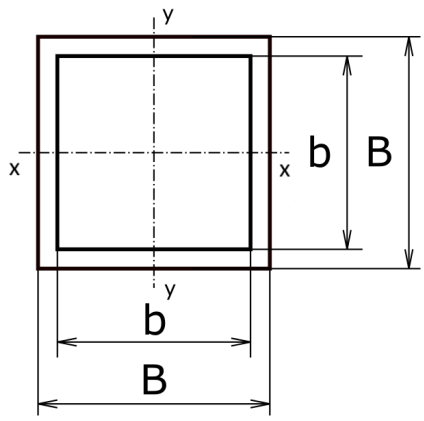


Figure 3.30: Profile scheme.

For these profiles, a study will be conducted on bending and buckling, which is suitable for their application. For the buckling study, the steps taken in section 3.4.5 will be repeated, only adapted to this type of piece.

The first step is to calculate the moment of inercia, the area and the radius of gyration:

$$I_{xx} = I_{yy} = \frac{B^4 - b^4}{12} = \frac{0.030^4 - 0.026^4}{12} = 2.94 \cdot 10^{-8}\ \text{m}^4 \tag{3.37}$$

$$A = 4 \cdot B \cdot t = 4 \cdot 0..030 \cdot 0.002 = 2.4 \cdot 10^{-4}\ \text{m}^2 \tag{3.38}$$

$$i = \sqrt{\frac{2.94 \cdot 10^{-8}}{2.4 \cdot 10^{-4}}} = 0.011\ \text{m} \tag{3.39}$$

The next step is to chose the column effective length factor, μ, whose value for this case, considering that both ends are pinned, is μ = 1.0.

Next, it's necessary to calculate the slenderness of the bar and the Euler slenderness, in order to determine the reduced slenderness ratio which the buckling resistance reduction factor is dependent of. All profiles have a 700 mm length l.

$$\lambda = \frac{\mu \cdot l}{i} = 63.23 \tag{3.40}$$

$$\lambda_1 = \pi \cdot \sqrt{\frac{E}{\sigma_y}} = 56.37 \tag{3.41}$$

$$\overline{\lambda} = \frac{\lambda}{\lambda_1} = 1.12 \tag{3.42}$$

where E and σ_y of aluminium 6063-T6 are 68.9 GPa and 214 MPa, respectively.

For this case, the imperfection factor corresponds to "c" with a value of 0.49. ϕ and χ are:

$$\phi = 0.5 \cdot (\overline{\lambda}^2 + \alpha \cdot (\overline{\lambda} - 0.2) + 1) = 1.35 \tag{3.43}$$

$$\chi = \frac{1}{\phi + \sqrt{\phi^2 - \overline{\lambda}^2}} = 0.47 \tag{3.44}$$

Multiplying the value of χ by the yield strength of the material, obtains the reduced strength, which allows to calculate the maximum axial force supported by the component. Therefore,

$$\sigma_{safe} = \chi \cdot \sigma_y = 101.19 \text{ MPa} \tag{3.45}$$

$$F_{adm} = \sigma_{safe} \cdot A = 24.29 \text{ kN} \tag{3.46}$$

Knowing that in a excessive case, a profile has to carry the weight of the two chucks, 651.38 N, which is lower than the obtained value, we confirm that it is suitable for this application.

In terms of bending analysis, the same length of 700 mm is considered to develop the bending moment diagram. To achieve this, it's considered a simple support in each end and applied a load correspondent of the weight of a chuck of 325,69 N at the two points where the counter-weight is located. The resulting outcome is as follows:

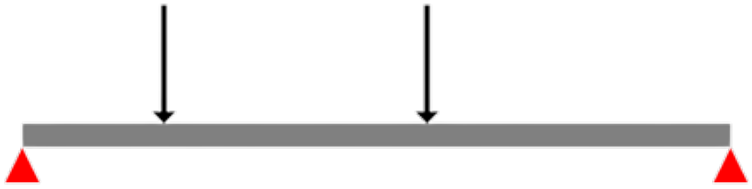


Figure 3.31: Forces diagram of the profiles.

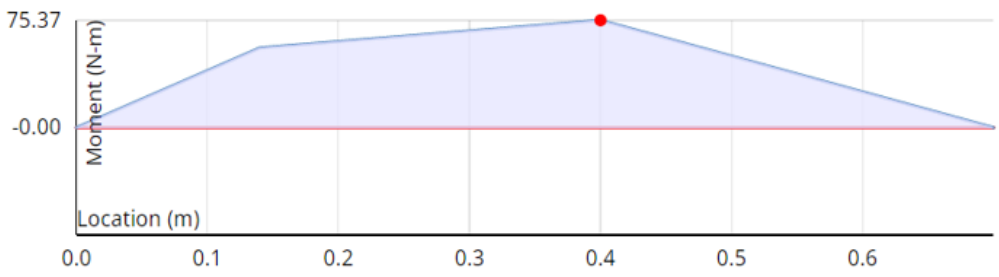


Figure 3.32: Bending moment diagram of the profiles.

Analyzing the diagram, we can determine that the maximum bending moment is 75.37 Nm. Now it is necessary to calculate the maximum stress experienced in the critical zone of the profile, which is located on the upper face of the section at a distance $\frac{B}{2}$ from the center.

$$\sigma_{max} = \frac{M_b \cdot \frac{B}{2}}{I} = \frac{75.37 \cdot \frac{0.030}{2}}{2.94 \cdot 10^{-8}} = 38.43 \text{ MPa} \tag{3.47}$$

Comparing it with the material's yield stress value, we find that it is significantly lower, indicating the safety of using these profiles.

3.6.2 Steel cables and pulleys

The pulleys are placed at the top of the profiles, so it was necessary to consider their design when looking for them. In the Orplex catalog, appendix E, it was possible to find a solution that allows the entry of a cable from underneath and exits from the side. the model chosen is the ETT-160-60 155.4.1, and a schematic of it can be seen in the following figure.

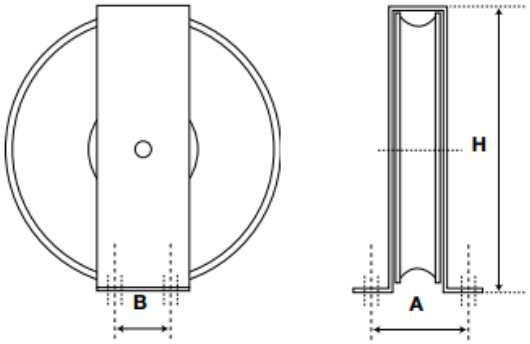


Figure 3.33: Pulley scheme.

Through the supplier, it's known that B is 20 mm, A is 46 mm and H is 66mm.

Two pulleys will be used for each counterweight, with each pair positioned parallel to the other. To determine whether these pulleys or the screws holding them support the weight without deforming, it is necessary to study the stiffness of the connections in relation to the supported weight.

To perform this study, it will be necessary to consider an imaginary displacement characterized by an angle θ. By considering the total distances from the base of the pulley and the number of bolts, it is possible to determine the forces exerted on the bolts when the counterweights act.

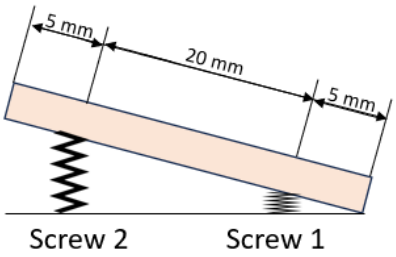


Figure 3.34: Imaginary displacement scheme.

For the purposes of this study, dimensions such as the 5mm distance between the holes and the end of the base have been assumed. Considering two bolts per row and the displacements as a function of the angle θ, we can obtain an equality of moments.

$$2 \cdot (K_p \cdot \theta \cdot 5) \cdot 5 + 2 \cdot (K_p \cdot \theta \cdot 25) \cdot 25 = T \cdot H \tag{3.48}$$

$$2 \cdot K_p \cdot \theta \cdot (5^2 + 25^2) = T \cdot H \tag{3.49}$$

where K_p is the bolts stiffness and T the tension force caused by the steel cable supporting the chucks weight, 33.2 kg.

The stiffness, for a certain angle θ, per row of bolts is then:

$$2 \cdot K_P \cdot \theta = \frac{332 \cdot 0.066}{0.005^2 + 0.025^2} = 33.71 \text{ N/mm} \tag{3.50}$$

To determine the force on each bolt, it is necessary to multiply the stiffness obtained by the distance to the contact point. Therefore, we obtain a supported force of 168.55 N and 842.77 N for each pair of bolts.

Next, it is necessary to determine the force that each bolt can support. Knowing that the pulleys involve the use of M5 bolts, we can find their effective area to determine this force through the yield strength. This area is determined in the section of the bolt with the smaller diameter of the thread, which, according to existing bolt standards, is the nominal diameter minus 1.6. Therefore, for this calculation, we consider a diameter of 3.4 mm.

$$Area = \frac{\pi \cdot 3.4^2}{4} = 9.08 \text{ mm}^2 \tag{3.51}$$

With the knowledge that this is a class 8.8 bolt, one can obtain its yield strength. It will be 0.8 times the 800 MPa indicated as the tensile strength for such a bolt class. Calculating then the force supported by each bolt:

$$F_{bolt} = 0.8 \times 800 \times 9.08 = 5811N \tag{3.52}$$

It's verified that the bolts support the force implied by the counterweights.

3.7 Base (23)

To support the entire system and facilitate its transportation, a dedicated base was designed. This component allows freedom of positioning of the two systems, bending and torsion. The base, measuring 1300x1050 mm, is a steel plate with 10 mm of thickness where components are bolted together. As shown in the following figure, the base features specific slots to maintain correct distances between parts.

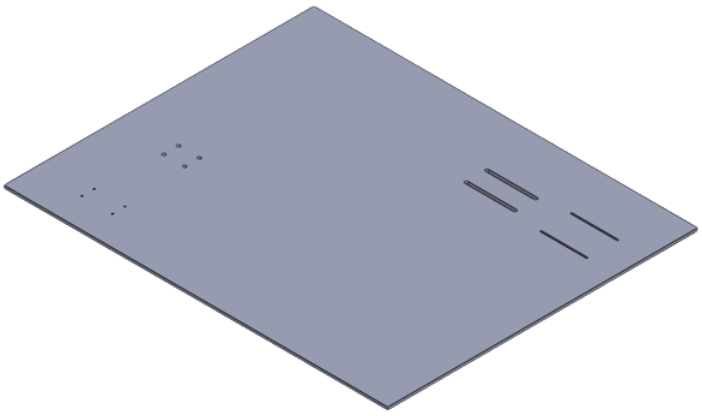


Figure 3.35: Base.

The holes and slots correspond to the torsion and bending systems, respectively. Since it's possible to test various specimens of different sizes, it's important for the system to accommodate this variability. For this purpose, the subsystems would need to have translational capacity. However, translational movement would be simpler if only one of them had this capability. As a result, it was decided that only the bending system would have the ability to move, implying only that the pulleys of the respective counterweight also have this ability. It's possible then to observe the slots where the fixation components of the subsystem will be secured using screws and nuts. These slots provide a path of 115 mm, sufficient to accommodate all the lengths of the test specimens.

3.8 Shafts sizing

Shafts play a crucial role in interconnecting different components of a mechanism. These shafts are used in a variety of conditions, so it's necessary to design the shaft taking into account the forces it will be subjected to, the boundary conditions and a safety factor. Through this process, the required shaft diameter can be accurately determined.

For each shaft, the first step involved determining the applied forces and representing them in a free body diagram. Subsequently, a bending moment diagram is derived, as it is the most suitable approach for analyzing these shafts. This process helps identify the critical zone of the shaft, where the highest bending moment is experienced. Using the material's mechanical properties

and the shaft's dimensions, an appropriate diameter is then calculated, taking into consideration a chosen safety factor.

All shafts within this mechanism are made of Ck45, which has an admissible stress of 310 MPa. It's worth noting that the shafts feature threaded cavities on both ends to facilitate their attachment using screws.

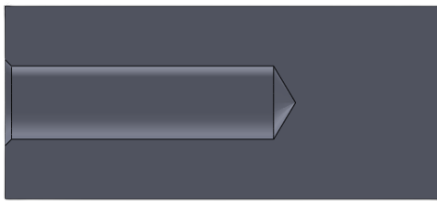


Figure 3.36: Threaded hole on the end of a shaft.

3.8.1 Shaft connecting the horizontal articulations (9)

The initial step involved creating a free body diagram of the system that encompasses the shafts to determine the forces acting on it. The forces F correspond to the forces exerted on the eyelets as a result of the moment M applied at the center of the mirror.

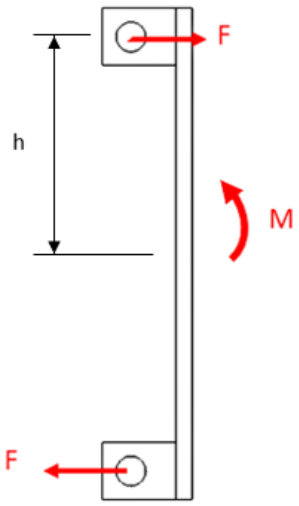


Figure 3.37: Free body diagram of section of the system.

Knowing that h = 132.5 mm and considering the maximum possible moment M = 210 Nm, we can calculate the forces F:

$$M = 2 \cdot F \cdot h \tag{3.53}$$

$$F = 792.45 \text{ N} \tag{3.54}$$

Since there are two eyelets in each end of the mirror, F_{eyelet} is in fact 396.23 N.

A bending moment diagram of the shaft is then developed. To achieve this, the shaft is considered pinned where is secured by the eyelets of the mirror and a load of 396.23 N is applied at the two points in contact with the horizontal articulation. This shaft has a length of 300 mm. The resulting outcome is as follows:



Figure 3.38: Forces diagram of the shaft (9).

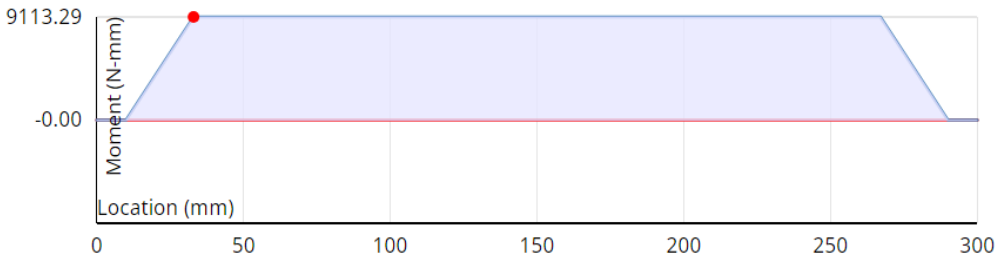


Figure 3.39: Bending moment diagram of the shaft (9).

Analyzing the diagram, we can determine that the maximum bending moment is 9113.29 Nmm. Next, proceeds the determination of the required diameter to withstand the load at the critical section, using the following expression:

$$d = \sqrt[3]{\frac{32 \cdot M_f \cdot n}{\sigma_{adm} \cdot \pi}} \tag{3.55}$$

Considering a safety factor n = 2, we obtain a value for the diameter d of 8.43 mm. This means that the shaft needs to have at least a 8.43 mm diameter to support the forces applied in this application. The shaft was designed with a diameter of 18 mm for aesthetic and practical reasons, as the eyelets and other holes do not benefit from being too small when connected to larger parts.

3.8.2 Shaft connecting the balance triangles and vertical articulations (10)

The free body diagram for the next case is depicted in the following image. The forces F correspond to the forces exerted on the vertical articulation connections as a result of the moment M applied at the center of the mirror.

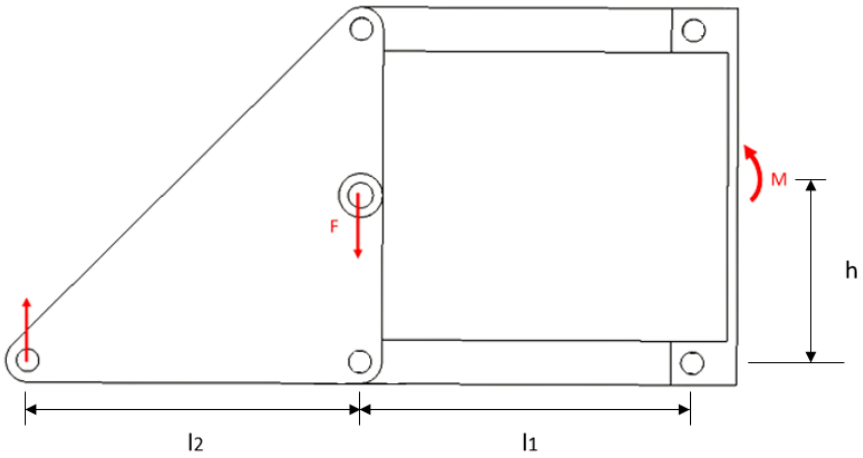


Figure 3.40: Free body diagram of section of the system.

Knowing that l_1 = 300.5 mm and is the distance between the first column of holes of the triangle and the mirror, l_2 = 265 mm and is the horizontal distance between the triangle holes, and considering the maximum possible moment M = 210 Nm, we can calculate the forces F:

$$M = F \cdot (-l_1) - F \cdot (-l_1 - l_2) \tag{3.56}$$

$$F = 792.45 \text{ N} \tag{3.57}$$

Since there are two articulations in each point, $F_{articulation}$ is in fact 396.23 N.

To achieve the bending moment diagram, it's considered pinned where the shaft is secured by the holes of the vertical articulation and applied a load of 396.23 N at the two points in contact with the balance triangles. This shaft has a length of 346 mm. The resulting outcome is as follows:



Figure 3.41: Forces diagram of the shaft (10).

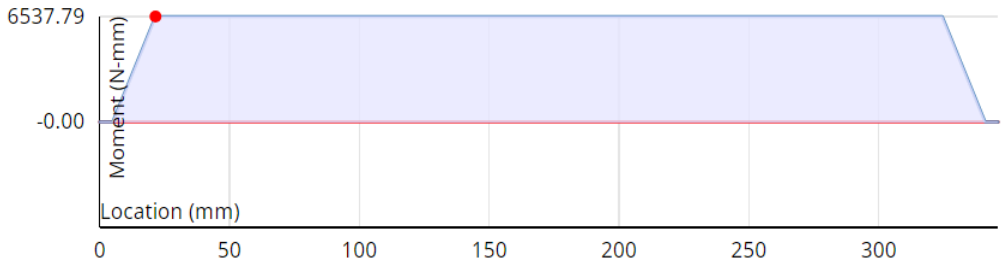


Figure 3.42: Bending moment diagram of the shaft (10).

Analyzing the diagram, we can determine that the maximum bending moment is 6537.79 Nmm. Next, proceeds the determination of the required diameter to withstand the load at the critical section. Using equation 3.55 with the same safety factor $n = 2$, we obtain a diameter of $d = 7.55$ mm.

To prevent deformation of the balancing triangles and maintain the distance between them, this shaft has the feature of changing its cross-section. Section change points are critical areas as they concentrate a lot of stress, requiring a specific assessment in that zone, characterized by the stress concentration factor K.

The shaft in question has a larger diameter D of 25 mm, a smaller diameter d of 18 mm, and a radius at the section change r of 1 mm, represented in appendix C. These dimensions are required to determine K_t on the respective graph, assuming that there is only bending in this case. It is necessary to know the value of r/d and D/d, which are 0.055 and 1.40, respectively.

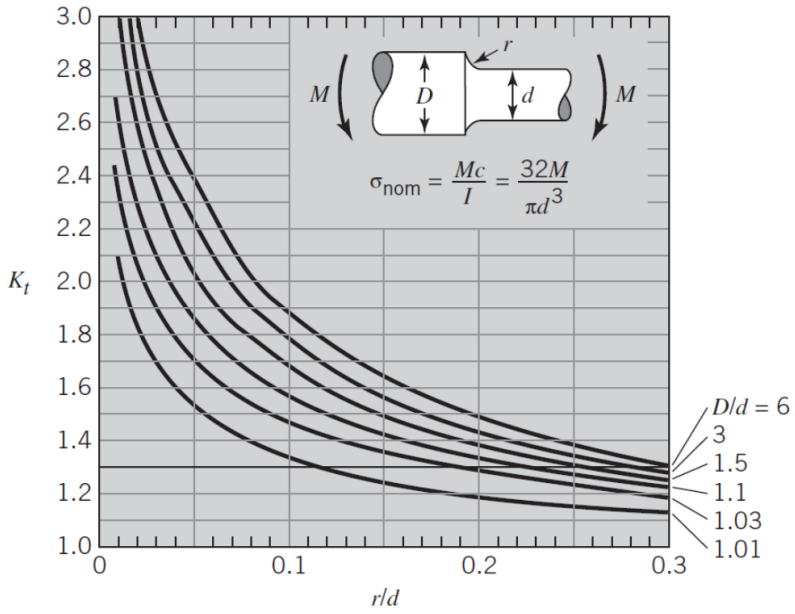


Figure 3.43: Stress concentration factor for shafts with a change in cross-section [46].

Analyzing the graph, we obtain a value of $K_t = 1.92$, approximately. The next step is to obtain the value of K_f:

$$K_f = 1 + q \cdot (K_t - 1) = 1.55 \tag{3.58}$$

where q represents the notch sensitivity index, with a value of 0.6 for this type of material.

To determine the maximum stress that this shaft can withstand, it is necessary to conduct a fatigue analysis by calculating the corrected fatigue limit stress.

$$\sigma_{fo}^{c} = C_1 \cdot C_2 \cdot C_3 \cdot C_4 \cdot \sigma_{fo} \tag{3.59}$$

where C_1 to C_4 are type of load, size effect, superficial finish and other factors correction factors, respectively. Considering a bending case, the smaller diameter of the shaft, and the fact that the component has been machined, it's possible to obtain:

- C_1 = 1;
- C_2 = 1.906;
- C_3 = 0.0215;
- C_4 = 1.

The fatigue limit stress is determined based on the material's tensile strength. For the given material σ_r = 580 MPa [50]. Since this stress is lower than 1400 MPa, it can be inferred that σ_{fo} is half of σ_r, which equates to 290 MPa. Thus, it can also be calculated that σ_{fo}^{c} = 11.868 MPa.

Finally, the last step is to calculate the equivalent static stress in order to make a comparison between it and the material's yield stress. That is given by the following expression.

$$\sigma_{est}^{eq} = \sigma_{med} + \frac{\sigma_{ced}}{\sigma_{fo}^{c}} \cdot K_f \cdot \sigma_a \tag{3.60}$$

The shaft is subjected to alternating pure loading, with zero mean stress. To calculate the alternating stress, will be used the maximum bending moment experienced by the shaft and its smallest diameter.

$$\sigma_a = \sigma_{nom} = \frac{32 \cdot Mb}{\pi \cdot d^3} = \frac{32 \cdot 6.538}{\pi \cdot 0.018^3} = 3699.63 \text{ Pa} \tag{3.61}$$

Finally, the equivalent static stress is obtained.

$$\sigma_{est}^{eq} = \frac{\sigma_{ced}}{\sigma_{fo}^{c}} \cdot K_f \cdot \sigma_a = 0.15 \text{ MPa} \tag{3.62}$$

With this value significantly below the yield strength of the material, it can be concluded that its application is safe.

3.8.3 Shaft connecting the vertical articulations to the support (29)

For this scenario, all external forces are already defined. It is known that the force in the two vertical articulations must be countered by the bearing fixed to the base.

To create the bending moment diagram, we apply a distributed load of 7.92 N/mm over the area in contact with the bearing, and we consider pinned, at each contact point with the articulations. The value of the load comes from the load obtained in equation 3.57, which will be borne by the area of the shaft in contact with the support, a section 100 mm long. This shaft has a length of 346 mm. The resulting outcomes as follows:



Figure 3.44: Forces diagram of the shaft (29).

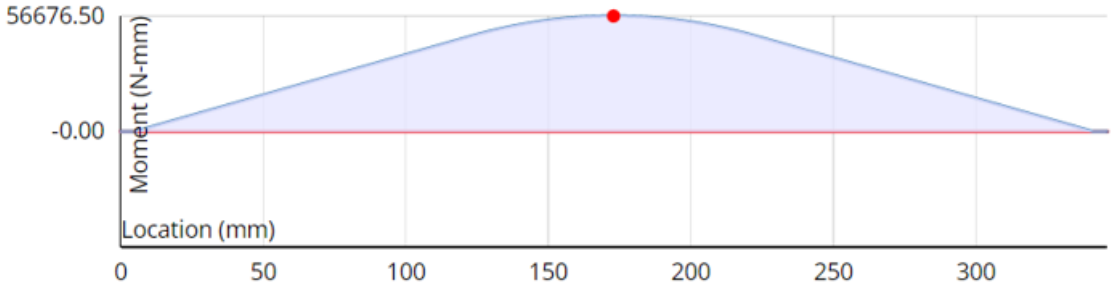


Figure 3.45: Bending moment diagram of the shaft (29).

Analyzing the diagram, we can determine that the maximum bending moment is 56676.5 Nmm. Next, proceeds the determination of the required diameter to withstand the load at the critical section. Using equation 3.55 with the same safety factor $n = 2$, we obtain a diameter of $d = 15.5$ mm. This means that the shaft needs to have at least a 15.5 mm diameter to support the forces applied in this application. The shaft was designed with a diameter of 18 mm for the same reasons as the previous.

3.8.4 Shaft connecting the balance triangles and eccentric system (9)

For this scenario, all external forces are already defined. It is known that the force applied by the eccentric system on the shaft must be countered by the two connections with the vertical articulations.

To create the bending moment diagram, we apply a load of 792.45 kN, obtained from equation 3.57, in the point contacting with the eccentric system, and we consider pinned, at each contact point with the articulations. This shaft has a length of 300 mm. The resulting outcomes as follows:

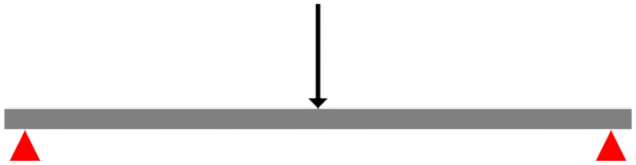


Figure 3.46: Forces diagram of the shaft (9).

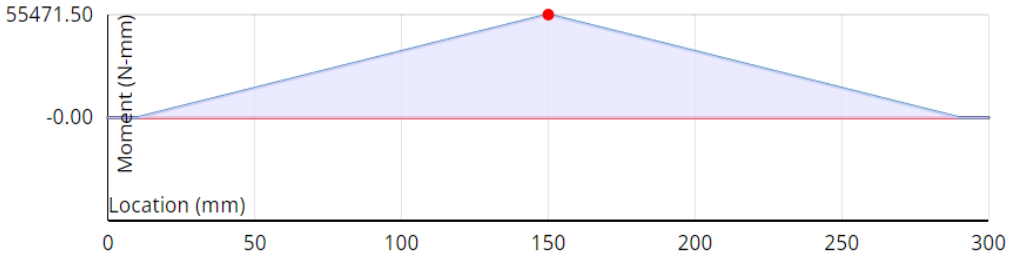


Figure 3.47: Bending moment diagram of the shaft (9).

Analyzing the diagram, we can determine that the maximum bending moment is 55471.5 Nmm. Next, proceeds the determination of the required diameter to withstand the load at the critical section. Using equation 3.55 with the same safety factor $n = 2$, we obtain a diameter of $d = 15.39$ mm. This means that the shaft needs to have at least a 15.39 mm diameter to support the forces applied in this application. The shaft was designed with a diameter of 18 mm for the same reasons as the previous.

3.8.5 Eccentric system's central shaft (20)

Like previous cases, all external forces are already defined. It is known that the force executed by the functioning of the eccentric system must be countered by the support fixed to the base.

To create the bending moment diagram, we apply a distributed load of 26.42 N/mm over the area that covers the eccentrics, and we consider pinned at each contact point with the supports. The value of the load comes from the load obtained in equation 3.57, which will be borne by the area of the shaft in contact with the eccentric, a section 30 mm long. This shaft has a length of 114 mm. The resulting outcomes as follows:

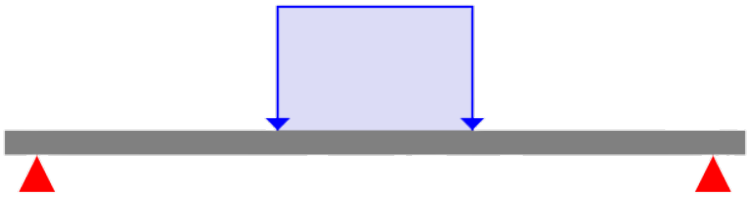


Figure 3.48: Forces diagram of the shaft (20).

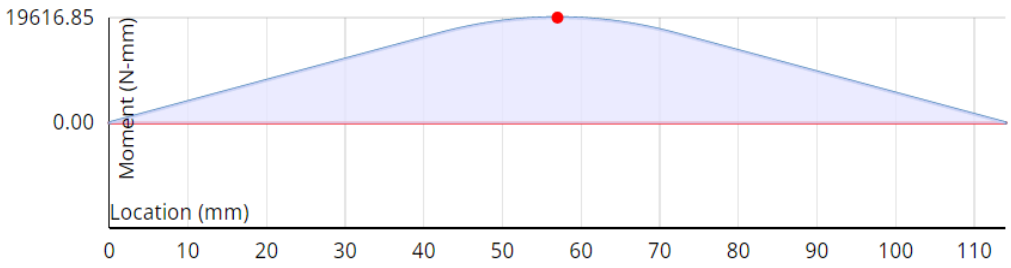


Figure 3.49: Bending moment diagram of the shaft (20).

Analyzing the diagram, we can determine that the maximum bending moment is 19616.85 Nmm. Next, proceeds the determination of the required diameter to withstand the load at the critical section. Using equation 3.55 with the same safety factor $n = 2$, we obtain a diameter of $d = 10.88$ mm. This means that the shaft needs to have at least a 10.88 mm diameter to support the forces applied in this application.

the shaft has been designed with a change of section that holds the shaft longitudinally in the middle of the supports. The largest diameter is 20 mm and the smallest is 15 mm. However, as the actuation component is not part of this project and this shaft might undergo changes due to its connection with the motor, stress concentration in this part will not be analyzed.

3.9 Bearings sizing

Bearings are crucial elements in the project as they facilitate rotational movements when placed between two components, thereby preventing their damage as well. In this project, two different types of bearings were used: plain bearings and ball bearings. The sizing of both types is detailed in the following sections.

3.9.1 Plain Bearings (34)

Permaglide plain bearings were chosen for the rotational movement of the components around the shafts. These bushings are a maintenance-free solution, providing excellent durability without requiring much attention.

As observed in the sections above, the maximum force to which each connection area of the shafts with other parts will be subjected is 396.23 N. This value will be used to verify the feasibility of the chosen bearing. The chosen model is the EGB1810-E40.



Figure 3.50: Permaglide bearing.

This piece has a width, B, of 10 mm and an inside diameter, D_i, of 18 mm. To reinforce the choice, the pressure applied by the force on the projected area of the interior of the bearing was calculated. The recommended value for applications of this type is 10 MPa.

$$P = \frac{F_{eyelet}}{A_p} = \frac{F_{eyelet}}{D_i \times B} = \frac{396.23 \text{ N}}{18 \text{ mm} \times 10 \text{ mm}} = 2.2 \text{ MPa} \tag{3.63}$$

Observing that the obtained pressure is approximately five times lower than the recommended 10 MPa, the choice and application of these bearings remain.

3.9.2 Ball Bearings (35)

The central shaft of the eccentric system must have free rotation, so it should not roll directly on the supports. Therefore, bearings were applied between the shaft and the supports to enable this rotational movement. The shaft on which the bearings will be placed has a diameter of 15 mm, so the bearings will have to follow this dimension. Also, so that the supports aren't oversized, we opted for a bearing with a small difference in inner and outer diameters. The bearings chosen are model 16004, appendix F. The dimensions of these bearings are provided in the following table and auxiliary figure.

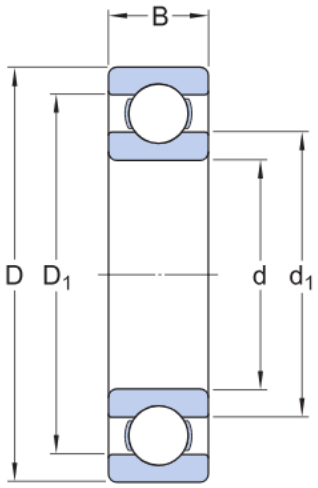


Figure 3.51: 16004 SKF bearing scheme.

Table 3.12: 16004 SKF bearing dimensions.

d [mm]	D [mm]	d_1 [mm]	D_1 [mm]	B [mm]
20	42	27.25	34.3	8

To determine if the bearing is suitable for this application, it's necessary to conduct both static and dynamic analyses. In the case of static loads, the bearing either has low rotation speeds or no rotation at all. This type of loading is responsible for inducing plastic deformation in bearings. To overcome this issue, it's necessary to calculate the static load capacity that the bearings must possess:

$$f_s = \frac{C_0}{P_0} \tag{3.64}$$

where f_s is the static load factor, C_0 the static load capacity and P_0 the equivalent static load.

This factor is the safety factor to ensure that the bearing doesn't undergo deformations, and it can vary according to the requirement:

Table 3.13: Variation of the safety factor [46].

f_s	Requirement
0.7 to 1.0	Low
1.0 to 1.5	Normal
1.5 to 2.5	High

Regarding the static load, this will be obtained through a combination of the radial force and axial force applied to the bearing:

$$P_0 = X_0 \cdot F_r + Y_0 \cdot F_a \tag{3.65}$$

where X_0 is the radial factor, Y_0 the axial factor, F_r the radial force and F_a the axial force.

For the case under consideration, the bearing is only subjected to radial force, hence $F_a = 0$ and $X_0 = 1$. Since two bearings are used in each side of the shaft, each one supports a quarter of the load, 198.11 N. In this way, we obtain:

$$P_0 = F_r = 198.11 \text{ N} \tag{3.66}$$

From the supplier, we know that the static load capacity, C_0, is 1.1 kN. Therefore, the static load factor is:

$$f_s = \frac{1.1}{0.19811} = 5.55 \tag{3.67}$$

Compared to table 3.13, the value obtained is above high, which confirms that it is a conservative choice.

For the dynamic loading, the bearing experiences considerable rotation speeds, meaning the rings rotate relative to each other. The sizing calculation is performed to ensure there is no premature bearing failure. Considering that the rotation speed is always constant, the value of the nominal life can be obtained from the operating life in hours given in millions, L_{10H}:

$$L_{10H} = \frac{(\frac{C}{P})^p}{60 \cdot n} \cdot 10^6 \tag{3.68}$$

where C is the dynamic load capacity, P the equivalent dynamic load, p the life exponent and n the rotational speed in rpm. The value of p varies depending on the type of bearing, with a value of $p = 3$ for ball bearings [56].

The calculation of the equivalent dynamic load, P, is done similarly to the equivalent static load, where:

$$P = X \cdot F_r + Y \cdot F_a \tag{3.69}$$

where X is the radial factor, Y the axial factor, F_r the radial force and F_a the axial force.

Once again, for the case study, the bearing is only subjected to radial force, so $F_a = 0$ and $X = 1$. Therefore, we obtain:

$$P = F_r = 198.11 \text{ N} \tag{3.70}$$

From the supplier, we know that C is 1.9 kN. Calculating the operating life in hours,

$$L_{10H} = \frac{(\frac{1.9}{0.39623})^3 \cdot 10^6}{60 \cdot 900} = 16335.29 \text{ hours} \tag{3.71}$$

This means that the bearings will be able to work for 16335.29 hours. Given the purpose of the machine, this figure is a good indicator of its durability.

3.10 Screws, Nuts and Washers

The fixation of all components in place require the application of screws and washers in the fixation system. Some fixations also need nuts to tighten the screws. All of these three types of components are selected from Fabory's website [54].

For the connection of the chucks (1) to the mirrors (2 and 3), will be applied four M10 screws in each, that will pass through the mirror, the mirror-chuck adaptor (11) and enter the chuck, for a total of eight screws. The M10 holes on the chuck have a depth of 25 mm, the adaptor a thickness of 5 mm and the mirror a thickness of 8 mm. This means that the screw can have a maximum length of 38 mm. Choosing a standardized length the nearest value is 35 mm, so to perform the fixation of these three parts the M10x35 DIN 912 zinc plated steel screws (25) are used. To apply these screws it will require a washer between the mirror and each screw, so eight washers are required. It will be used DIN 125-1A zinc plated steel M10 140 HV plain washers (29).

For all the shafts guiding and connecting the mirrors, balance triangles (5 and 6) and articulations (4 and 7), M8 screws are used to prevent its movement. Each shaft uses two screws, one in each end, so a total of twenty eight screws in the machine. The M8 holes on every shaft have a depth of 25 mm, meaning that the screw can have a maximum length of 25 mm. Choosing a standardized length close to it was 20 mm, so the screws used are M8x20 DIN 912 zinc plated steel (27). Similar to the other cases, applying these screws implicates applying a washer in each one. Twenty eight DIN 9021 zinc plated steel M8 140 HV plain washers (26) will be used. This kind of washer was used because it needed to have an outside diameter bigger than the shaft's diameter in order to contact with the outside component and fix the shaft in place.

Where two abutting components rub against each other, there is a need for a separating element between the two to prevent damage. In these scenarios are used washers. In the whole machine are used twenty plain washers DIN 912 zinc plated steel M18 140 HV (31).

Each system has two connections to the base, one for the eccentric system and one for the vertical articulation. The concept of these two connections is to have screws that go through their supports and the base, and underneath are tightened by nuts, separated from the base with washers.

In the support (8), are used four M10 nuts to tighten four M10 screws, in each. The chosen nuts are zinc plated steel DIN 934 hexagon nuts (30). The screws have to go through the holes of the support that have a depth of 50 mm, the base with a thickness of 10 mm and the nuts with a thickness of 8 mm. This means that the screw should have a minimum length of 68 mm plus two times the nut's pitch, which is 1.5 mm. Choosing a standardized length the most adequate value is 75 mm, so to perform this fixation the M10x75 DIN 912 zinc plated steel screws (28) are used. In total are required eight of these screws and nuts. To apply these nuts it will require a washer between it and the base, so eight washers are required. It will be used the same DIN 125-1A zinc plated steel M10 140 HV plain washers (24) as before.

In the eccentric system's support (21), are used another four M5 nuts to tighten four M5 screws, in each. The chosen nuts are zinc plated steel DIN 934 hexagon nuts (38). The screws have to go through the holes of the support that have a depth of 5 mm, the base with a thickness of 10 mm

and the nuts with a thickness of 4 mm. This means that the screw should have a minimum length of 19 mm plus two times the nut's pitch, which is 0.80 mm. Choosing a standardized length the most adequate value is 25 mm, so to perform this fixation the M5x25 DIN 912 zinc plated steel screws (39) are used. In total are required eight of these screws and nuts. To apply these nuts it will require a washer between it and the base, so eight washers are required. It will be used the same DIN 125-1A zinc plated steel M5 140 HV plain washers (40) as before.

In the eccentric locking mechanism, is used a nut to tighten the spring plunger. It is a M3 DIN 439 zinc plated nut (33) also supplied by Fabory.

Also in the eccentric system, to connect the two parts of the cranks, are used M5x12 DIN 912 zinc plated steel screws (36). In total are required 4 screws.

Finally, the screws used in the jaw adaptors (13 and 14) are M12x25 DIN 912 zinc plated steel screws (37), and each adaptor is secured by two of this components, which means twelve screws in total.

3.11 Design for Manufacturing

To achieve the final designed, it will require the procurement of certain parts and the manufacturing of others. For the latter, it is necessary to define the materials and processes that will be used, as well as completing their manufacturing drawings. All parts, procured and manufactured, will then be listed on the complete bill of materials.

Almost every part except the screws, nuts and washers is submitted to a custom manufacturing process of some kind. For this project, the parts are not exposed to any special environmental conditions. The materials' mechanical properties are the only selection criteria, in order to ensure that failure can be avoided. As such, all the designed parts for this project will be made from Ck45.

The manufacturing process for these components primarily involves turning, drilling, milling and boring operations. Turning is utilized to achieve high levels of concentricity, ensuring precise dimensional control by rotating the workpiece on a lathe while a cutting tool removes material. Drilling is extensively employed to create holes of various sizes and depths, relying on the rotation of a drill bit and axial force to cut through the material. Milling is employed using a rotating milling cutter with multiple teeth to remove material and achieve the desired shape, size, and surface finish. Lastly, boring is used to achieve greater accuracy of the diameter of a hole, performed exclusively on internal surfaces. In addition to these processes, some parts are welded and laser-cut.

Both supports will have similar manufacturing processes, mostly differing in the outer shape and diameters of the holes. The manufacturing process involves cutting the pieces to the desired dimensions, with the desired thickness, then drilling the four fixing holes in the base. Finally, boring the centre hole through which the respective shaft will pass in each bracket.

The mirrors, triangles and horizontal joints are made up of small parts that are welded together to form the total component. For these parts and the vertical joints, the process will first involve

cutting the material to the desired dimensions for the outer edge. Drilling would then take place at the various desired points, with the diameter of each hole in question. The preferred welding method is angle welding, due to its efficiency and simplicity. Regarding the eyelets, as well as the cylinders welded to the triangles, it was not possible to properly design the parts to weld all the necessary faces. This project involved changing the dimensions of the parts, which could result in changes to all the calculations made. For this reason, the project only takes account of welding on the faces indicated for this purpose. The solution to this problem would be to modify the dimensions of the parts to the materials' mechanical properties are the only selection criteria, in order to ensure that failure can be avoided.

Both the chuck-mirror adaptor and all the shafts will be manufactured mainly by turning. By removing material during turning, it is possible to create customised cylindrical shapes, in the case of the adapter and the shaft with section change. The four small holes in the adapter and the threaded holes at the ends of the shafts will be drilled. For the centre hole of the adapter, we opted for boring.

As for the eccentrics and locking cap, their main bodies will be obtained by turning. The grooves on the outer surface of the fixed eccentric will be milled, using a cutter with a splitter that allows for an equal distance between the grooves. The notch in the free eccentric will also be made in this form. The holes in the protruding face of this eccentric will be drilled. All the interior holes and details on this face will be obtained by boring.

The base consists of a sheet of metal in which the slots and holes are obtained by milling and drilling, respectively.

The key and both connecting rod parts of the eccentric system are obtained by cutting the material and then milling it. The connecting rod parts are also manufactured by drilling the connection holes.

Finally, the adapters designed for the grips will mostly be obtained by milling, outlining their main shape and the details of the guide at their base. The holes for these parts and the original grips will be drilled. The recesses for the screw heads on the adapters will also be milled.

The technical drawings respective to all manufactured parts mentioned above can be found in appendix C.

The aim of this work was to focus on the body and operation of the machine itself, which is why the technical drawings for the parts of the counterweight structure were not made at this stage. However, the solution is presented in the report, with all the structural calculations carried out.

3.12 System Actuating Power Requirements

Although the actuating component is not part of this project, the power required by the system was calculated. The motor provides the necessary torque for the eccentric system to rotate and thereby transmit motion to the rest of the system. It's known that the highest power will be required

during the upward movement to the maximum position of the eccentrics. This occurs because the system transitions from a position of lower effort to a position of maximum effort.

The first step is to calculate the torque required for this movement. Knowing that the maximum total eccentricity is 10 mm and the maximum force is 792.453 N, the necessary torque is:

$$T = F \cdot e = 792.453 \cdot 0.010 = 7.925 \text{ Nm} \tag{3.72}$$

Since power is a function of torque and rotational speed, it's possible to obtain its value. Based on the work and the market studied in chapter 2, a frequency value of 15 Hz will be considered to carry out the necessary power study. The frequency of 15 Hz corresponds to a rotational speed of 94.248 rad/s.

$$P = T \cdot n = 7.925 \cdot 94.248 = 746.869 \text{ W} = 0.747 \text{ kW} \tag{3.73}$$

This means that in order to be able to carry out tests in this frequency range, the system requires 0.747 kW of power in the eccentric system shaft.

3.13 Chapter Summary

In conclusion, the design entails a combination of parts being procured and others being manufactured. All of the parts that constitute the overall system, such as the mirrors, articulations, shafts and eccentrics, will be made of Ck45.

The essential specifications for surface roughness, dimensions, and tolerances have been laid out, guaranteeing that the design and manufacturing details for each part contribute to the end goal of the system. These specifications must be followed during the production process to guarantee the components' quality and functionality.

This chapter has given a general overview of the pieces that need to be created, their designs, and the materials and methods used to make them. These specifics set the groundwork for the project successful completion and enable accurate and controlled testing of multiaxial fatigue effects.

Chapter 4

Conclusion

In the final chapter of this dissertation, the final conclusions from the research conducted in this work are presented. The key findings and insights gained throughout the research process are summarized, providing a culmination to the dissertation. By presenting the conclusions and work suggestions, it brings a sense of closure to the study, while opening ways to further investigation and improvement of the design of multiaxial fatigue testing machines.

4.1 Final Conclusions

The main objective of this dissertation has been achieved through the design of a combined bending and torsion fatigue testing machine. Within the different stages of this work, it is possible to define the objectives achieved and the final characteristics of the machine obtained.

The designed machine consists of two main independent systems, torsion and bending. This independence between systems means that a single machine can carry out tests with three different types of load, either jointly or individually. Within each system there are three subsystems: the main body, which allows the system to adapt to the conditions imposed; the eccentric, which applies the loads to the system; and the counterweight solution, which prevents the bushings from interfering with the tests.

The specimens used as a reference in the machine design follow the standard ASTM E2207-02 standard, which provides the dimensions and geometry of the specimens accepted in the project. This standard was followed due to the lack of standardisation of these parameters for the exact type of test studied in this work. The machine accepts specimens with outer section diameters from 16.5 mm to 37 mm, with section lengths from 59.4 mm to 166.5 mm, respectively. This range already takes into account the limitations imposed by the chucks, as larger specimens would need both larger chucks and higher permissible loads.

In terms of permissible load, the value corresponds to the maximum permissible load for the chucks, which is set at 210 Nm.

The mechanism allows the application of torsional and bending moments that allow the desired test specimens to be tested within the stipulated limits. This is done through a four-bar mechanism

that allows the system to adapt to the natural conditions imposed by the specimen when subjected to loads.

In order to apply cyclic loads with previously defined amplitudes, an eccentric system was designed to allow the stroke to vary depending on the desired moment to be applied to the test piece. This eccentric system is constantly rotating during tests, applying cyclic loads. The rotation of the free eccentric around the fixed eccentric allows the stroke to change, which causes the load to change. A conversion table, table 3.11, was made for the final stroke corresponding to each tooth number in the pre-defined position, the upper one.

Most of the components are designed from scratch, specifically for this application. The material of choice for this was Ck45 due to its affordability and mechanical properties suited to the application. Some parts require welding, but the vast majority are manufactured by drilling, milling and turning.

Also, although the actuator part was not part of this project, the power needed to apply a motor to act on the shaft of the eccentric systems for tests at 15 Hz was calculated. The required power is 0.747 kW.

One of the main challenges faced was to find a solution to counteract the weight of the clamping chucks chosen. This solution increased the volume and weight of the machine, as well as its complexity.

In summary, the designed machine proposes concepts that, once validated and produced, would be promising in this area of study, opening up new horizons in these types of machine designs. Clear advantages of this project are the range of specimens accepted, the possibility of carrying out only torsion or bending tests, the mobility of the machine and the low complexity of the main body. However, some disadvantages are the weight of the chucks, as well as the limitations they impose on the system and the need to create a system to counteract this weight. Also a disadvantage is the non-infinite number of possible strokes for application, which are limited by the number of teeth.

4.2 Future Works

As future work, the improvement of the disadvantages mentioned above would be important, as well as the improvement of other aspects.

The project of new lightweight chucks with the same wide range of specimen dimensions would be imperative in a new project. The reduction in weight and machine obstruction would be beneficial and cost-effective, as well as practical.

Furthermore, finding a different solution to vary the stroke would be interesting, allowing for a greater range of load amplitudes in tests, expanding the study of material behavior under these conditions. It could be designed a similar system that includes a greater number of possible positions or work on a new concept.

The use of finite element analysis software would be interesting to analyze the critical sections of the machine during its operation, not yet performed due to time constraints. This rigorous

method could highlight sections with a high concentration of stresses that could potentially affect the results obtained in tests.

Finally, to complete this project, it would be important to design the electrical and actuator system specifically for this machine. To do so, it would be necessary to define the most suitable frequency range for the desired tests and choose a motor that preferably allows for power regulation.

All of these proposed tasks support the advancement and evolution of knowledge in the field of multiaxial fatigue, especially in cases involving combined torsion and bending.

References

[1] Darrell Socie and Gary Marquis. *Multiaxial fatigue*. SAE International, 1999.

[2] V M Radhakrishnan. Multiaxial fatigue-an overview, 1995.

[3] Ishvari Fernanda, Zuñiga Telllo, Jorge L Avila Ambriz, Gonzalo M Dominguez Almaraz, Julio C Verduzco Juarez, Erasmo Correa Gomez, and Ishvari F Zuñiga Tello. Design and construction of a torsion fatigue machine: Torsion fatigue tests on two industrial aluminum alloys. *U.P.B. Sci. Bull., Series D*, 2017.

[4] S. Suresh. *Fatigue of Materials*. Cambridge University Press, 2 edition, 1998.

[5] Marco Antonio Meggiolaro, Jaime T P Castro, and Rodrigo de Moura Nogueira. A fast rotating bending fatigue test machine. Associacao Brasileira de Engenharia e Ciencias Mecanicas - ABCM, 2 2018.

[6] Nondestructive Evaluation Physics : Materials — nde-ed.org. https://www.nde-ed.org/Physics/Materials/Mechanical/FractureToughness.xhtml. [Accessed 20-07-2023].

[7] Harro Ranter. ASN Aircraft accident de Havilland DH-106 Comet 1 G-ALYP Elba — aviation-safety.net. https://aviation-safety.net/database/record.php?id=19540110-1. [Accessed 08-09-2023].

[8] Office of Rail and Road. Train derailment at hatfield: A final report by the independent investigation board. Technical report, Office of Rail and Road, 2006.

[9] Tessa Axsom. Stress Concentrations: How to Identify and Reduce Them in Your Designs | Fictiv — fictiv.com. https://www.fictiv.com/articles/stress-concentrations-how-to-ide. [Accessed 14-08-2023].

[10] Ruel Billones, Josephine K. Liwang, Kierra Butler, Letitia Graves, and Leorey N. Saligan. Dissecting the fatigue experience: A scoping review of fatigue definitions, dimensions, and measures in non-oncologic medical conditions, 2021.

[11] Boris Stratula, Alexander Nikitin, and I. Nikitin. Critical plane and multiaxial criteria for in-phase and antiphase cyclic loading. *Procedia Structural Integrity*, 13:1402–1407, 01 2018.

[12] William H Munse, Karl A Stambaugh, Paul R Van Mater Jr, and SENSOR DATA INTEGRATION INC CONCORD MA. Fatigue performance under multiaxial loading. 1990.

[13] A. Fernández Canteli, E. Castillo, S. Blasón, J.A.F.O. Correia, and A.M.P. de Jesus. Generalization of the weibull probabilistic compatible model to assess fatigue data into three domains: Lcf, hcf and vhcf. *International Journal of Fatigue*, 159, 2022.

[14] Yong Bai and Wei-Liang Jin. Chapter 24 - mechanism of fatigue and fracture. In Yong Bai and Wei-Liang Jin, editors, *Marine Structural Design (Second Edition)*, pages 477–487. Butterworth-Heinemann, second edition edition, 2016.

[15] Ashish Thakur. How does fatigue life depend on the test frequency of the component?, 04 2020.

[16] Daniel Hendrickson. Fatigue failure due to variable loading, 2017.

[17] Alfredo Ribeiro, José Correia, António Silva, and Abilio De Jesus. Evolution of fatigue history. 2011.

[18] Wojciech Macek, Stanisław Zawiślak, Adam Deptuła, and Robert Ulewic. Fatigue testing machines and apparatus. *Zeszyty Naukowe. Quality. Production. Improvement*, 2019.

[19] J B Geetha Shree. Fatigue analysis of truss, 2015.

[20] Amr Shaat and Amir Fam. Axial loading tests on short and long hollow structural steel columns retrofitted using carbon fibre reinforced polymers. *Canadian Journal of Civil Engineering*, 33:458–470, 02 2011.

[21] Axial Load Fatigue Testing Machine | Torontech — torontech.com. https://www.torontech.com/axial-load-fatigue-testing-machine. [Accessed 10-08-2023].

[22] Mechanics of Materials: Axial Load xBB; Mechanics of Slender Structures | Boston University — bu.edu. https://www.bu.edu/moss/mechanics-of-materials-axial-load/. [Accessed 10-08-2023].

[23] Zainul Huda. *Torsion in Shafts*, pages 189–198. Springer International Publishing, 2022.

[24] materials - torsionload — princeton.edu. https://www.princeton.edu/~maelabs/hpt/materials/torsionload.htm. [Accessed 10-08-2023].

[25] Torsion Testing — admet.com. https://www.admet.com/testing-applications/test-types/torsion-testing/. [Accessed 10-08-2023].

[26] Lance Lachica. Get The Highest Performance Dynamic Fatigue Torsion Test Machines — testresources.net. https://www.testresources.net/test-machines/torsion-test-machines/560-series-torsion-test-machine/. [Accessed 10-08-2023].

[27] Fabio Marcelo, Peña Bustos, César Augusto, and Álvarez Vargas. Design and construction of a torsional fatigue testing machine operated by inertial loads. pages 46–55, 2012.

[28] HG Vyas. Comparative study of hollow and solid shaft for the application in eight speed gear box. *IJRAR-International Journal of Research and Analytical Reviews*, 2018.

[29] Bakr Noori Khudhur. Finite element analysis of the boom of crane loaded statically, 2013.

[30] P D Soden, M A Millar, B A Adeyefa, and Y S Wong. Loads, stresses, and deflections in bicycle frames. *The Journal of Strain Analysis for Engineering Design*, 21(4):185–195, 1986.

[31] Lance Lachica. Bend Test Machines — testresources.net. https://www.testresources.net/test-machines/by-test-type/bend-test-machines/. [Accessed 10-08-2023].

[32] Four Point Bending System (4PB) — matest.com. https://www.matest.com/en/product/b210-kit-stand-alone-servo-pneumatic-four-point-bending-system-4pb. [Accessed 10-08-2023].

[33] John Pang and F.X. Che. Isothermal cyclic bend fatigue test method for lead-free solder joints. *Journal of Electronic Packaging*, 129, 2007.

[34] Patrick N.B. Anongba. What are the differences between three point and four point bending tests?, 10 2017.

[35] Three Point and Four Point Bending | Penn Center for Musculoskeletal Disorders | Perelman School of Medicine at the University of Pennsylvania — med.upenn.edu. https://www.med.upenn.edu/pcmd/3pt-4pt-bending.html. [Accessed 10-08-2023].

[36] J. Brian Jordon, Harish Rao, Robert Amaro, and Paul Allison. Chapter 6 - extreme conditions and environments. In J. Brian Jordon, Harish Rao, Robert Amaro, and Paul Allison, editors, *Fatigue in Friction Stir Welding*, pages 119–136. Butterworth-Heinemann, 2019.

[37] Advances in Multiaxial Fatigue — astm.org. https://www.astm.org/stp1191-eb.html. [Accessed 16-08-2023].

[38] Fadiga multiaxial não proporcional no ANSYS Workbench — esss.co. https://www.esss.co/blog/fadiga-multiaxial-nao-proporcional-ansys-workbench-2/. [Accessed 16-08-2023].

[39] Vinícius Por and Zanardi Vieira. Projeto de graduação 2 fadiga multiaxial: avaliação comparativa entre os métodos da mínima circunferência, métododa caixa e método do momento de inércia - universidade de brasilia, faculdade de tecnologia, departamento de engenharia mecânica, 2017.

[40] K S Kim, X Chen, C Han, and H W Lee. Estimation methods for fatigue properties of steels under axial and torsional loading, 2002.

[41] 8850 series axial-torsion system ±100 kn, ±1000 nm / ±250 kn, ±2000 nm, 2022.

[42] Axial Torsion Test Machines — testresources.net. https://www.testresources.net/test-machines/axial-torsion-test-machines/. [Accessed 17-08-2023].

[43] Fumio Ogawa, Yusuke Shimizu, Stefano Bressan, Takahiro Morishita, and Takamoto Itoh. Bending and torsion fatigue-testing machine developed for multiaxial non-proportional loading. *Metals*, 2019.

[44] G. S. A. Shawki and A. A. Mashhour. A fatigue-testing machine for combined bending and torsion. *Experimental Mechanics*, 14:196–201, may 1974.

[45] Joseph Edward Shigley, Larry D Mitchell, and H Saunders. Mechanical engineering design. 1985.

[46] Robert L Norton. *Machine design*. Prentice Hall, 2010.

[47] Standard practice for strain-controlled axial-torsional fatigue testing with thin walled tubular specimens. Standard, ASTM International, 2010.

[48] A Ashwin, R B Hari Lakshman, C B Chand Swaroop, M Vignesh, R Vaira Vignesh, and R Padmanaban. Predicting the wear rate of aluminum alloy aa2024-t351 using hybrid linear function and radial basis function. *IOP Conference Series: Materials Science and Engineering*, 561(1), 2019.

[49] Special Metals. Inconel® alloy 718. https://www.specialmetals.com/documents/technical-bulletins/inconel/inconel-alloy-718.pdf, 2023. Accessed: September 10, 2023.

[50] Ansys granta edupack software, ansys, inc., cambridge, uk, year (www.ansys.com/materials).

[51] Elmar Wilczek. *Statische Berechnung Eines Rohrkrummers mit Realen Randbedingungen*. Phd thesis, Institut fur Leichtbau, Aachen Universitat, 1984.

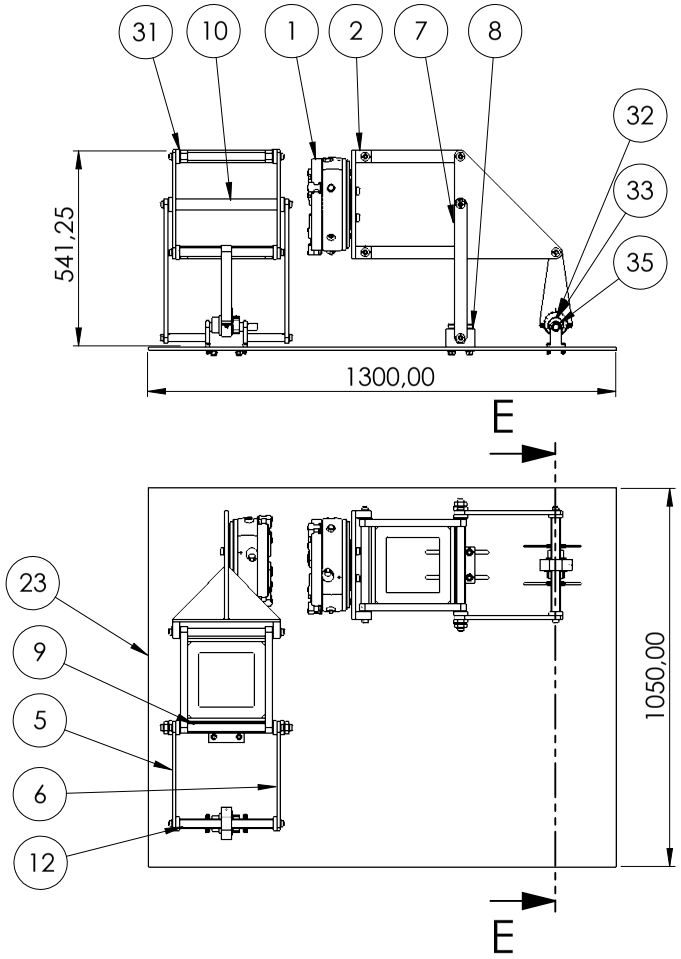
[52] British Standard. Eurocode 3—design of steel structures—. *BS EN*, 1(1):2005, 1993.

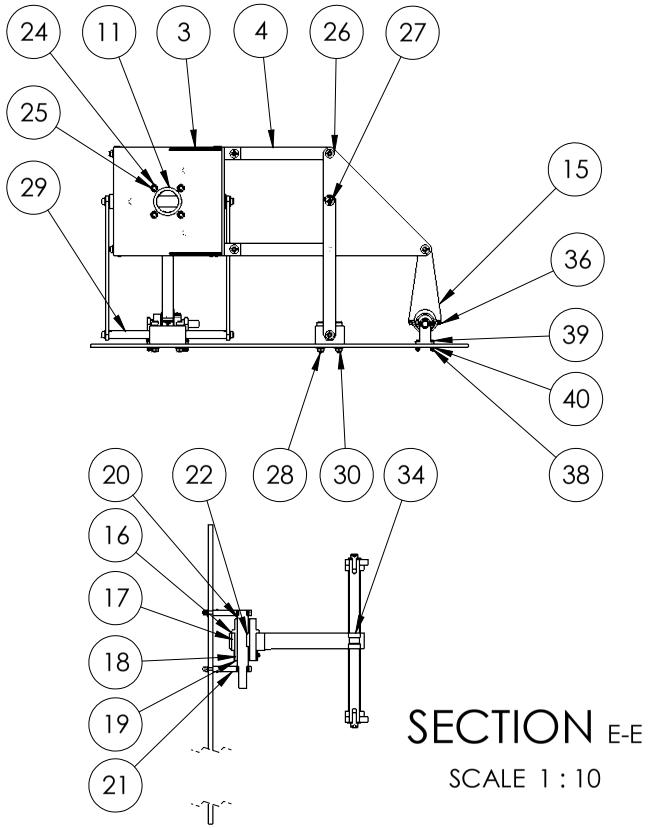
[53] H. Mäkelt. *Mechanical Presses*. Taylor & Francis Group, 1968.

[54] Fabory Portugal — fabory.com. https://www.fabory.com/pt. [Accessed 12-09-2023].

Appendix A

Final Design technical drawings





SECTION E-E

SCALE 1 : 10

	Nome	Data				Folha	1/1
Des.	Beatriz Ferreira	18/09/2023	A4	inegi		Massa (g)	
						Tratamento	
ISO 2768 ISO 13920 - EB		mK	mm	Escala-1:15		Material	
Referência		**Mechanical Drawing**				**Quantidade**	

SOLIDWORKS Educational Product. For Instructional Use Only.

Appendix B

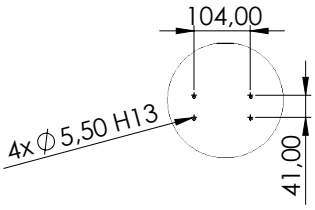
BOM - Bill of Materials

Number	Name	Description	Quantity
1	SCHUNK-0819013 ROTA-S plus2_0 250-62 C5-SFG	Ø62 mm; 210 Nm Supplier: SCHUNK	2
2	2023.body.1	Bending Mirror Material: Ck45	1
3	2023.body.2	Torsion Mirror Material: Ck45	1
4	2023.body.3	Horizontal Articulation Material: Ck45	4
5	2023.body.4	Right Triangle Material: Ck45	2
6	2023.body.5	Left Triangle Material: Ck45	2
7	2023.body.6	Vertical Articulation Material: Ck45	4
8	2023.body.7	Support Material: Ck45	2
9	2023.body.8	Shaft Ø18 mm Material: Ck45	10
10	2023.body.9	Shaft Ø25 mm Material: Ck45	2
11	2023.body.10	Adaptor Material: Ck45	2
12	2023.body.11	Spacer Material: Ck45	4
13	2023.body.12	Jaw Adaptor 1 Material: Ck45	6
14	2023.body.13	Jaw Adaptor 2 Material: Ck45	6
15	2023.eccentric.1	Superior Part of Crank Material: Ck45	2
16	2023.eccentric.2	Inferior Part of Crank Material: Ck45	2
17	2023.eccentric.3	Free Eccentric Material: Ck45	2
18	2023.eccentric.4	Fixed Eccentric Material: Ck45	2
19	2023.eccentric.5	Locking Cap Material: Ck45	2
20	2023.eccentric.6	Shaft Ø15 mm Material: Ck45	2
21	2023.eccentric.7	Support Material: Ck45	4
22	2023.eccentric.8	Key Material: Ck45	2
23	2023.base.1	Base Material: Ck45	1
24	Washer DIN 125-1 A 10.5 38130.100.001	DIN 125-1 A 10.5 Supplier: Fabory	16

25	Cylinder head screw DIN 912 M10x35 07160.100.035	DIN 912 M10x35 Supplier: Fabory	8
26	Washer DIN 9021 8.4 38210.080.001	DIN 9021 8.4 Supplier: Fabory	28
27	Cylinder head screw DIN 912 M8x20 07160.080.020	DIN 912 M8x20 Supplier: Fabory	28
28	Cylinder head screw DIN 912 M10x75 53570.100.075	DIN 912 M10x75 Supplier: Fabory	8
29	2023.body.14	Shaft Ø18 mm Material: Ck45	2
30	Hexagon nut DIN 934 M10 01300_100_001	DIN 934 M10 Supplier: Fabory	8
31	Washer DIN 125-1 A 19 38130.180.001	DIN 125-1 A 19 Supplier: Fabory	20
32	K0310_03	Spring Plunger M3 Supplier: Fabory	2
33	Hexagon nut DIN 439 B M3 11360.030.001	DIN 439 B M3 Supplier: Fabory	2
34	egb1810-e40	Permaglide Bearing Supplier: Schaeffler	44
35	SKF_61802_ir	Ball Bearing 16004 Supplier: SKF	8
36	Cylinder head screw DIN 912 M5x12 07160_050_012	DIN 912 M5x12 Supplier: Fabory	4
37	Cylinder head screw DIN 912 M12x25 07160.120.025	DIN 912 M12x25 Supplier: Fabory	12
38	Hexagon nut DIN 934 M5 01300.050.001	DIN 934 M5 Supplier: Fabory	8
39	Cylinder head screw DIN 912 M5x25 07160.050.025	DIN 912 M5x25 Supplier: Fabory	8
40	Washer DIN 125-1 A 5.3 38130.050.001	DIN 125-1 A 5.3 Supplier: Fabory	8

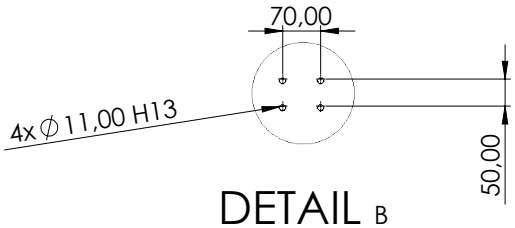
Appendix C

Technical drawings



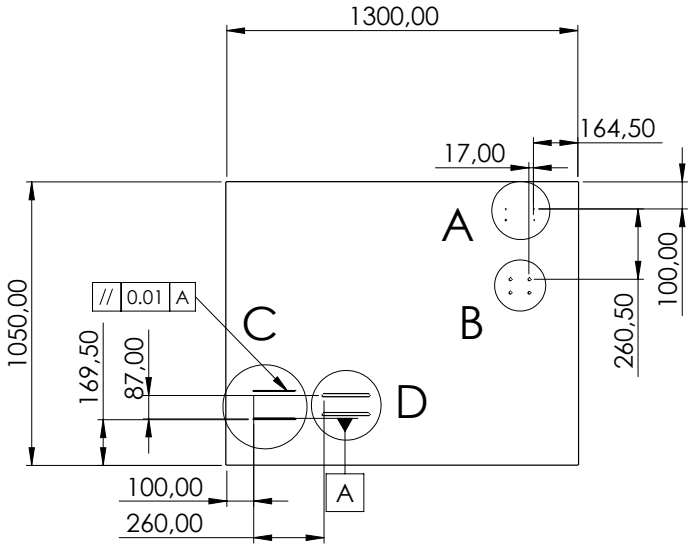
DETAIL A

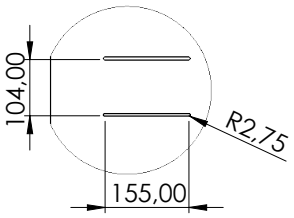
SCALE 1 : 10



DETAIL B

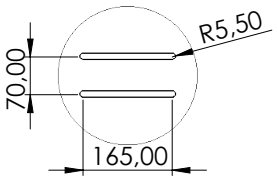
SCALE 1 : 10





DETAIL C

SCALE 1 : 10



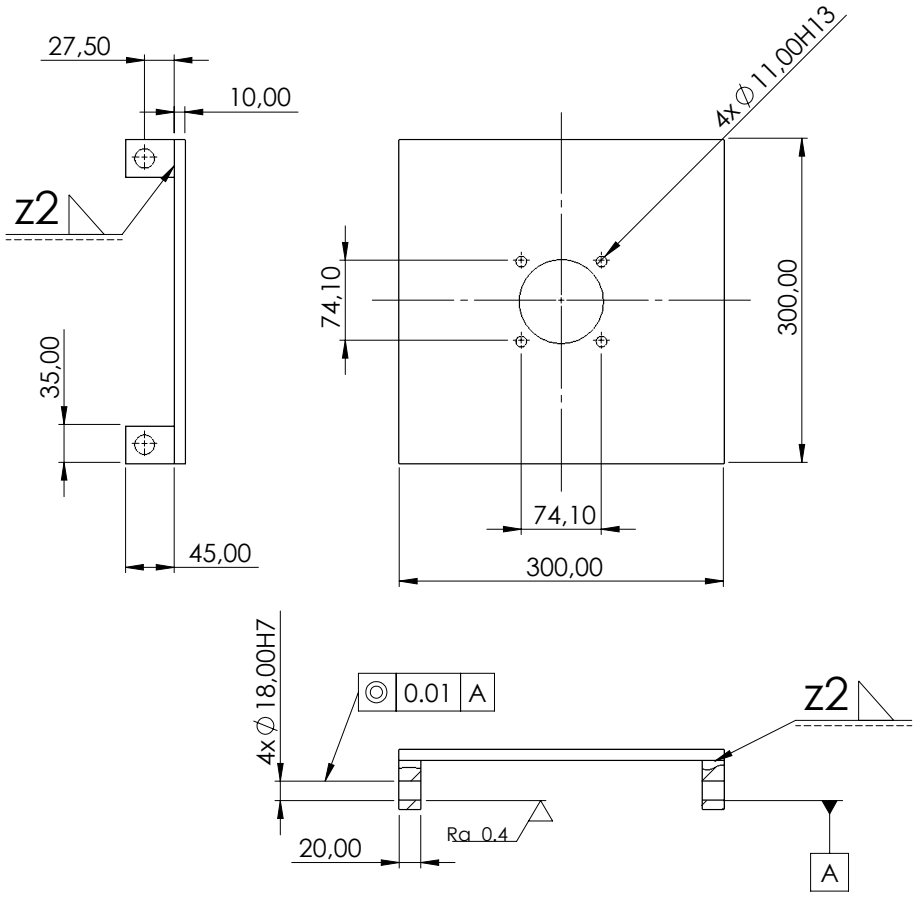
DETAIL D

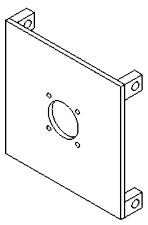
SCALE 1 : 10

t = 10 mm

	Nome	Data				Folha	1/1
Des.	Beatriz Ferreira	12/09/2023	A4	inegi		Massa (g)	
						Tratamento	
ISO 2768	mK	mm	Escala-1:50			Material	
Referência	**2023.base.1**					**Quantidade**	

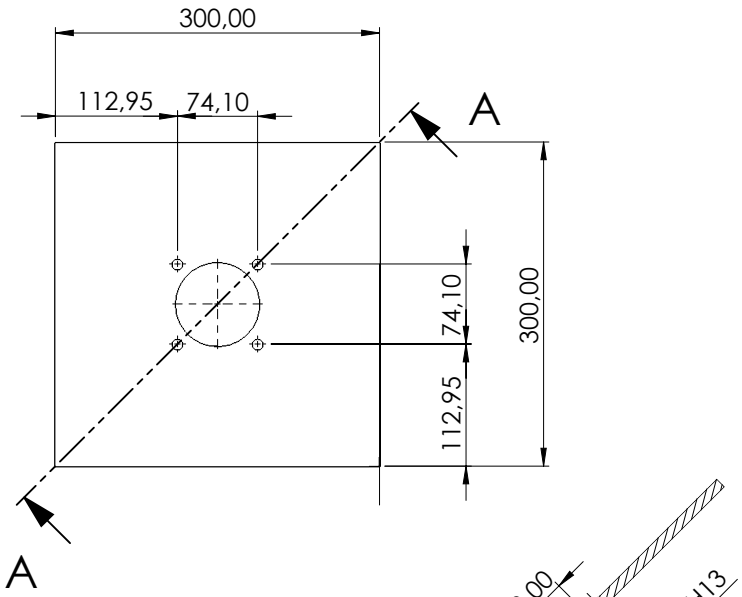
SOLIDWORKS Educational Product. For Instructional Use Only.

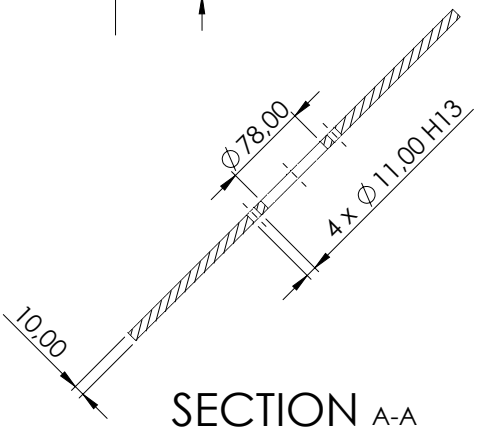




	Nome	Data				Folha	1/1
Des.	Beatriz Ferreira	11/09/2023	A4	inegi		Massa (g)	
						Tratamento	
ISO 2768 ISO 13920		mK	mm	Escala-1:5		Material	
Referência	**2023.body.1**					**Quantidade**	

SOLIDWORKS Educational Product. For Instructional Use Only.

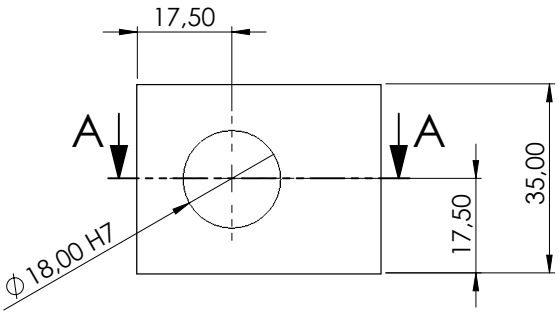


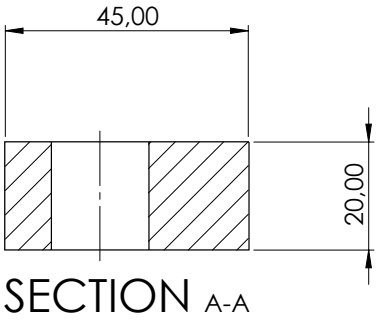


SECTION A-A

	Nome	Data				Folha	1/1
Des.	Beatriz Ferreira	16/09/2023	A4	inegi		Massa (g)	
						Tratamento	
ISO 2768		mK	mm	Escala-1:5		Material	
Referência		**2023.body.1.1**				**Quantidade**	

SOLIDWORKS Educational Product. For Instructional Use Only.

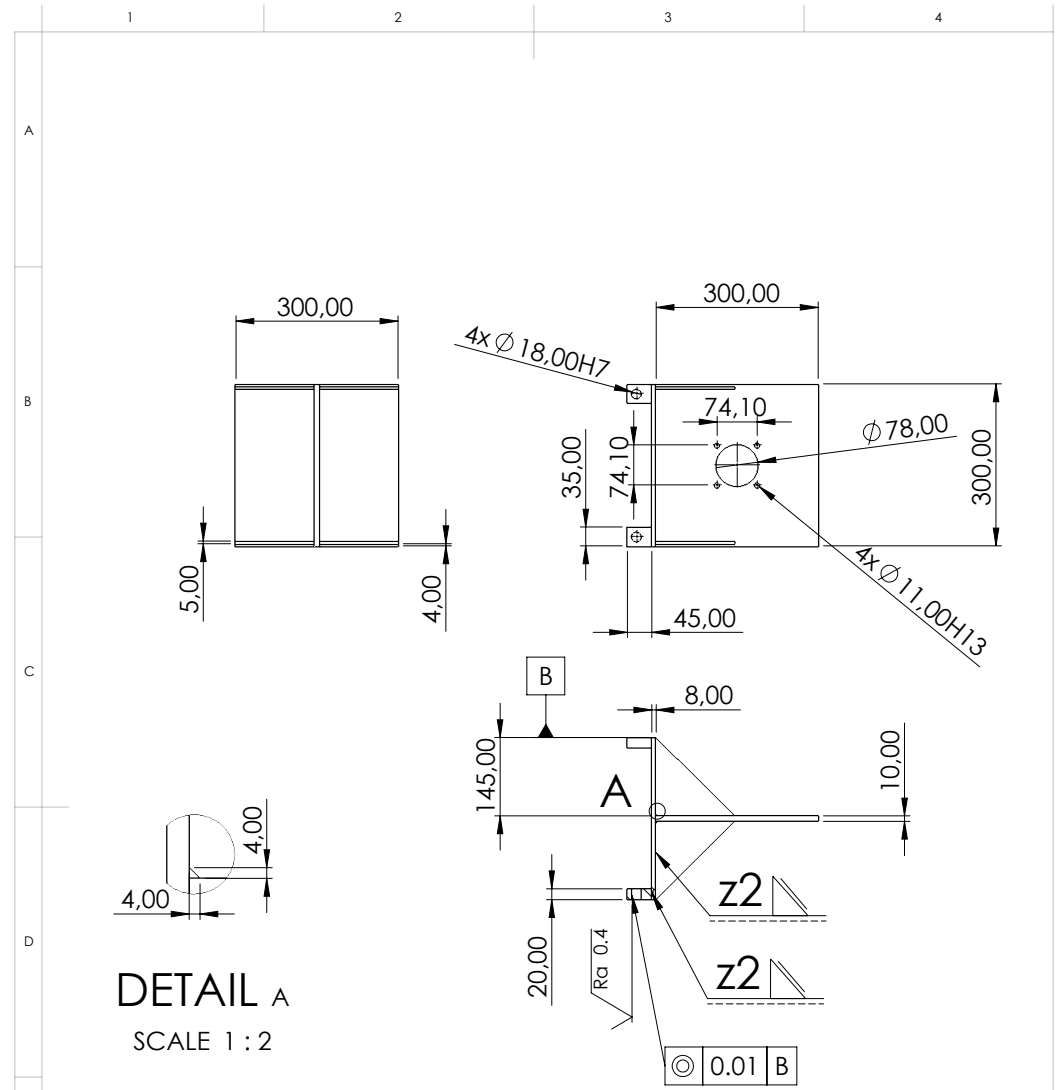




SECTION A-A

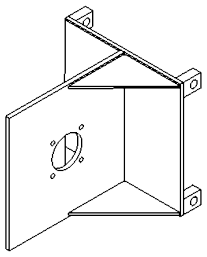
	Nome	Data				Folha	1/1
Des.	Beatriz Ferreira	16/09/2023	A4	inegi		Massa (g)	
						Tratamento	
ISO 2768	mK	mm	Escala-1:1			Material	
Referência	**2023.body.1.2**					**Quantidade**	

SOLIDWORKS Educational Product. For Instructional Use Only.



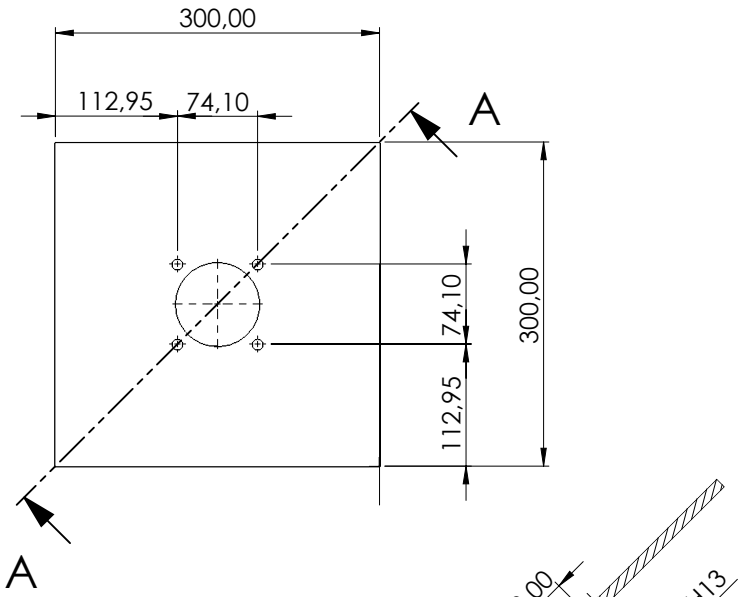
DETAIL A

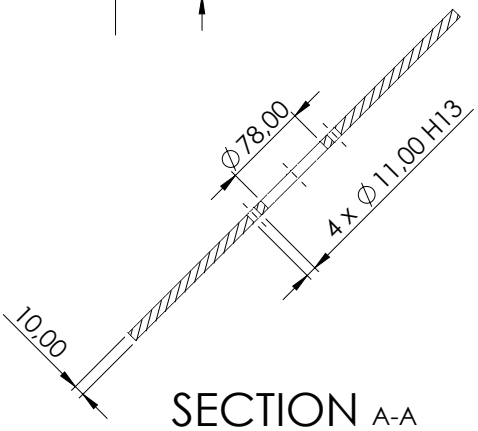
SCALE 1 : 2



	Nome	Data				Folha	1/1
Des.	Beatriz Ferreira	11/09/2023	A4	inegi		Massa (g)	
						Tratamento	
ISO 2768 ISO 13920 - BE		mK	mm	Escala-1:10		Material	
Referência		**2023.body.2**				**Quantidade**	

SOLIDWORKS Educational Product. For Instructional Use Only.

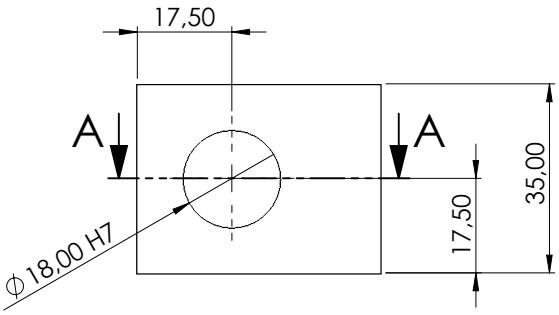


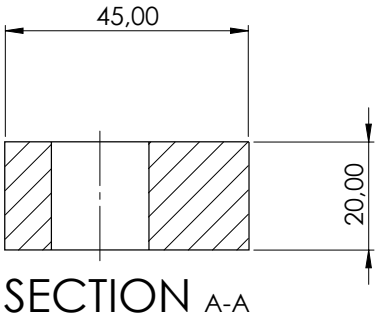


SECTION A-A

	Nome	Data				Folha	1/1
Des.	Beatriz Ferreira	16/09/2023	A4	inegi		Massa (g)	
						Tratamento	
ISO 2768		mK	mm	Escala-1:5		Material	
Referência		**2023.body.1.1**				**Quantidade**	

SOLIDWORKS Educational Product. For Instructional Use Only.

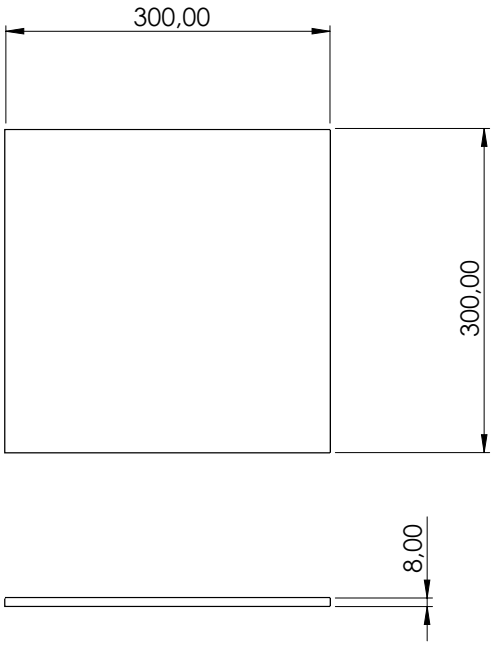




SECTION A-A

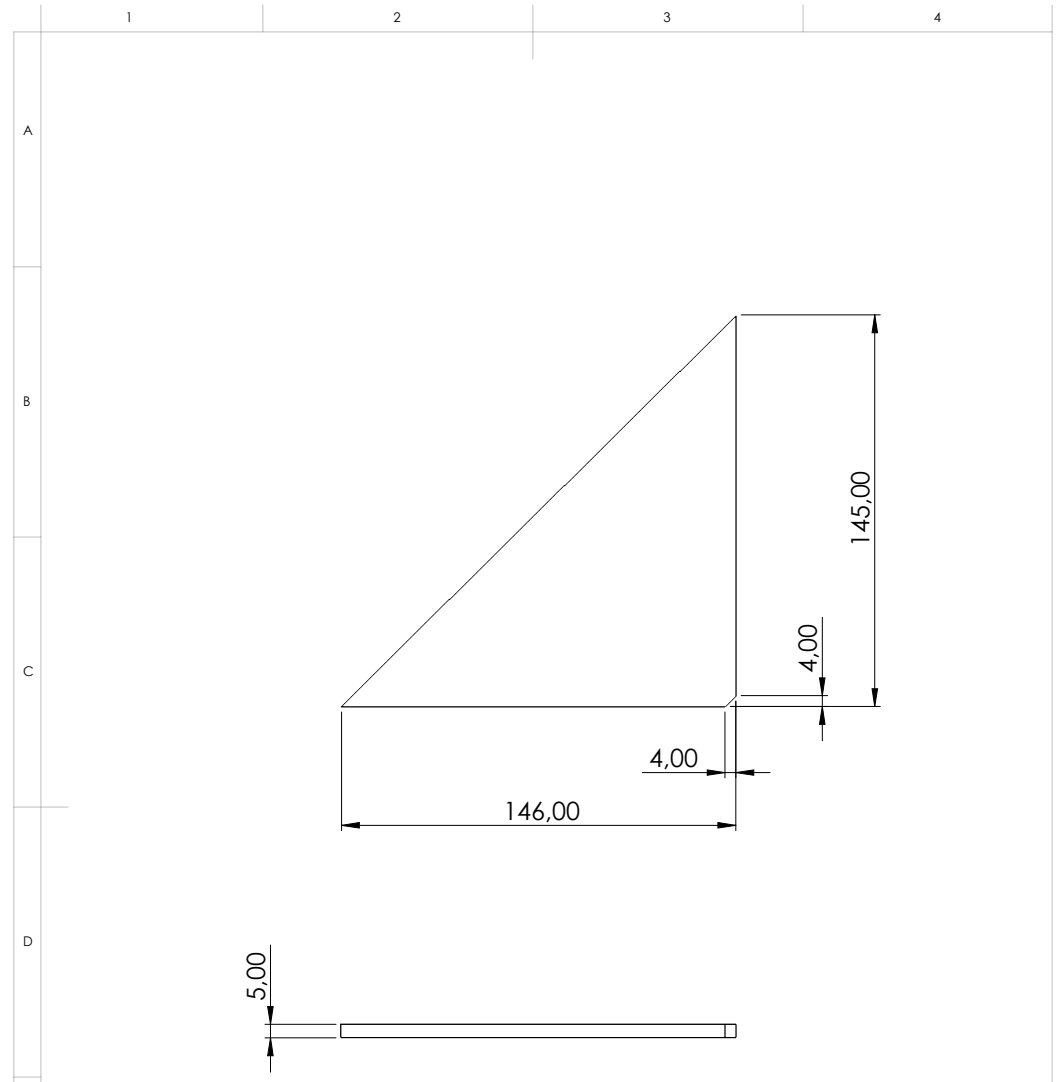
	Nome	Data				Folha	1/1
Des.	Beatriz Ferreira	16/09/2023	A4	inegi		Massa (g)	
						Tratamento	
ISO 2768	mK	mm	Escala-1:1			Material	
Referência	**2023.body.1.2**					**Quantidade**	

SOLIDWORKS Educational Product. For Instructional Use Only.



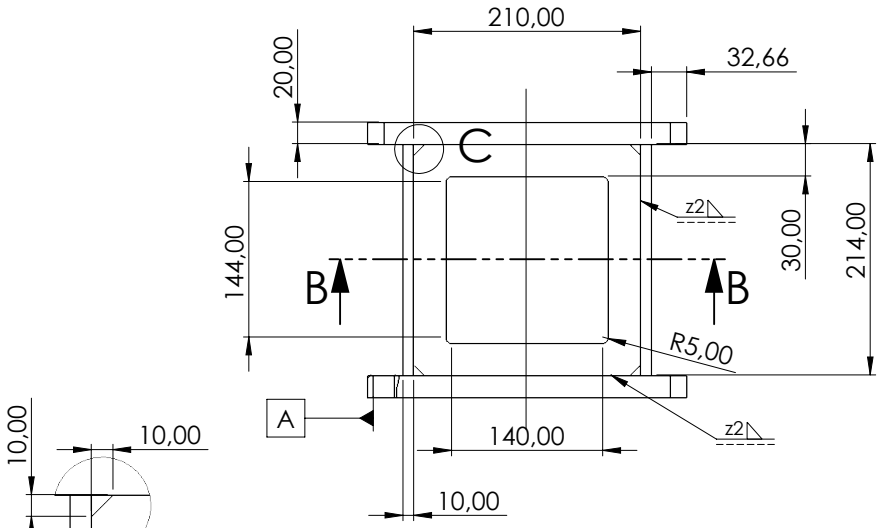
	Nome	Data				Folha	1/1
Des.	Beatriz Ferreira	16/09/2023	A4	inegi		Massa (g)	
						Tratamento	
ISO 2768		mK	mm	Escala-1:5		Material	
Referência	**2023.body.1.3**					**Quantidade**	

SOLIDWORKS Educational Product. For Instructional Use Only.



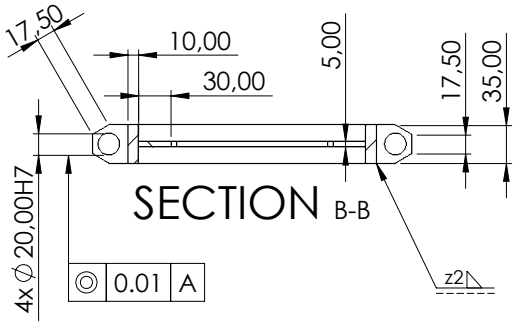
	Nome	Data				Folha	1/1
Des.	Beatriz Ferreira	16/09/2023	A4	inegi		Massa (g)	
						Tratamento	
ISO 2768		mK	mm	Escala-1:2		Material	
Referência	**2023.body.1.4**					**Quantidade**	

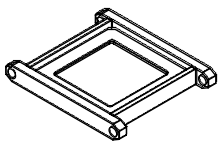
SOLIDWORKS Educational Product. For Instructional Use Only.



DETAIL C

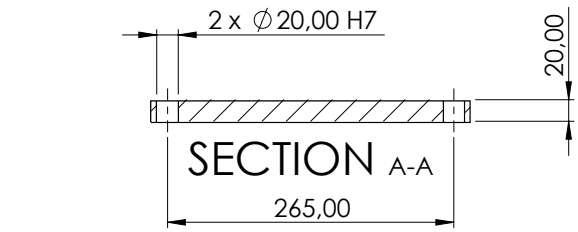
SCALE 2 : 5

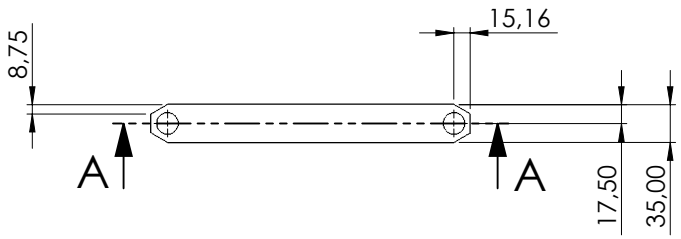




	Nome	Data				Folha	1/1
Des.	Beatriz Ferreira	12/09/2023	A4	inegi		Massa (g)	
						Tratamento	
ISO 2768 ISO 13920 - BE		mK	mm	Escala-1:5		Material	
Referência		**2023.body.3**				**Quantidade**	

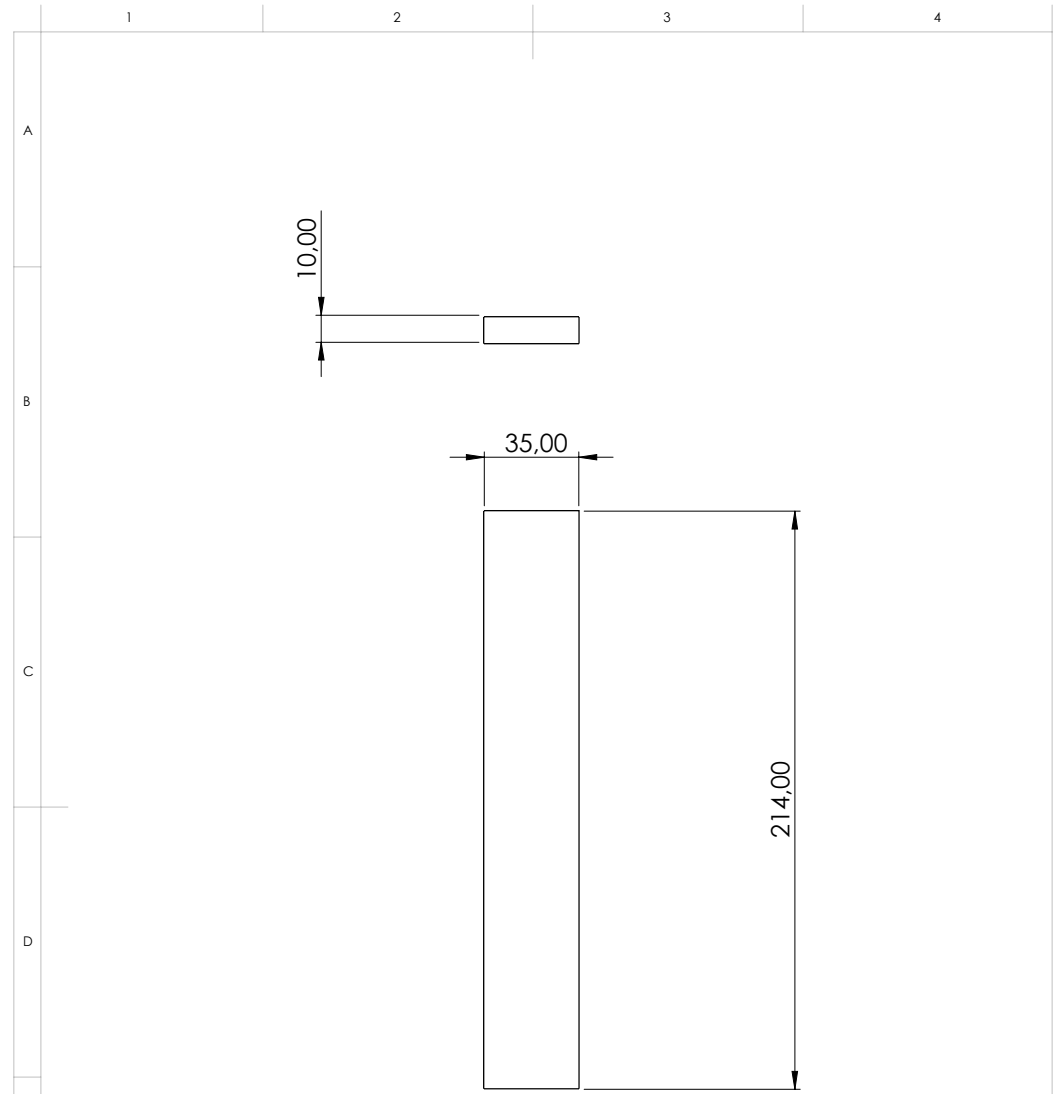
SOLIDWORKS Educational Product. For Instructional Use Only.





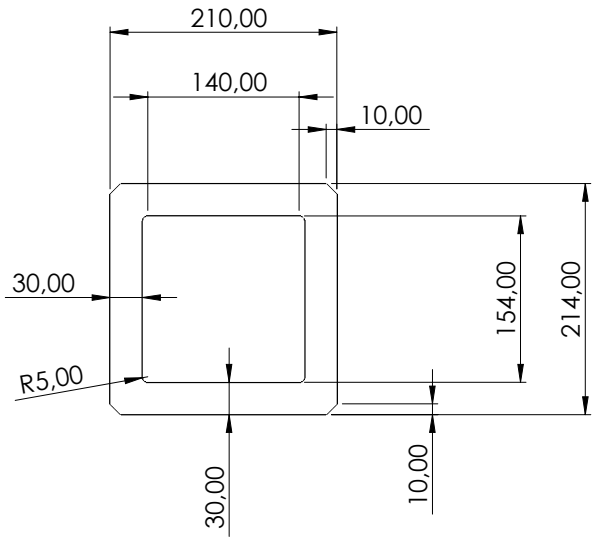
	Nome	Data				Folha	1/1
Des.	Beatriz Ferreira	18/09/2023	A4	inegi		Massa (g)	
						Tratamento	
ISO 2768	mK	mm	Escala-1:5			Material	
Referência	**2023.body.3.1**					**Quantidade**	

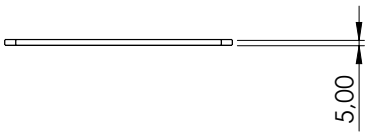
SOLIDWORKS Educational Product. For Instructional Use Only.



	Nome	Data				Folha	1/1
Des.	Beatriz Ferreira	18/09/2023	A4	inegi		Massa (g)	
						Tratamento	
ISO 2768	mK	mm	Escala-1:2			Material	
Referência	**2023.body.3.2**					**Quantidade**	

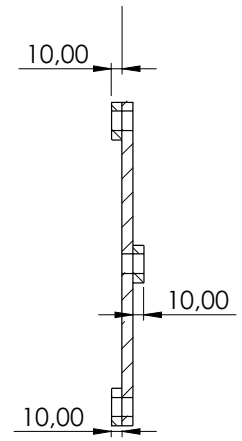
SOLIDWORKS Educational Product. For Instructional Use Only.



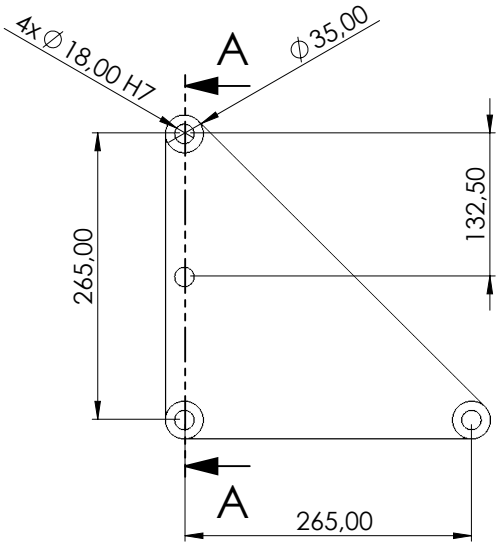


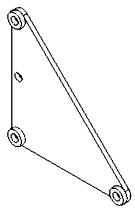
	Nome	Data				Folha	1/1
Des.	Beatriz Ferreira	18/09/2023	A4	inegi		Massa (g)	
						Tratamento	
ISO 2768		mK	mm	Escala-1:5		Material	
Referência		**2023.body.3.3**				**Quantidade**	

SOLIDWORKS Educational Product. For Instructional Use Only.



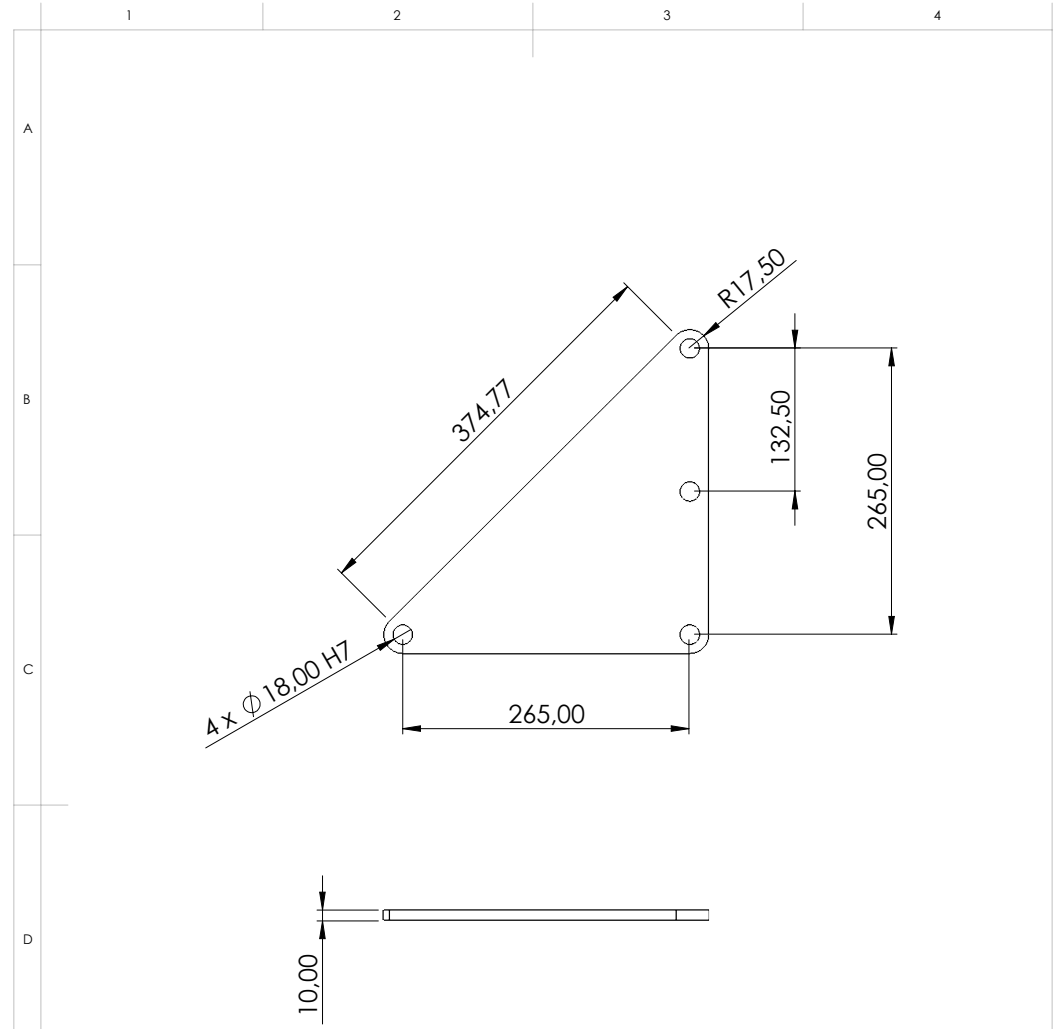
SECTION A-A





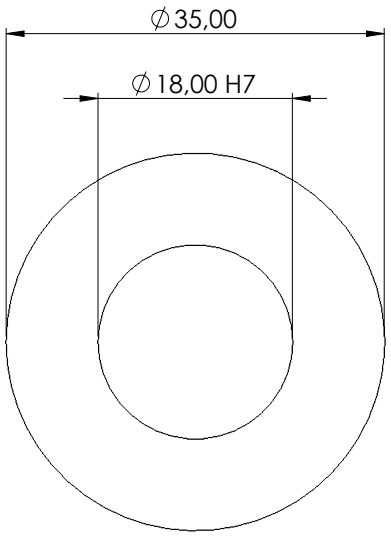
	Nome	Data				Folha	1/1
Des.	Beatriz Ferreira	11/09/2023	A4	inegi		Massa (g)	
						Tratamento	
ISO 2768 ISO 13920 - BE		mK	mm	Escala-1:5		Material	
Referência		**2023.body.5**				**Quantidade**	

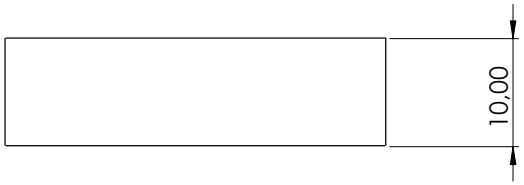
SOLIDWORKS Educational Product. For Instructional Use Only.



	Nome	Data				Folha	1/1
Des.	Beatriz Ferreira	17/09/2023	A4	inegi		Massa (g)	
						Tratamento	
ISO 2768	mK	mm	Escala-1:5			Material	
Referência	**2023.body.5.1**					**Quantidade**	

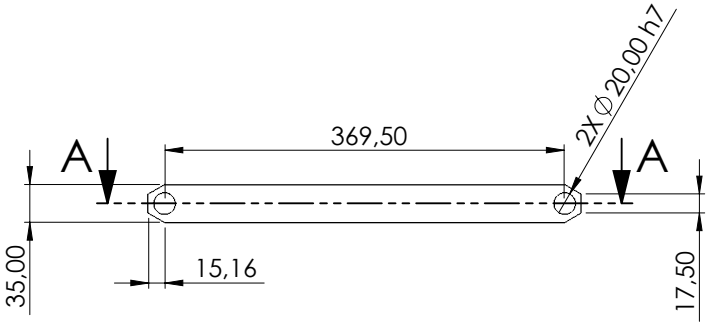
SOLIDWORKS Educational Product. For Instructional Use Only.

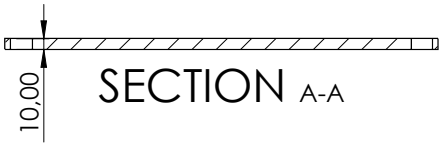


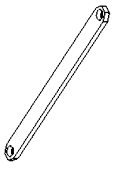


	Nome	Data				Folha	1/1
Des.	Beatriz Ferreira	17/09/2023	A4	inegi		Massa (g)	
						Tratamento	
ISO 2768	mK	mm	Escala-2:1			Material	
Referência	**2023.body.5.2**					**Quantidade**	

SOLIDWORKS Educational Product. For Instructional Use Only.

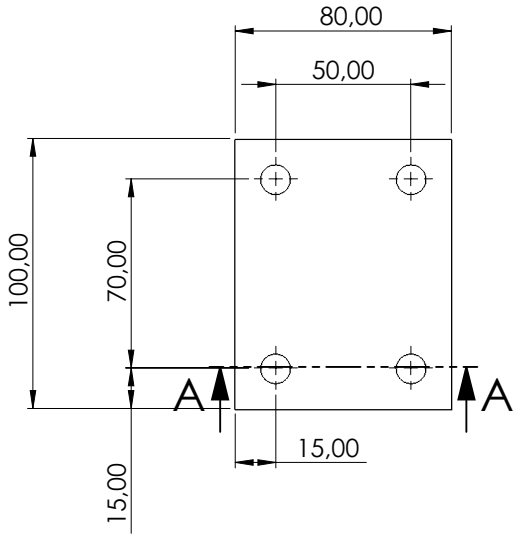


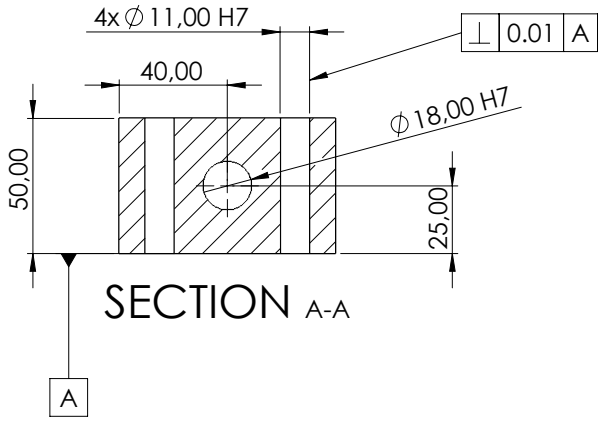


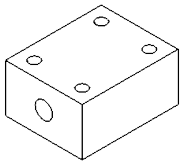


	Nome	Data				Folha	1/1
Des.	Beatriz Ferreira	11/09/2023	A4	inegi		Massa (g)	
						Tratamento	
ISO 2768	mK	mm	Escala-1:5			Material	
Referência	**2023.body.6**					**Quantidade**	

SOLIDWORKS Educational Product. For Instructional Use Only.



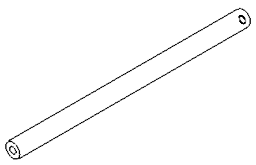




	Nome	Data				Folha	1/1
Des.	Beatriz Ferreira	11/09/2023	A4	inegi		Massa (g)	
						Tratamento	
ISO 2768	mK	mm	Escala-1:2			Material	
Referência	**2023.body.7**					**Quantidade**	

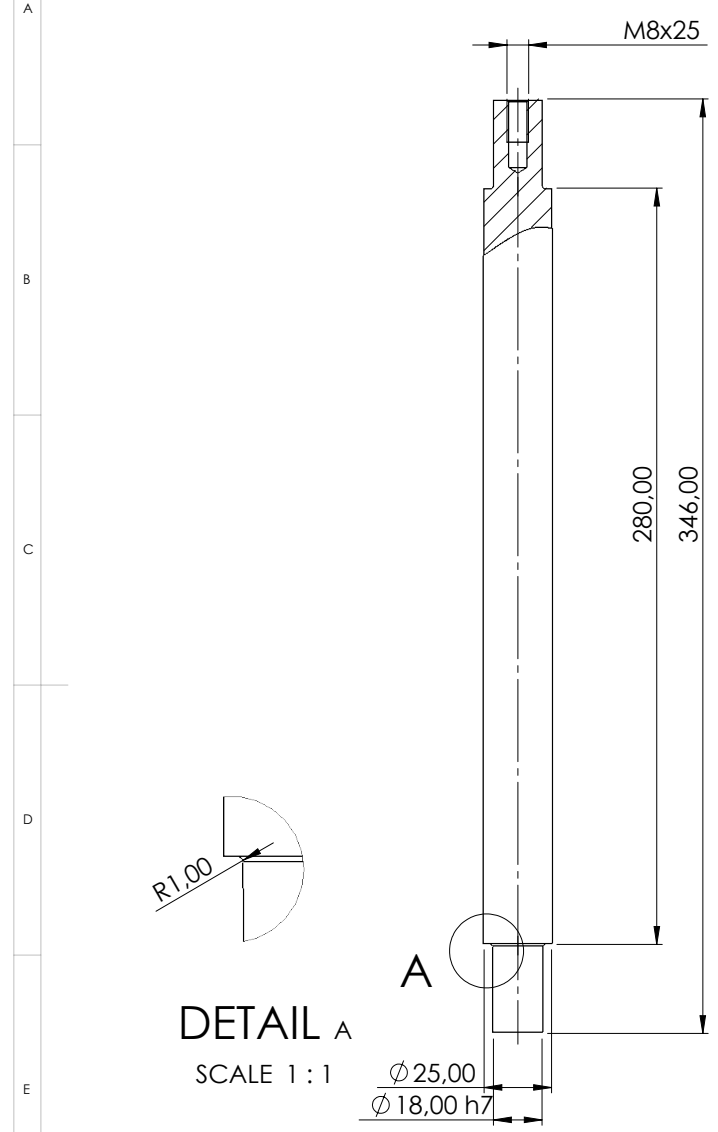
SOLIDWORKS Educational Product. For Instructional Use Only.

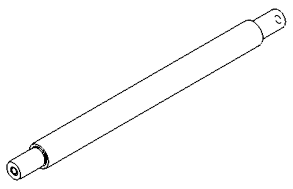




	Nome	Data				Folha	1/1
Des.	Beatriz Ferreira	12/09/2023	A4	inegi		Massa (g)	
						Tratamento	
ISO 2768		mK	mm	Escala-1:5		Material	
Referência		**2023.body.8**				**Quantidade**	

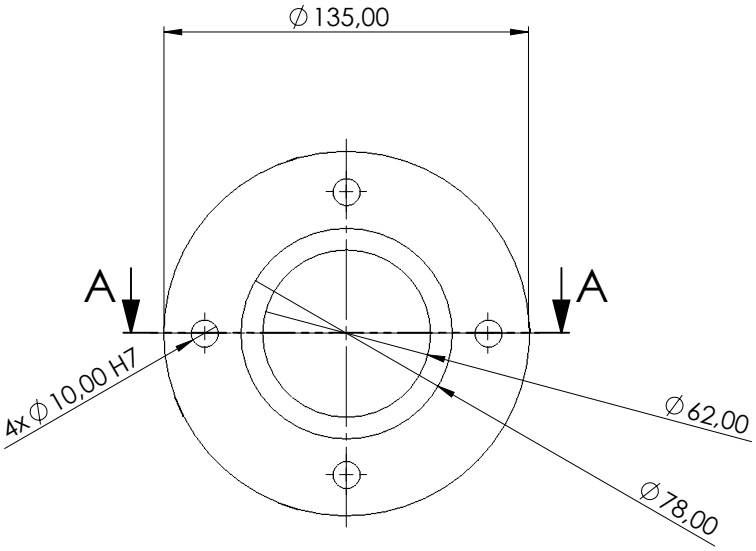
SOLIDWORKS Educational Product. For Instructional Use Only.

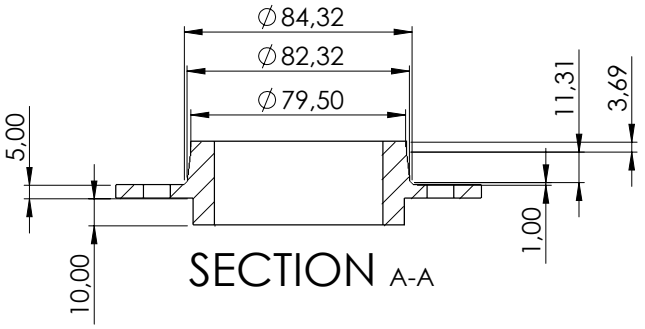


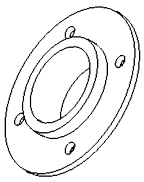


	Nome	Data				Folha	1/1
Des.	Beatriz Ferreira	12/09/2023	A4	inegi		Massa (g)	
						Tratamento	
ISO 2768		mK	mm	Escala-1:5		Material	
Referência		**2023.body.9**				**Quantidade**	

SOLIDWORKS Educational Product. For Instructional Use Only.

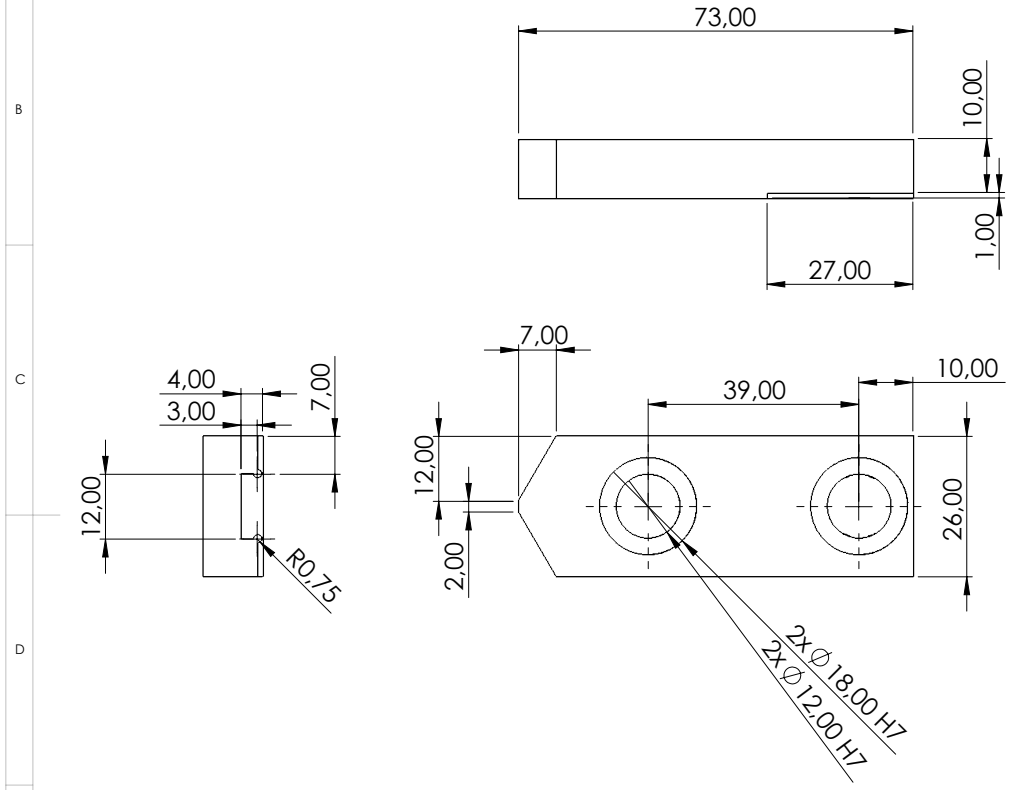






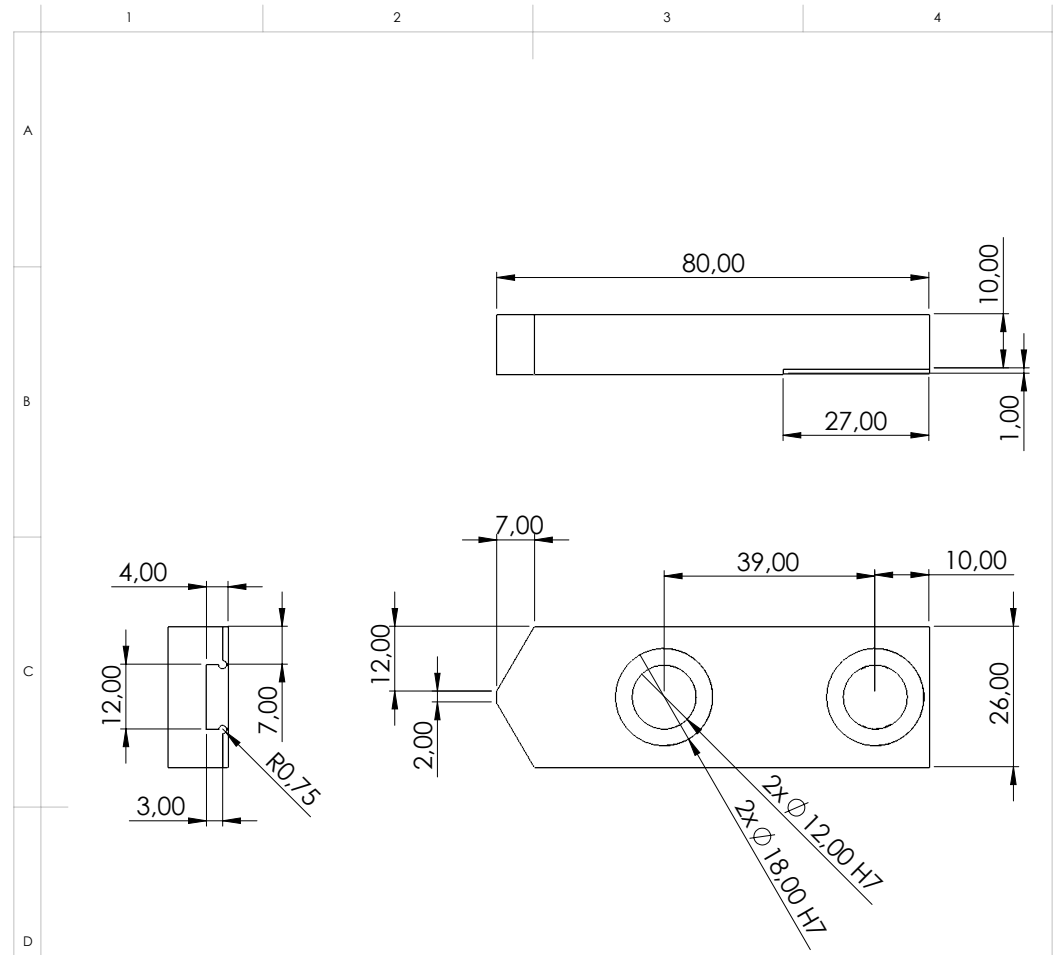
	Nome	Data				Folha	1/1
Des.	Beatriz Ferreira	11/09/2023	A4	inegi		Massa (g)	
						Tratamento	
ISO 2768		mK	mm	Escala-1:2		Material	
Referência		**2023.body.10**				**Quantidade**	

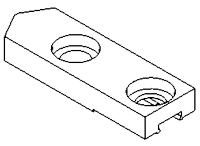
SOLIDWORKS Educational Product. For Instructional Use Only.



	Nome	Data				Folha	1/1
Des.	Beatriz Ferreira	12/09/2023	A4	inegi		Massa (g)	
						Tratamento	
ISO 2768	mK	mm	Escala-1:1			Material	
Referência	**JawAdaptor119**					**Quantidade**	

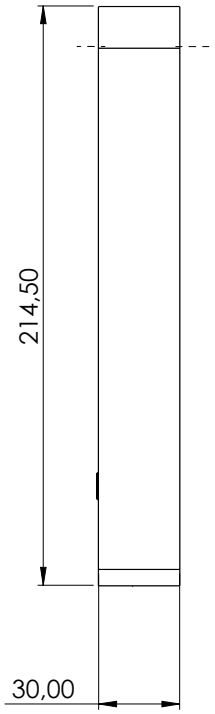
SOLIDWORKS Educational Product. For Instructional Use Only.

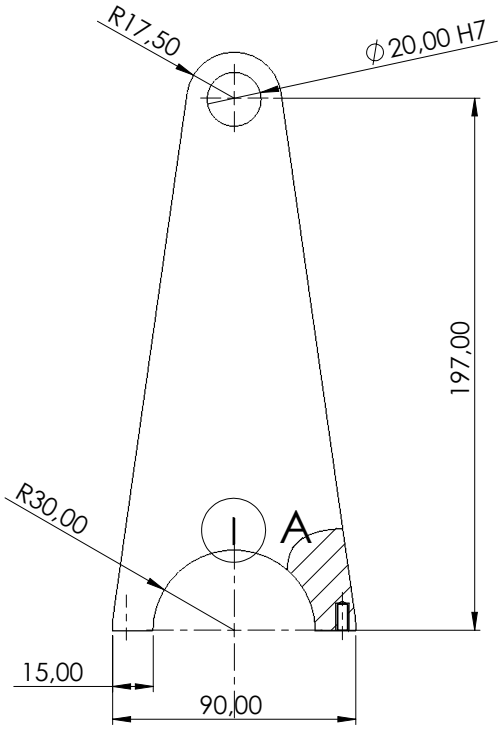


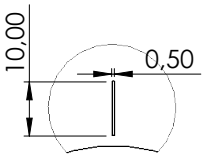


	Nome	Data				Folha	1/1
Des.	Beatriz Ferreira	12/09/2023	A4	inegi		Massa (g)	
						Tratamento	
ISO 2768		mK	mm	Escala-1:1		Material	
Referência	**JawAdaptor126**					**Quantidade**	

SOLIDWORKS Educational Product. For Instructional Use Only.

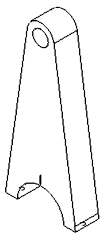






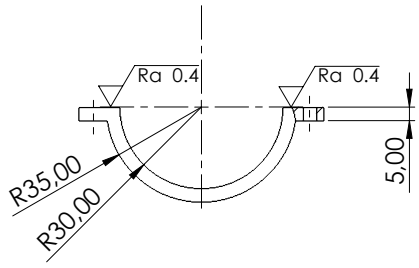
DETAIL A

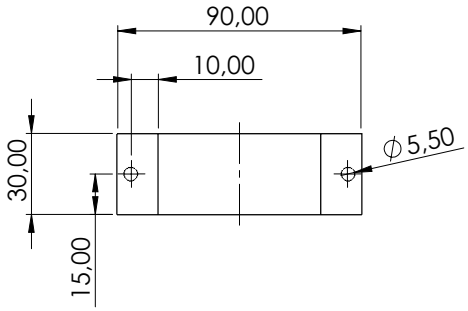
SCALE 1 : 1

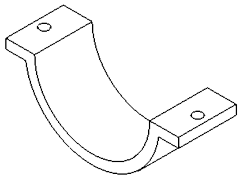


	Nome	Data				Folha	1/1
Des.	Beatriz Ferreira	12/09/2023	A4	inegi		Massa (g)	
						Tratamento	
ISO 2768		mK	mm	Escala-1:2		Material	
Referência		**2023.eccentric.1**				**Quantidade**	

SOLIDWORKS Educational Product. For Instructional Use Only.

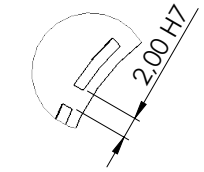




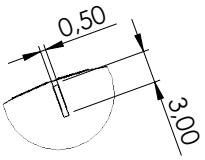


	Nome	Data				Folha	1/1
Des.	Beatriz Ferreira	12/09/2023	A4	inegi		Massa (g)	
						Tratamento	
ISO 2768	mK	mm	Escala-1:2			Material	
Referência	**2023.eccentric.2**					**Quantidade**	

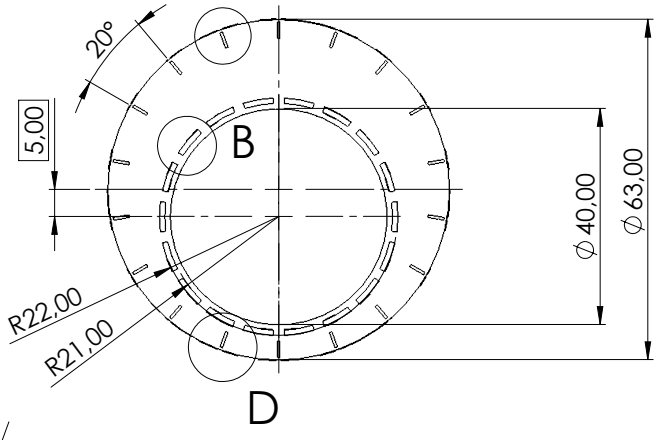
SOLIDWORKS Educational Product. For Instructional Use Only.

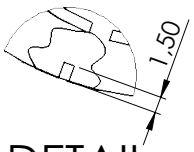


DETAIL B
SCALE 2 : 1

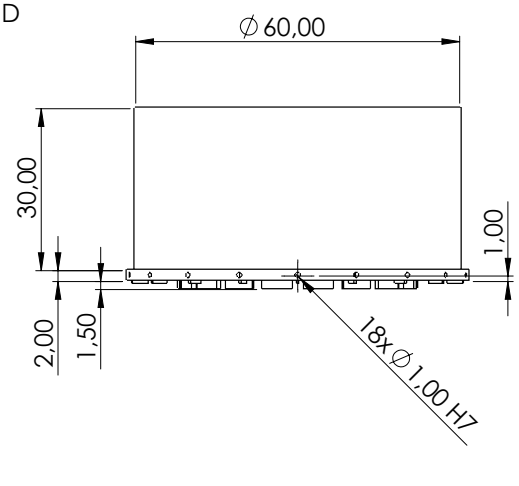


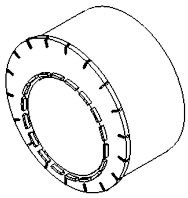
DETAIL C
SCALE 2 : 1





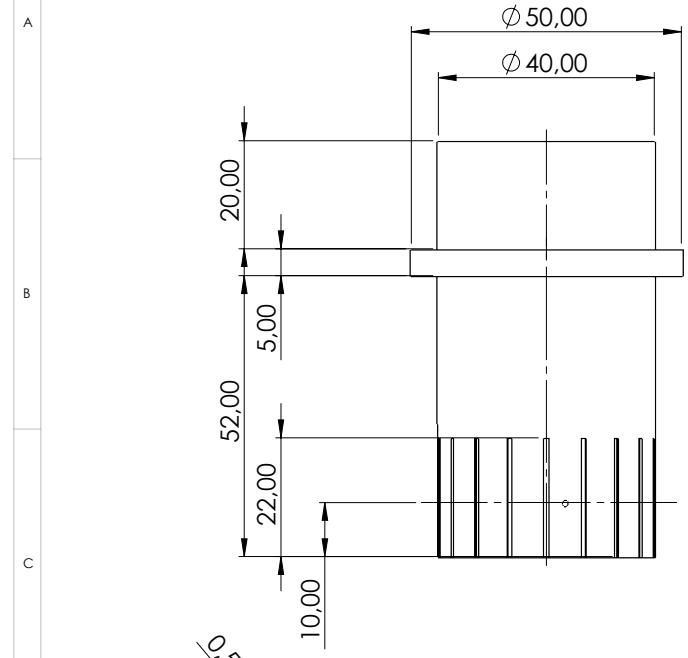
DETAIL D
SCALE 2 : 1

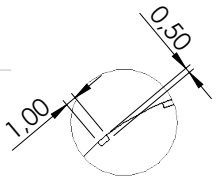




	Nome	Data				Folha	1/1
Des.	Beatriz Ferreira	12/09/2023	A4	inegi		Massa (g)	
						Tratamento	
ISO 2768	mK	mm	Escala-1:1			Material	
Referência	**2023.eccentric.3**					**Quantidade**	

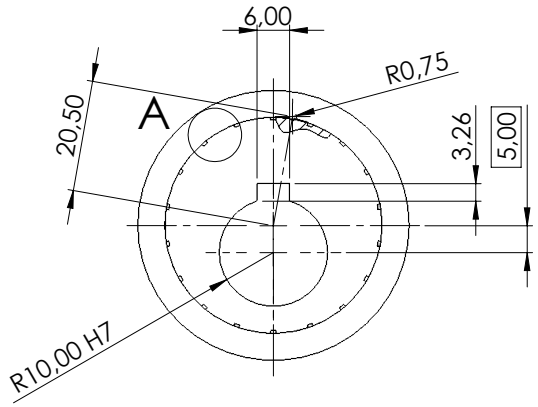
SOLIDWORKS Educational Product. For Instructional Use Only.





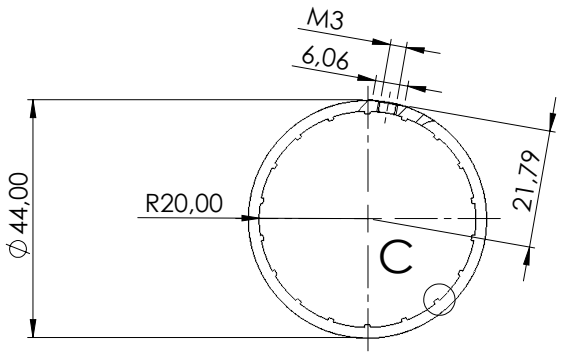
DETAIL A

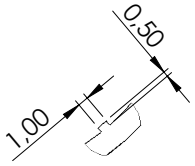
SCALE 2 : 1



	Nome	Data				Folha	1/1
Des.	Beatrz Ferreira	12/09/2023	A4	inegi		Massa (g)	
						Tratamento	
ISO 2768	mK	mm	Escala-1:2			Material	
Referência	**2023.eccentric.4**					**Quantidade**	

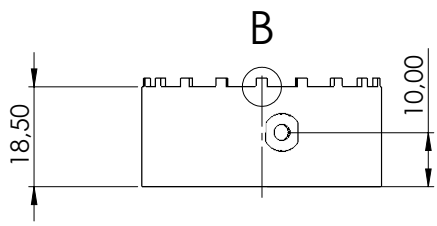
SOLIDWORKS Educational Product. For Instructional Use Only.

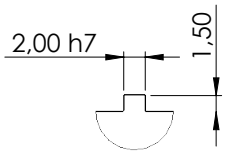




DETAIL C

SCALE 2 : 1



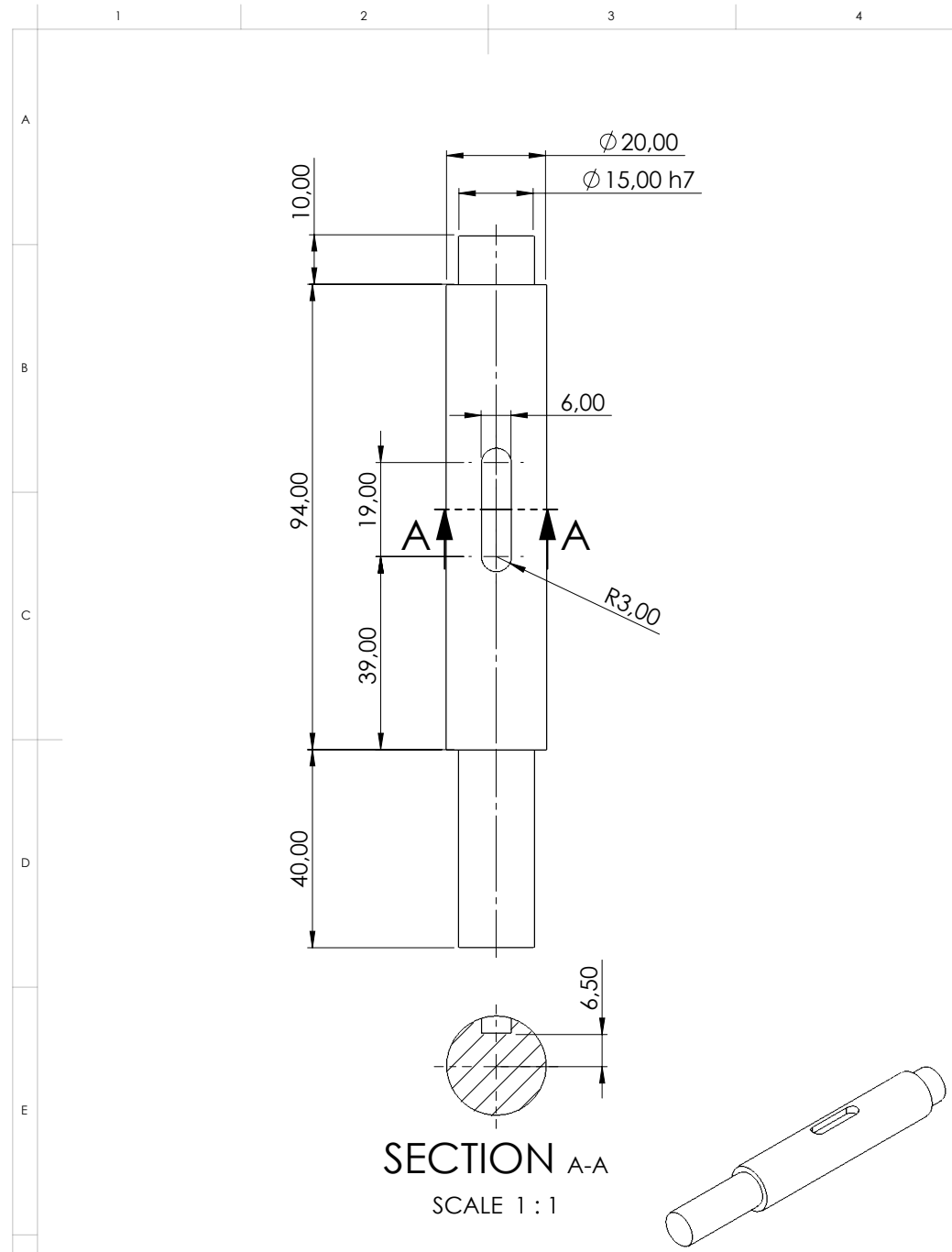


DETAIL B

SCALE 2 : 1

	Nome	Data				Folha	1/1
Des.	Beatriz Ferreira	12/09/2023	A4	inegi		Massa (g)	
						Tratamento	
ISO 2768	mK	mm	Escala-1:1			Material	
Referência	**2023.eccentric.5**					**Quantidade**	

SOLIDWORKS Educational Product. For Instructional Use Only.

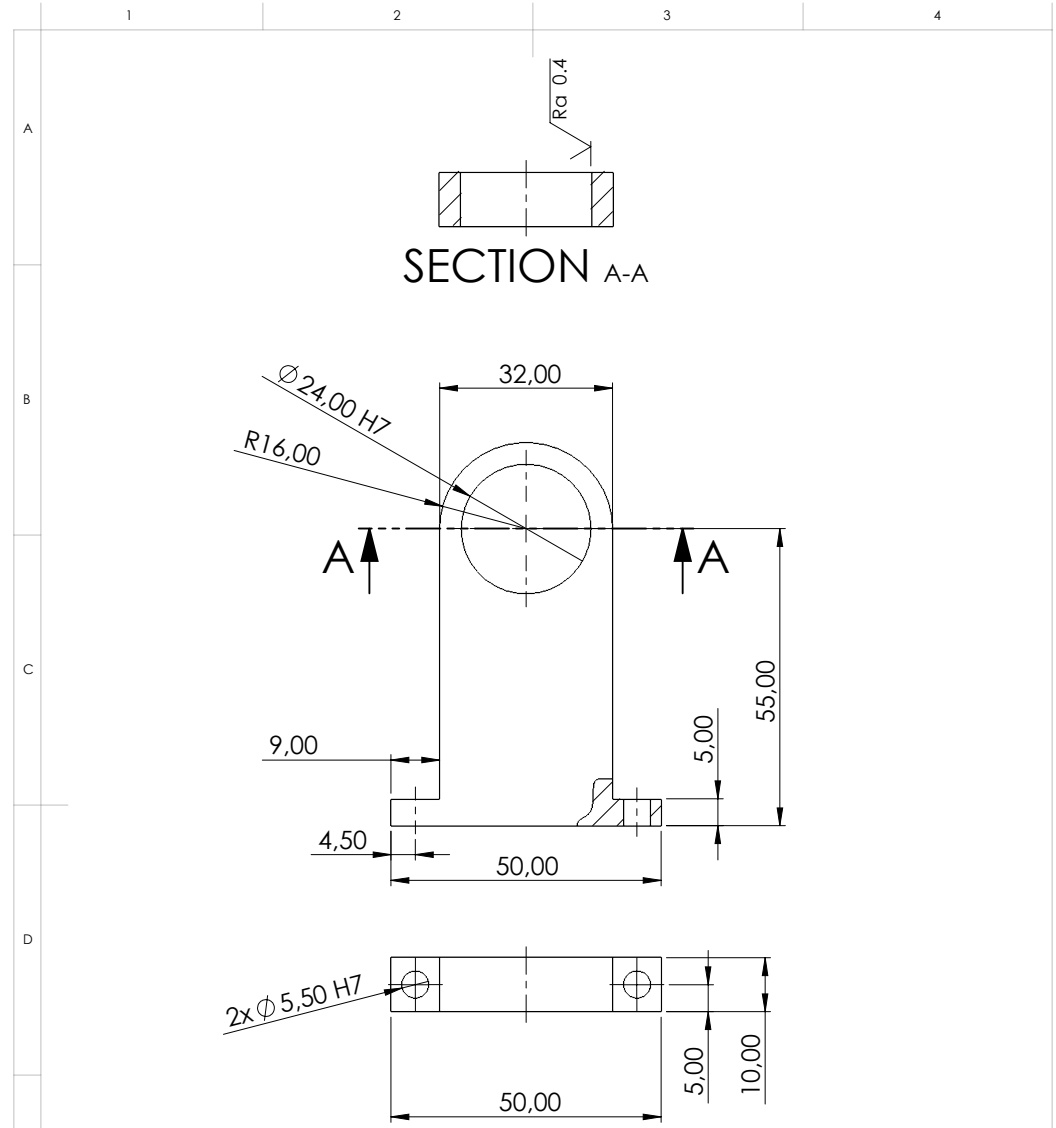


SECTION A-A

SCALE 1 : 1

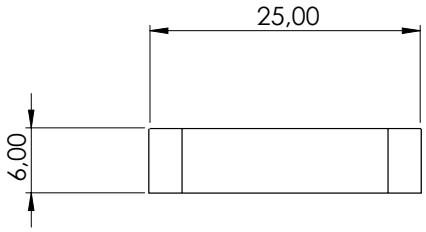
	Nome	Data				Folha	1/1
Des.	Beatriz Ferreira	12/09/2023	A4	inegi		Massa (g)	
						Tratamento	
ISO 2768		mK	mm	Escala-1:2		Material	
Referência		**2023.eccentric.6**				**Quantidade**	

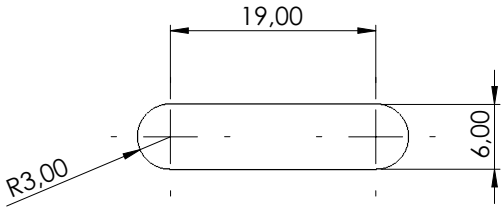
SOLIDWORKS Educational Product. For Instructional Use Only.

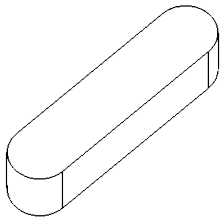


	Nome	Data				Folha	1/1
Des.	Beatriz Ferreira	12/09/2023	A4	inegi		Massa (g)	
						Tratamento	
ISO 2768	mK	mm	Escala-1:1			Material	
Referência	**2023.eccentric.7**					**Quantidade**	

SOLIDWORKS Educational Product. For Instructional Use Only.





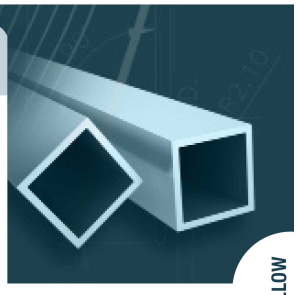


	Nome	Data				Folha	1/1
Des.	Beatriz Ferreira	12/09/2023	A4	inegi		Massa (g)	
						Tratamento	
ISO 2768	mK	mm	Escala-2:1			Material	
Referência	**2023.eccentric.8**					**Quantidade**	

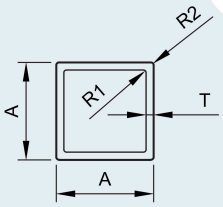
SOLIDWORKS Educational Product. For Instructional Use Only.

Appendix D

Wispeco Catalog



HOLLOW



SECTION NO.	RANGE	A	T	R1	R2	Kg/m	PAINT PERIMETER	ANODIZED PERIMETER
42357	> 10mm	11.80	1.20	0.30	0.30	0.138	100	100
50055		12.00	1.20	0.30	0.30	0.140	100	100
55783		12.70	1.50	0.30	0.30	0.182	100	100
42326		15.00	1.20	0.30	0.30	0.179	100	100
57018		16.00	1.20	0.30	0.30	0.193	100	100
53664		16.00	1.60	0.30	0.30	0.248	100	100
42912		18.00	1.20	0.30	0.30	0.219	100	103
54060		19.00	1.50	0.30	0.30	0.285	100	108
50060		19.00	1.60	0.30	0.30	0.302	107	107
50059		19.00	3.20	0.30	0.30	0.548	100	101
42406	> 20mm	20.00	1.10	0.30	0.30	0.226	100	116
55884		20.00	1.10	3.90	5.00	0.202	100	104
52493		20.00	1.30	0.30	1.00	0.261	100	113
42179		20.00	1.50	0.60	0.60	0.301	100	114
10871		20.00	1.50	0.30	0.30	0.301	100	114
00193		20.00	1.60	0.30	0.30	0.319	100	113
56060		20.00	2.00	0.30	0.30	0.391	100	111
50064		21.00	1.20	0.30	0.30	0.257	100	120
42435		21.00	1.30	0.40	0.40	0.277	100	139
00012		22.20	2.00	1.20	3.20	0.418	100	119
50382		22.50	2.00	0.75	2.50	0.432	100	122
50065		24.00	1.20	0.30	0.30	0.296	100	138
42390		24.00	1.30	0.30	0.30	0.319	100	139
58881		25.00	1.20	0.30	0.30	0.310	100	144
50347		25.00	1.30	2.00	1.30	0.343	100	143
56616		25.00	1.40	0.30	0.30	0.358	100	143
50066		25.00	1.50	0.30	0.30	0.382	100	143
42178		25.00	1.50	0.30	0.80	0.381	100	142
54927		25.00	1.60	0.30	0.30	0.405	100	143
55408		25.00	2.00	0.90	0.90	0.500	100	139
53916		25.00	2.00	4.00	6.00	0.452	100	129
50609		25.00	3.00	0.30	0.30	0.716	100	137
10628		25.40	2.00	0.30	0.30	0.507	102	145
00022		25.40	3.18	0.70	3.96	0.731	100	133
55162		25.90	1.90	0.30	0.30	0.494	103	147
56693		27.20	1.50	1.00	0.30	0.416	105	155
11433	> 30mm	30.00	1.60	0.30	0.30	0.492	120	144
42886		30.00	2.00	0.30	0.50	0.608	120	172
56692		31.00	1.60	0.30	0.30	0.510	124	180
00101		31.80	3.20	0.63	0.63	0.993	126	176
55144		33.60	1.50	0.30	0.30	0.522	134	195
10223		38.00	1.70	1.00	0.30	0.667	152	221
00041		38.00	2.00	0.30	1.27	0.777	150	218
42274		38.00	3.00	1.00	2.00	1.132	149	212
50070		38.00	3.00	0.30	0.30	1.139	151	215
55899	> 40mm	40.00	2.00	0.30	0.30	0.825	160	232
56965		40.00	2.50	0.30	0.30	1.017	160	230
56207		40.00	3.00	0.30	0.30	1.204	160	228
42938		44.00	3.00	2.00	0.50	1.343	175	250
53996		44.00	3.00	3.00	0.30	1.355	176	250
58335	50mm	50.00	1.50	0.30	0.30	0.789	200	294
56655		50.00	2.00	0.50	2.50	1.028	196	287
11173		50.00	3.00	0.30	0.30	1.529	200	288
56066		50.00	6.00	0.30	0.30	2.864	200	275
00256		50.80	3.20	1.60	1.60	1.653	200	288
56924	> 60mm	60.00	2.00	0.30	0.30	1.258	240	352
56081		60.00	3.00	0.30	0.30	1.855	239	347
42145		63.50	6.40	1.60	6.36	3.877	243	343
56121	> 70mm	70.50	2.50	0.30	0.30	1.830	278	409
11517		76.00	2.00	0.30	0.30	1.605	304	448
50075		76.20	1.70	0.30	0.30	1.374	304	450
59049		76.20	3.20	0.30	0.30	2.534	304	444
42371		77.80	2.00	0.30	0.30	1.644	311	458
55210	> 100mm	100.00	2.00	0.30	0.30	2.126	399	591
13029		100.00	3.50	0.30	0.30	3.644	400	586
55906		100.00	6.00	0.30	0.30	6.119	399	575
55126		114.50	2.00	0.40	0.40	2.441	457	678

Material Specifications
All material will be Aluminium 6063-T6 unless specified or requested. All lengths can be supplied in 6m lengths. Longer lengths can be supplied on special request.

Surface Finish
All lengths are available in mill finish, powder coated or anodised.

TUBING
Square 2
Rectangular 3-4
Round 5-6

ANGLES
Equal Leg 7
Unequal Leg 8

CHANNELS
Equal Leg 9-10
Lipped & Top Hat 11

MISC
T & H Sections 12

BARS
Flat Bar 13
Hexagon Bar 14
Square Bar 14
Round Bar 14

Appendix E

Orplex Catalog

PULLEY TYPE ETT 160 COMPLETE WITH BRACKET - FOR WIRE ROPE Quick Ref: 155.4

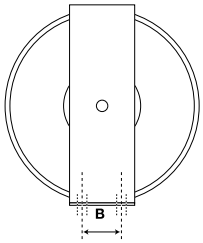
- WEBI Galvanised cast iron pulley with bearing and pressed steel bracket
- Complete with bearing and fixing bolt
- Material finish - galvanised cast iron
- Capacities from 100 kg to 400 kg
- To suit 3 mm - 5 mm wire rope (see specification PDF for full details)
- For use with manual and powered winches (any applications where rope needs to be diverted)
- SWISS MADE "ETTER"

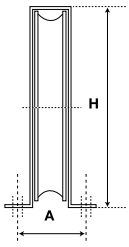
ETT-160 PULLEY COMPLETE WITH BRACKET - FOR WIRE ROPE

Material - galvanized cast iron pulley with pressed steel bracket

Product code		ETT - 160-60 155.4.1	ETT - 160-80 155.4.2	ETT - 160-100 155.4.3	ETT - 160-120 155.4.4
Diameter of pulley	(mm)	60	80	100	120
Groove for wire cable Ø	(mm)	3	4	4	5
Load Capacity	(kg)	100	200	300	400
A	(mm)	46	60	78*	70
B	(mm)	20	24	42	46
H	(mm)	66	88	109	130
Mounting hole Ø	(mm)	5	6	7	10
Weight per item	(kg)	0,35	0,6	1,1	1,6


© winchshop.co.uk





Appendix F

SKF Bearing Technical Sheet



16004

Rolamento rígido de esferas

Os rolamentos rígidos de esferas de uma carreira são particularmente versáteis, possuem baixo atrito e são otimizados para baixo ruído e baixa vibração, o que permite uma alta velocidade de rotação. Eles suportam cargas radiais e axiais em ambas as direções, são fáceis de montar e requerem menos manutenção do que muitos outros tipos de rolamentos.

- Modelo simples, versátil e robusto
- Baixo atrito
- Capacidade de alta velocidade
- Suporta cargas radiais e axiais em ambas as direções
- Requer pouca manutenção

Overview

Dimensões

Diâmetro do furo	20 mm
Diâmetro externo	42 mm
Largura	8 mm

Desempenho

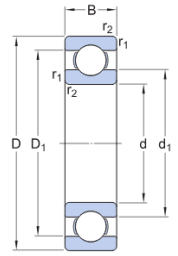
Classificação de carga dinâmica básica	7.28 kN
Classificação de carga estática básica	4.05 kN
Velocidade de referência	38 000 r/min
Velocidade-limite	24 000 r/min
Classe de desempenho SKF	SKF Explorer

Propriedades

Rasgos de entrada	Sem
Número de carreiras	1
Recurso de localização, anel externo do rolamento	Nenhum
Tipo de furo	Cilíndrico
Gaiola	Metal laminado
Arranjo pareado	Não
Folga interna radial	CN
Material, rolamento	Aço para rolamentos
Revestimento	Sem
Vedação	Sem
Lubrificante	Nenhum
Recurso de relubrificação	Sem

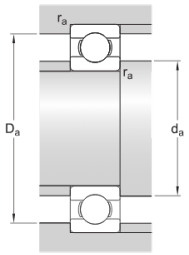
Especificações técnicas

Classe de desempenho SKF	SKF Explorer



Dimensões

d	20 mm	Diâmetro do furo
D	42 mm	Diâmetro externo
B	8 mm	Largura
d_1	≈ 27.25 mm	Diâmetro do ressalto
D_1	≈ 34.3 mm	Diâmetro do ressalto
$r_{1,2}$	min. 0.3 mm	Dimensão de chanfro



Dimensões do encosto

Diâmetro do encosto do eixo	d_a	min. 22 mm
Diâmetro do encosto do mancal	D_a	max. 40 mm
Raio de concordância do eixo ou filete do mancal	r_a	max. 0.3 mm

Dados de cálculo

Appendix G

Fabory Spring Plunger Technical Sheet

FABORY



Posicionadores com mola, sextavado interior e esfera, força de mola padrão Aço inoxidável 1.4305 M3

Referência	58517.030.001
Marca	-
UBB	500689799830
UNSPSC	31162807
EAN	
Emb. de 10	Apenas embalagem completa

Parâmetros técnicos

Material (comprimento)	Aço inoxidável (Inox)
Encaixe	Sextavado interior
Rosca	Métrica
D	M3
Material técnico	1.4305
Info	Material: Manga 1.4305. Bola 1.4034. Mola 1.4310. Versão: Brilhante. Bola, endurecida.

Normas

Especificação técnica

D	M3
D_1	1.5
F1 = springiness beginning in N	1.5
F2 = springiness end in N	3
H	0.4
L	9
S	1.5

Desenho técnico

